DISSERTATION

ALGAE-TO-FUEL PATHWAYS: INTEGRATION OF CULTIVATION STUDIES, PROCESS MODELING, TECHNO-ECONOMIC ANALYSES, AND LIFE CYCLE ASSESSMENTS

Submitted by

Peter H. Chen

Department of Mechanical Engineering

In partial fulfillment of the requirements

For the Degree of Doctor of Philosophy

Colorado State University

Fort Collins, Colorado

Spring 2022

Doctoral Committee:

Advisor: Jason C. Quinn

Thomas Bradley
Anthony Marchese
Kenneth Reardon

ABSTRACT

ALGAE-TO-FUEL PATHWAYS:
INTEGRATION OF CULTIVATION STUDIES, PROCESS MODELING, TECHNO-ECONOMIC ANALYSES, AND LIFE CYCLE ASSESSMENTS

Researchers have recognized the potential of microalgae for renewable fuels for several decades, with a sharp increase in interest in the past decade. Though progress in algal cultivation and conversion has been substantial, commercialization of algal fuels has not yet been achieved. Economic metrics must be balanced with renewable fuel goals such that algal fuels can be competitive with conventional petroleum fuels. Through process modeling, techno-economic analysis (TEA), and life cycle assessment (LCA), the work in this dissertation seeks to illuminate improvements to algal fuel systems and outline the steps required to advance algal fuels toward commercialization.

This work heavily focuses on hydrothermal liquefaction (HTL), a thermochemical process that converts whole wet biomass into biocrude, a petroleum crude oil analog. An aqueous phase, a gaseous phase, and a solid phase are created alongside the primary biocrude product. The aqueous phase of HTL notably contains a high content of nitrogen, which could potentially be recycled back to algae cultivation. At a scale where algal biofuels would meet a significant portion of transportation fuel needs, the demand for nutrients, specifically nitrogen and phosphorus, would exceed current global agricultural production. While recycling the aqueous phase could alleviate the demand for fresh nutrients in algae cultivation, it also contains toxic components, which include heterocyclic nitrogen compounds and phenolic compounds.

The first phase of this research is an experimental component that focuses on methods for improving the recyclability of nutrients in the aqueous phase. A novel use of adsorbents (activated carbon and ion-exchange resins) was discovered for reducing the presence of components that are toxic to algae growth.

The second research phase is a comprehensive modeling effort of the HTL process. A process model was developed in *Aspen Plus* from a robust assessment of current literature. These results are fed into TEA and LCA models to fully demonstrate the effects that process uncertainties have on the viability of HTL. For example, the high-temperature conditions that define HTL require the material to maintain a subcritical liquid state, which complicates the assessment of accurate thermochemical properties due to the required pressure. To clarify this issue, the work in this research phase compares the estimated performance of algal HTL between different thermodynamic models. HTL environmental metrics beyond global warming potential and net energy ratio are also discussed for the first time. Uncertainties in conversion performance are bounded through a scenario analysis that manipulates parameters such as product yield and nutrient recycle (as discussed in the first research phase) to establish a range of economic results and environmental impacts. The work is supplemented with a publicly available model to support future hydrothermal liquefaction assessments and accelerate the development of commercial-scale systems.

The third and final research phase compares HTL with a fractionation train called Combined Algal Processing (CAP) and takes into consideration the possibility of integrating HTL downstream of CAP. CAP can be described as a pretreatment and fermentation step followed by a lipid extraction step to extract carbohydrates and lipids, respectively, for fuel products. However, CAP cannot convert proteins to fuels, making the process highly dependent

on feed composition from the cultivation stage. HTL's advantage over CAP is its relative agnosticism to composition, but it requires greater capital costs and is more energetically intensive. A fuzzy logic approach is proposed to compare CAP and HTL process models through relevant performance metrics and to map algal feed conditions that lead to optimal algae-to-fuel pathways. Thresholds are set for fuzzy membership functions in relevant performance objectives: minimum fuel selling price (MFSP), global warming potential (GWP), and net energy ratio (NER). The membership functions yield "satisfaction scores" for each objective and factor into an overall satisfaction score. Individual and overall satisfaction scores for each pathway are mapped to the full range of feed compositions (proteins, carbohydrates, and lipids). A composition-based algal growth model was then implemented to perform an uncertainty analysis through Monte Carlo simulations. The impact on satisfaction scores from varying other key process model parameters, such as algae productivity, individual process yields, process operating parameters, and life cycle inventory uncertainty are highlighted in these select scenarios.

ACKNOWLEDGMENTS

I would like to thank my graduate committee – Dr. Bradley, Dr. Marchese, and Dr. Reardon – for their support and attention toward this work. I want to highlight Dr. Quinn as an incredibly supportive and positive advisor through my entire time at Colorado State University, who has maintained steadfast leadership before and during the COVID-19 pandemic. The Quinn research group has provided excellent feedback on my work. Lastly, I must thank my friends and my parents, Zhizheng Chen and Lihua Liu, for their unwavering personal support throughout my time in graduate school.

The work in this research was funded by DOE awards DE-EE0008245, DE-EE0008245, and DE-EE0008515. Opinions, findings, conclusions, or recommendations expressed here are those of the author(s) and do not necessarily reflect the view of the U.S. Department of Energy.

TABLE OF CONTENTS

CH. 1: RESEARCH INTRODUCTION

The impending effects of climate change have left humanity with increasingly difficult challenges to solve. The Intergovernmental Panel on Climate Change (IPCC) reports the current trajectory of global warming and outlines sectors that must evaluate and implement mitigation strategies to avoid catastrophic global warming [1,2]. The transportation sector is a key facet of modern society that inherently poses large impacts on the world, both beneficial – with respect to quality of life – and detrimental via air pollution and greenhouse gas emissions. Approximately 14% of global greenhouse gas emissions in 2010 were attributed to transportation, 95% of which were derived from fossil fuels [2]. The world population is projected to increase from 7.7 billion (as of 2020) to 9.7 billion by 2050 and 11 billion by 2100 [3]. This increase in population will create a higher demand for motorized transportation and increase the need for energy security, especially in rapidly growing developing countries. The projected growing worldwide market for easily transportable energy and leaves a large opportunity to develop renewable fuels.

In the United States, corn has already seen success as a biofuel feedstock. Most American fuel stations carry gasoline with up to 10% ethanol [4]. However, conventional biofuels like corn ethanol only comprise one small step toward lowering transportation emissions. The Renewable Fuel Standard mandates only a 20% decrease in life-cycle greenhouse gas emissions for conventional biofuel but imposes a stricter 50% decrease in GHG emissions for other fuel categories. The RFS also caps corn ethanol production at 15 billion gallons per year, resulting in a biofuel "blend wall". Biodiesel is another fuel category that can be derived from land crops like soy and jatropha but is not produced in the same quantities as ethanol [5]. Together, food-based feedstocks make up a category called first-generation biofuels. A major disadvantage of first-

generation biofuels is the conflict with resources for food production, sometimes referred to as the “food versus fuel” problem [6]. Indirect land use change has also controversially been cited as a detriment to the sustainability of first-generation biofuels [7,8]. Second-generation feedstocks are comprised of abundant lignocellulosic sources like wood and agricultural waste. Though investment in second-generation biofuels began in the 2010s, the recalcitrant nature of such feedstocks results in high production costs and commercial lignocellulosic fuel plants are exceptionally limited or nonexistent to this day [5,9].

Third-generation biofuels are created from algae and provide notable advantages over first- and second-generation biofuels. The algal biofuel production chain is composed of a sequence of cultivation, harvesting and dewatering, conversion, fuel upgrading, transportation and distribution, and end use via combustion. In the cultivation stage, algae can potentially achieve biodiesel productivity rates one or two orders of magnitude greater than land crops per unit area of land [10]. An added benefit is the ability for algae to grow on non-arable land, avoiding a major conflict often cited in the food versus fuel problem associated with first-generation biofuels. Despite these advantages, numerous production challenges throughout the value chain have prevented third-generation biofuels from seeing large-scale commercialization. Biomass and conversion costs are major obstacles [11–14], leading to many efforts to further improve algae productivity and fuel yields. Freshly harvested and dewatered algae contain 80 wt% water or more [12], which limits the number of viable technologies that can process algal biomass into a renewable fuel product. There exists a need to assess potential improvements and solutions to these production challenges if third-generation biofuels are to ever contribute meaningfully to the fight for energy security and climate change mitigation.

Techno-economic analysis (TEA) and life cycle assessment (LCA) are powerful tools that can measure the performance and sustainability of novel technologies such as algal biofuel plants. TEA and LCA are intricately tied to process modeling by linking calculated material and energy flows to economic and life cycle inventory, respectively. Typically, the key TEA metric for renewable fuels is the minimum fuel selling price (MFSP), which is the price that a renewable fuel plant can sell a unit of fuel over the plant's lifetime to break even in investment. LCA quantifies the environmental impacts of material and energy flows to air, water, and land. LCA impacts vary in relevance to certain processes; in the context of climate change, global warming potential (GWP) is the most important impact. However, this part of this dissertation will touch upon other oft-overlooked LCA impact categories like eutrophication and human health impacts.

Through the combination of rigorous process modeling, TEA, and LCA, this work answers some questions posed by current literature on algae-to-fuel pathways. Processes across the algal biofuel system boundary, from cultivation to end use, are covered in this dissertation. The first research phase is an experimental component that addresses the viability of treating a nutrient-rich stream from a fuel conversion process called hydrothermal liquefaction (HTL) to improve the recyclability of nitrogen for algae cultivation, which would solidify a major assumption about closing the nutrient supply loop. The following research phase then addresses HTL in detail by varying some of the key parameters that are often assumed to be fixed in literature. The final phase is a holistic comparison of HTL to another algae-to-fuel pathway, Combined Algal Processing [11] via a "fuzzy logic" scoring methodology. This dissertation is intended to inform future research about some of the key factors required for commercial-scale algal biofuel production to succeed as a sustainable renewable energy source.

CH. 2: REMEDIATION OF HYDROTHERMAL LIQUEFACTION AQUEOUS PHASE FOR IMPROVED ALGAL NUTRIENT RECYCLE [a]

2.1 Introduction

Algal biomass has many applications, ranging from bioenergy to nutritional supplements. Algae are heralded as one of the most promising biomass feedstocks thanks to the cells' highly efficient photosynthetic light-to-biomass conversion [15]. Other key advantages of algae as a bioenergy feedstock include the ability to be cultivated on non-arable land, which avoids conflicting land use with agricultural crops, and utilization of waste flue gas and wastewater streams as substrate and nutrient supplies. However, one major challenge in large-scale deployment of algal biomass production is sustainable nutrient supply. Accelerating biomass production at the agricultural scale to levels that could meet national renewable fuel production milestones would push the demand for nitrogen and phosphorus between 32% and 49% of the world surplus supply [16]. Thus, approaches for sustainable nutrient supply need to be considered. One such approach is to consider recycling nutrients from conversion processes to reduce the demand for fresh nutrients and improve the sustainability footprint of the overall algae production process.

One conversion process considered for bioenergy production is hydrothermal liquefaction (HTL). HTL is a thermochemical conversion technology that produces bio-crude oil and other products from a wet biomass feed. A continuous HTL process operates at moderate temperatures (250 – 400 °C) and high pressures (20 – 22 MPa) to keep reactions in a subcritical (liquid) state.

---

[a] This chapter was published as a peer-reviewed journal article: Chen, P.H., Venegas Jimenez, J.L., Rowland, S.M., Quinn, J.C., Laurens, L.M.L., 2020. Nutrient recycle from algae hydrothermal liquefaction aqueous phase through a novel selective remediation approach. Algal Res. 46. https://doi.org/10.1016/j.algal.2019.101776

Along with bio-crude oil, other products such as gases (carbon dioxide and methane), bio-char, and an aqueous phase (HTL-AP) containing nutrients and organic compounds are produced. One advantage of HTL is the ability to process wet biomass feeds. A large variety of feedstocks have been evaluated, including slurries of terrestrial biomass such as forest residue and corn stover [12]. Algae is a highly synergistic feedstock with HTL as it can be processed without cost-prohibitive and environmentally unsustainable drying prior to downstream conversion [17].

While the bio-crude oil is the desirable product, the partitioning of carbon, nitrogen, and phosphorus to other HTL product fractions presents an opportunity for improving the sustainability of the system through nutrient recycle [12]. Bio-crude oil production in HTL can be manipulated by changing the operating conditions. Bio-crude yields range between 30% and 60% of the biomass feed [18]. A small fraction is converted to gas and char, with the remaining majority of the biomass partitioned to HTL-AP. One HTL process model in Elliott et al. [19] is assumed to have integration of HTL-AP nutrient recycle back to algal cultivation without treatment. This meets the same conclusion of other recent work, albeit after some dilution [20]. Jones et al. [21] assumes 90% of nitrogen in the aqueous phase can be recycled back to algal cultivation without any reduction in growth. However, many other algal HTL assessments acknowledge that nutrient recycle technology needs further development due to the demonstration of poor growth from toxic compounds that accompany the HTL-AP [22,23]. Experimental studies report inhibited algal growth in recycled HTL aqueous phase, even at diluted levels [20,24,25]. Though success was shown in Godwin et al. [26] in recycling HTL-AP for algal polycultures, it was also demonstrated that monocultures were far less tolerant to untreated HTL-AP. It is important to evaluate whether these toxic effects can be reduced or eliminated, as to be a sustainable conversion technology, it is expected that HTL needs to

integrate nutrient recycle. The extent of toxicity of HTL-AP derived from *Chlorella vulgaris* has been shown to depend highly on algal species. Edmundson et al. [20] showed that in equivalent media, dilutions of HTL-AP sustained the growth of *Chlorella sorokiniana* compared with standard medium, but severely inhibited the growth of *Scenedesmus obliquus*. The contrast in growth was enough that further studies with *S. obliquus* were excluded. Overall, a survey of literature shows that some sustainability assessments assume seamless integration of HTL-AP, but past experimental work conflicts with this assumption by demonstrating that untreated recycled HTL-AP reduces productivity due to the formation of toxic compounds in the HTL process.

In previous experimental work, reduced algae productivity has been attributed to the complexity and diversity of compounds found in HTL-AP that are toxic to algae. Compound families in HTL-AP that have demonstrated algal growth inhibition include phenolics (phenol and its derivatives) and heterocyclic nitrogen compounds such as 2-piperidinone, 2-pyrrolidinone, and pyrazine [27]. Several treatments to remediate HTL-AP toxicity have been studied. Activated carbon has been reported to adsorb toxic cyclic nitrogen compounds and its adsorbent effects have been demonstrated in the application of HTL-AP nutrients to anaerobic digestion [28–31]. Studies of recycling effluent back to algal cultures, however, were not found. An alternative adsorbent family is resins, which have been demonstrated to remove toxic phenolic compounds from rice straw-derived HTL-AP [32]. Few results for resin remediation have been reported despite including a much wider variety of potential treatments than activated carbon. No studies were found that addressed resins as an algal HTL-AP treatment. Lastly, polyvinylpyrrolidone (PVPP) is an established resin adsorption treatment for other applications, most notably in removing phenolics from wine and beer [33,34]. Similar to resins, the

application of PVPP to algal HTL-AP has yet to be demonstrated. Adsorption methods present an unexplored field of HTL-AP treatments that can potentially remediate issues with toxicity in algae.

While achieving sustainability benchmarks requires nutrient recycle from HTL, the impact on productivity is more complicated than seamless integration as assumed in a variety of economic and environmental assessments. The viability of aqueous phase recycle depends on the degree to which recycled nutrients can replace fresh media components without toxic inhibition. Based on the current state of the field, there exists a potential for recycling HTL-AP catered toward the growth of specific algal strains through toxicity reduction. Despite data supporting the use of adsorption treatments on HTL-AP, work in algal cultivation has been limited in both scope and quantity. Very little information is available on the molecular profiling of the effects of remediation of process streams, beyond standard characterization of the raw HTL-AP as part of an elemental profiling [35].

This study focuses on the replacement of fresh nitrogen in media using nitrogen in HTL-AP. Effects on the growth of *Chlorella vulgaris* and *Desmodesmus armatus* monocultures are compared across various nitrogen replacement levels. The goals of this study were 1) to determine the maximum tolerance each species has for HTL-AP derived from *Chlorella vulgaris*, 2) to identify novel remediation treatments on HTL-AP that effectively remove toxic compounds, and 3) to compare compositional profiles of algae grown on standard media against algae grown with HTL-supplied nutrients. To achieve these, treatments such as activated carbon and resins not mentioned in literature for HTL-AP remediation (Dowex 50WX8, a strongly acidic cation-exchange resin, and PVPP, a polymeric polyphenol adsorbing resin) were evaluated in terms of impact on growth and health of algae cultures as media nutrients are replaced by

HTL-AP. To elucidate the impact of the treatments, a detailed elemental composition of the pre- and post-treatment HTL-AP was determined, with a novel application of the in-depth molecular profiling of the organics in the HTL-AP before and after Dowex 50WX8 treatment by Fourier transform ion cyclotron resonance (FT-ICR) mass spectrometry. The impact of this work is aimed toward establishing an improved technology suite for sustainable nutrient recycling from the aqueous waste streams of thermochemical algae conversion technologies such as HTL.

2.2 Materials and methods

2.2.1 HTL aqueous phase

HTL product streams were produced in a continuous HTL system operated at Pacific Northwest National Laboratory (PNNL) [12] in September 2017. The feedstock for the HTL process was a 22 wt% *Chlorella vulgaris* biomass slurry produced at Global Algal Innovations in Lihue, Kauai, Hawaii. The HTL-AP stream was collected in bulk during the process and included the start-up, steady-state, and system post-flush streams. The system post-flush collection resulted in a dilution of the collected steady-state HTL-AP by approximately 1.5x; the bulk sum of the three streams comprises the HTL-AP used in this study. The initial compositional data from this collection were provided by PNNL along with the material. The compositional data accompanying the HTL AP collection was the basis for initial calculations of nitrogen concentrations in medium recipes. A revised compositional analysis, outlined below, was used for discussion purposes and for quantifying changes from the treatments performed. Minor inconsistencies in reported data were observed between the measured nutrient concentrations, which did not affect the conclusions of this work.

Approximately 8 L of the final bulk HTL-AP was procured in April 2018 from the PNNL HTL conversion team [19]. All HTL-AP was filtered through a 0.2 µm aPES membrane filter for

sterile media preparation and kept frozen until utilization in biological assays. Samples of HTL-AP were submitted to a contract laboratory (Huffman Hazen Laboratories, Golden, CO) for compositional analysis on total carbon, total organic carbon, ammonia nitrogen, Kjeldahl nitrogen, orthophosphate, total phosphorus, sulfate, and total sulfur. Standard water testing methods [36] were used for the analysis of the HTL-AP by a commercial analytical testing laboratory, with the following representing a high-level overview:

Organic carbon was measured by acidification of a sample aliquot with HCl, followed by O_2 sparging to remove inorganic carbon as CO_2. Instrument analysis was performed by high temperature combustion, followed by colorimetric determination of CO_2 production. Total carbon was measured at NREL with a high-temperature total organic carbon (TOC) analyzer with a non-dispersive infrared (NDIR) detector (Shimadzu). Ammonia nitrogen (NH_4^+-N) was measured by distilling a sample aliquot into boric acid solution and titrating with HCl to a bromocresol green and methyl red indicator end point. Kjeldahl nitrogen was measured by treating a sample aliquot with H_2SO_4 to convert organic nitrogen to ammonia. The sample was then distilled into boric acid solution and titrated with HCl to a bromocresol green and methyl red indicator end point. Orthophosphate and sulfate were measured by ion chromatography with ion detector. Phosphorus and sulfur were measured by inductively coupled plasma atomic emission spectroscopy (ICP-AES).

2.2.2 HTL-AP remediation

Three treatments were explored in this study: activated carbon (AC), Dowex 50WX8 (DX; ion-exchange resin), and polyvinylpolypyrrolidone (PVPP; polymer resin). Granular coconut-derived AC (EM Industries, Inc.) was added to untreated HTL-AP at a loading of 100 g AC per L HTL-AP and mixed for three days. A previous study on AC for HTL-AP conducted

treatments at adsorbent loading levels varying from 0 to 30 wt% (0 to 300 g AC L^{-1}) for 24 hours [30], which showed that the selected loading reduced the number of GC/MS peaks by approximately half. The ion-exchange resin Dowex 50WX8 (46.4 dry wt%) was added to untreated HTL-AP at a load of 200 g L^{-1} wet resin HTL-AP for three days. This adsorbent loading was chosen as a comparable dry weight fraction to AC. The Dowex 50WX8 resin was selected for its expected ability to remove negatively charged components. Another resin, PVPP, was added to untreated HTL-AP at loads of 20 g resin per L HTL-AP (PVPP20) and 50 g resin per L HTL-AP (PVPP50) and allowed to mix at a residence time of three days. The lower concentrations of PVPP compared to DX and AC loadings were selected because of the projected lower polyphenolics content in the HTL-AP. The information in section 2.4 indicates that phenolics are part of the molecular composition of the HTL-AP, and consistent with previously published data [35]; however, our data is not quantitative. One detailed quantitative assessment of HTL-AP from *Chlorella vulgaris* measured phenolics at about 2% of the total organic carbon (TOC), averaging 500 mg L^{-1} [37]. It was also assumed that PVPP may be difficult to economically scale up at higher loading. All treated HTL-AP aliquots were filtered again through a 0.2 µm aPES membrane filter. Samples of treated HTL-AP were also submitted to Huffman Hazen Laboratories for compositional analysis.

2.2.3 Algae cultivation and analysis

Chlorella vulgaris UTEX 395 and wild-type *Desmodesmus armatus* were selected as they represent commercially-relevant species with high bioenergy potential. These species are closely related to *Chlorella sorokiniana* and *Scenedesmus obliquus*, respectively, which have been studied for their response to HTL-AP toxicity and have shown to have vastly contrasting tolerance [20]. Cultures of *C. vulgaris* were grown in modified Bold's basal medium (mBBM)

adjusted to pH 6.9. *D. armatus* cultures were grown in modified artificial seawater medium (MASM). MASM was adjusted to pH 8 with HCl. Media recipes are tabulated by molar concentration in Table A - 1. All media recipes were adjusted from literature recipes to contain 10 mM nitrogen. Media nitrogen was derived from ammonium chloride (NH_4Cl) or sodium nitrate ($NaNO_3$) for mBBM or MASM, respectively, for control cultures. Toxicity experiments were carried out with HTL-AP or a combination of the HTL-AP and the control nitrogen source. HTL-AP dilutions were calculated from the original compositional analysis from PNNL. Growth data were collected from duplicate monocultures of *C. sorokiniana* and *D. armatus* cultivated in varying dilutions of HTL-AP.

We included a variance in HTL-AP dilutions to investigate toxicity limits. *C. vulgaris* cultures were tested for HTL-AP toxicity tolerance at HTL-AP dilutions of 200x, 150x, 100x, and 50x HTL-AP (18%, 24%, 35%, and 71% nitrogen replacement, respectively). *D. armatus* cultures were tested with MASM-diluted untreated HTL-AP at dilutions of 200x and 25x (representing 18% and 141% nitrogen replacement, respectively). Each experiment was performed in sterilized 500 mL Erlenmeyer flasks with foam tops for gas exchange. Cultures started with a working volume of 125 mL. Each control and treatment were inoculated in duplicate. Flasks were placed on a 130-rpm shaker in a 24 – 26 °C, 50 μE m^{-2} s^{-1} light environment. No CO_2 or air sparging was included with gas exchange limited to the foam tops. Samples of approximately 1 mL per flask were taken periodically. Volume lost to evaporation or sample removal was not replenished. Growth was measured by optical density at 750 nm (OD_{750}) with a Beckman Coulter DU 800 spectrophotometer. All spectrophotometer blanks were taken with the respective medium of the sample culture measured, e.g. OD_{750} measurements for *C. vulgaris* controls were blanked with mBBM; 100x DX cultures were blanked with DX-treated

HTL-AP diluted 100x in mBBM; and so forth. Blanks were replaced periodically to prevent turbidity buildup from contamination. Each of these OD_{750} measurements were plotted against the culture time from inoculation to develop a growth curve for the carbon-limited linear phase. A line of best fit was developed for the linear section for each average growth curve, where the slope of the line indicates the linear growth rate. Culture pH was also monitored with each OD_{750} sample using a Hach H135 Minilab portable pH meter. Contamination was monitored by microscopy samples throughout each experiment.

Samples for compositional analysis were collected upon completion of experiments. Aliquots of 50 mL from each culture flask were centrifuged at 3,000×g RCF for 5 minutes at 4 °C. Supernatant was separated from biomass pellets by decanting and stored in a -20 °C freezer. The remaining biomass pellets were lyophilized and stored at -20 °C. Samples of supernatant were analyzed at NREL by a Shimadzu TOC-L Total Organic Carbon Analyzer. Compositional tests on supernatant included total carbon (TC) and total organic carbon via non-purgeable organic carbon (NPOC). Inorganic carbon (IC) content was calculated by the difference between TC and NPOC measurements. Biomass composition was analyzed by GC/MS and by assays for carbohydrate, lipid, and protein content using NREL-developed standard laboratory procedures, as described before [38–41].

2.2.4 Ultra-high resolution mass spectrometry characterization of aqueous phase organics molecular composition

To isolate the HTL-AP organics for in depth molecular profiling, the untreated, AC-treated, and DX-treated HTL-AP samples were first evaporated under gentle stream of nitrogen, after which the dried samples were extracted and desalted with a series of organic solvents. Samples were first extracted twice with a mixture of methylenechloride:isopropyl alcohol

(DCM:IPA) at a ratio of 75:25. The samples were then extracted twice with DCM:IPA (1:2) and lastly with DCM:IPA 10:90. All extracts were combined and evaporated under nitrogen and the mass recovery of salts and residual organics were then measured and reported as a weight fraction of the initial, dried, HTL-AP sample in Table 1. The dried samples were extracted/desalted with a series of organic solvents.

Table 1. Mass yield of salts and organics from aqueous samples (AC = activated carbon, DX = Dowex 50WX8). All data shown are shown as single data points from representative extractions of the HTL-AP.

Sample	Salts and residual organics (% mass)	Extracted organic compounds (% mass)	Residual salts (% mass)
Untreated	4.4	2.0	2.4
AC treatment	2.9	0.1	2.7
DX treatment	2.8	1.2	1.6

Extracts were re-dissolved in DCM at a concentration of 1 mg mL^{-1}, then further diluted in methanol (MeOH) to a final concentration of 100 µg mL^{-1}. Formic acid was added at 0.1 v/v% to aid with ionization for positive-ion electrospray. Samples were analyzed with a Bruker 7T SolariX XR Fourier Transform Ion Cyclotron Resonance (FT-ICR) mass spectrometer with magnitude mode data processing. Nebulization was conducted with a nebulizer pressure of 0.4 bar, dry gas flow rate of 3 L min^{-1}, and dry temperature of 200 ^{o}C. The capillary voltage was 4000 V and the end plate was set to -500 V. Samples were directly infused at a flow rate of 5 µL·min^{-1}. Twenty co-added spectra (4 megaword) were collected with an accumulation time of 200 ms and a m/z range of 100.4 – 1500, with an average resolving power of 260,000 at m/z 400 at a 1.95 s transient time. An external calibration was performed with sodium trifluoroacetate clusters prior to data analysis and spectra were internally calibrated on a Kendrick mass series of ions with an N_2O_2 heteroatom class and a double bond equivalent (DBE) value of 7 prior to data processing. Peaks were picked using the Bruker DataAnalysis software at six standard deviations above the average noise value. The peak list was imported into PetroOrg software

(software.petroorg.com; Omics, Tallahassee, FL), and elemental formulas were iteratively assigned to each identified peak within a tolerance of 0.5 ppm, similar to an approach described previously [35]. Based on assignment parameters (Table A - 2), the conditions in assignment order #1 were applied, followed by the conditions in assignment order #2 to the remaining unassigned peaks. This procedure was followed until all conditions were used. For both samples, the root mean square (RMS) mass error for all assignments was less than 500 ppb, and the percent relative abundances assigned were 84.3% for the untreated sample and 74.6% for the DX-treated sample. Calculations of H/C, O/C, and N/C as well as data sorting and visualization were performed in *R* and *Excel*. Histograms were created using the ggMarginal function in statistical data processing software *R version 3.5.0* [42] and 100 bins were used.

Because FTMS data collected for the AC treated samples showed inconclusive results on molecular profiling, and the growth studies indicated little benefit to the AC treatment, we only moved forward with the in-depth molecular annotation and elemental formula assignments for the DX treated samples and discussed in section 3.5.

2.2.5 Statistical analysis

All experimental cultivation experiments were run in biological duplicate, and the statistical evaluation of significance was carried out based on the standard error on the mean. For the FT-ICR MS data, the comparisons of the assigned molecular formulae were carried out in the statistical software *R version 3.5.0* [42]. All compositional data were collected in triplicate and the standard deviation is included as a metric of the technical measurement uncertainty.

2.3 Results and discussion

2.3.1 HTL-AP compositional analysis

To support the estimation of nutrient recycling from raw HTL-AP, detailed compositional analyses were determined by Huffman Hazen Laboratories (Table 2). Bulk HTL-AP fluid was sent to NREL stored in non-inert conditions for several months prior to being used for this experimental work. Throughout this study, the original and accompanying analysis for NH_4^+-N concentration in untreated HTL-AP was used as the basis for determining nitrogen replacement of HTL-AP in media. Analyses from the NREL and Huffman Hazen laboratories, returned NH_4^+-N content in the raw HTL-AP 29% higher than the original analysis from PNNL. Initial growth experiments used an amount of nitrogen higher than originally intended. Based on calculations from the original analysis, the maximum untreated HTL-AP concentration required for full nitrogen replacement in media was a 25x dilution. With the NREL analysis, this represents a 141% nitrogen replacement. While this exceeds the targeted nitrogen replacement, it does not represent a level of free ammonia that would severely inhibit growth for *Chlorella*. A study by Wang et al. [43] found a short term (hours) EC_{50} of approximately 98 mM NH_4^+/NH_3 in some *Chlorella*, a much higher concentration than the 10 mM used in this study. In a similar vein, Konig et al. [44] demonstrated no inhibition in *Chlorella* grown in 10 mM NH_3 at pH 9.0. By contrast, another study by Azov & Goldman concluded that *Scenedesmus obliquus* struggled to grow around pH 8.4 due to free ammonia inhibition derived from 10 mM NH_4Cl [45]. It is likely that other Desmids like *Desmodesmus armatus* could suffer from a similar level of free ammonia inhibition at high pH, which makes it difficult to discern whether inhibitory effects in HTL-AP come from high NH_4-N or from other compounds. Nevertheless, Edmundson et al. also

concluded that *Scenedesmus* was unable to grow in untreated HTL-AP while *Chlorella sorokiniana* could [20], indicating that HTL-AP tolerance is highly species-dependent.

Several aliquots of the filtered, untreated HTL-AP were treated with AC, DX, or PVPP as described above. After AC treatment, the brown color in HTL-AP liquid was completely removed to produce a clear filtrate, which is a unique observation among the remediation treatments outlined in this study. Both DX- and PVPP-treated HTL-AP kept their brown color after filtration, unlike the AC-treated liquid. Samples of treated HTL-AP, including the untreated control, were submitted to Huffman Hazen Laboratories (Golden, CO) for carbon, nitrogen, phosphorus, and sulfur content analysis (Table 2).

Table 2. Compositional analysis of untreated and treated hydrothermal liquefaction-aqueous phase (HTL-AP) (Huffman Hazen Laboratories, Golden, CO). Units are in ppm and derived from a single data point of measurements by a contract laboratory on representative material after treatment.

	Untreated	**AC 100 g L^{-1}**	**DX 200 g L^{-1}**	**PVPP 20 g L^{-1}**	**PVPP 50 g L^{-1}**
Dissolved solids	45.6×10^3	29.5×10^3	26.7×10^3	—	—
Total carbon	26.9×10^3	12.1×10^3	15.7×10^3	24.8×10^3	24.5×10^3
Total organic carbon	18.4×10^3	7.2×10^3	14.2×10^3	18.6×10^3	18.7×10^3
Total alkalinity	28.4×10^3	26.8×10^3	6.24×10^3	26.5×10^3	27.5×10^3
NH_4^+-N	6.1×10^3	5.2×10^3	1.9×10^3	5.8×10^3	6.0×10^3
Kjeldahl nitrogen	8.6×10^3	6.4×10^3	3.8×10^3	8.1×10^3	8.4×10^3
Organic nitrogen[1]	2.5×10^3	1.2×10^3	1.9×10^3	2.3×10^3	2.4×10^3
Orthophosphate[2]	40	—	26	26	26
Phosphorus[2]	16	—	14	17	19
Sulfate	485	525	496	546	566
Sulfur	382	222	336	334	325

[1] Calculated as the difference between Kjeldahl nitrogen and NH_4^+-N.
[2] Phosphate and phosphorus levels excluded from report due to disparity between control and AC treatment measurements.

AC-treated HTL-AP had 61% of its organic carbon content removed, compared to only 23% organic carbon removal in the DX-treated HTL-AP. The trend is reversed, however, when analyzing nitrogen removal; only 13% of NH_4^+ and 26% of Kjeldahl nitrogen (total nitrogen excluding NO_3^- and NO_2^-) was removed in the AC treatment, while 68% of NH_4^+ and 56% of

Kjeldahl nitrogen was removed from the DX treatment. Thus, it is likely that the DX treatment would exhibit a reduced inhibitory effect on algae growth due to the removal of toxic nitrogen-containing compounds. Despite the greater removal of total nitrogen from the DX treatment, the AC treatment removed more organic nitrogen than the resins as expected from previous studies in literature [28–31]. Removal of components from PVPP was negligible; neither the 20 g L^{-1} nor the 50 g L^{-1} loading treatments altered the carbon and nitrogen content from the control by more than 9% (Table 2). Higher PVPP loading was not tested, as any improvement in viability would be offset by the equivalent unit cost of PVPP, which is at least an order of magnitude higher than other treatments.

2.3.2 Growth on untreated HTL-AP

Five untreated HTL-AP dilutions (control, 200x, 150x, 100x, and 50x) were initially tested to establish the baseline tolerance of *Chlorella vulgaris* UTEX 395. The linear growth rates for these trials are compared in Figure 1 with growth curves presented in Figure A - 1.

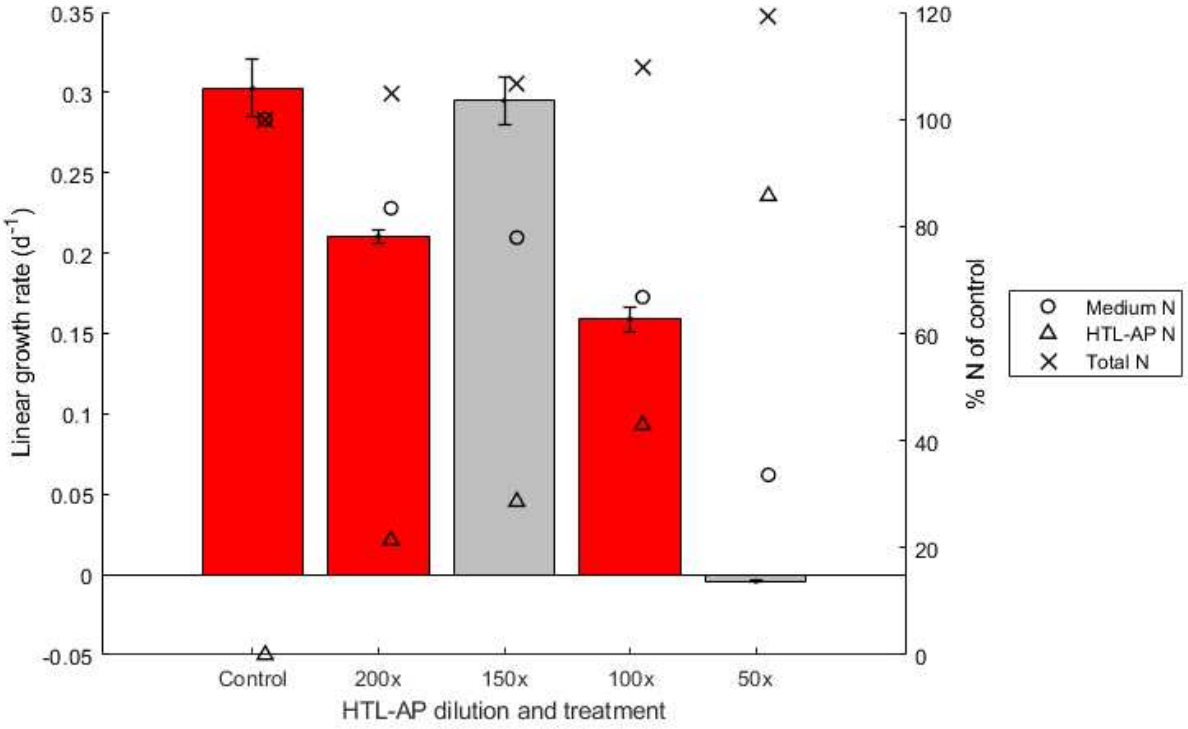

Figure 1. Linear growth rates of C. vulgaris on untreated hydrothermal liquefaction-aqueous phase (HTL-AP) dilutions in modified Bold's Basal Medium (mBBM). Markers indicate the actual amount of nitrogen derived from medium, HTL-AP, and the total. All data for the growth conditions are shown as the average ± standard error of duplicate cultures (n = 2). Data anomalies are reported but are grayed out. The 150x HTL-AP dilution culture unexpectedly grew better than the 200x HTL-AP dilution; the trend has not since been replicated. The 50x HTL-AP dilution exhibited no growth.

The linear growth rate of the control culture was 0.303 ± 0.018 d^{-1}. The growth rate of this study was lower than a similar study (1.38 d^{-1}) primarily due to a twofold difference in light (50 µE m^{-2} s^{-1} in this study compared to 100 µE m^{-2} s^{-1} in [46]). Growth was completely inhibited at a 50x dilution (71% nitrogen replacement) of HTL-AP. It is speculated that HTL-AP toxicity from either heterocyclic nitrogen compounds or phenolics is the cause of some of the observed growth reduction. At a 100x dilution (35% nitrogen replacement), HTL-AP inhibited *C. vulgaris* growth to 0.159 ± 0.008 d^{-1}, a 47 ± 7% decrease from the control. According to the growth rates from this experiment, the absolute HTL-AP toxicity threshold for *C. vulgaris* lies

between a 100x and 50x dilution. It can be extrapolated from this trend that a full nitrogen replacement offered by untreated HTL-AP at 25x dilution would not support growth of *C. vulgaris*. Growth was similar to the control at 150x HTL-AP dilution (24% nitrogen replacement). It is uncertain why the growth rate at 150x dilution exceeds growth at a higher dilution at 200x (0.211 ± 0.004 d^{-1}, 30% reduction from control). Given the decreased growth rate of *C. vulgaris* in 200x HTL-AP compared to the control in further experiments, it is likely that the growth rate of the 150x dilution culture is an outlier, as growth in the 150x dilution would be expected to fall in between the 200x and 100x dilutions. However, because these data were collected as duplicate biological experiments, we decided to include the data here, but present them as possible anomalies in Figure 1.

Similarly, in initial experiments with untreated HTL-AP, wild-type *Desmodesmus armatus* was tested at 200x and 25x dilutions in MASM. *D. armatus* showed growth inhibition at all dilutions in MASM (Figure 2). *D. armatus* grew in control MASM media at a linear rate of 0.082 ± 0.004 d^{-1}. Even in a 200x dilution (17% nitrogen replacement), *D. armatus* achieved a linear growth rate of 0.026 ± 0.001 d^{-1}, which is a 69 ± 5% reduction compared to the control medium. *D. armatus* is a comparable relative to *Scenedesmus obliquus* (by the family Scenedesmaceae), the latter of which was demonstrated by Edmundson et al. [20] to have low tolerance to HTL-AP. *D. armatus* completely failed to grow in a 25x dilution (141% nitrogen replacement) of HTL-AP. These results indicate that *D. armatus* is not suited for growth on raw HTL-AP, potentially due to a high sensitivity to compounds in HTL-AP.

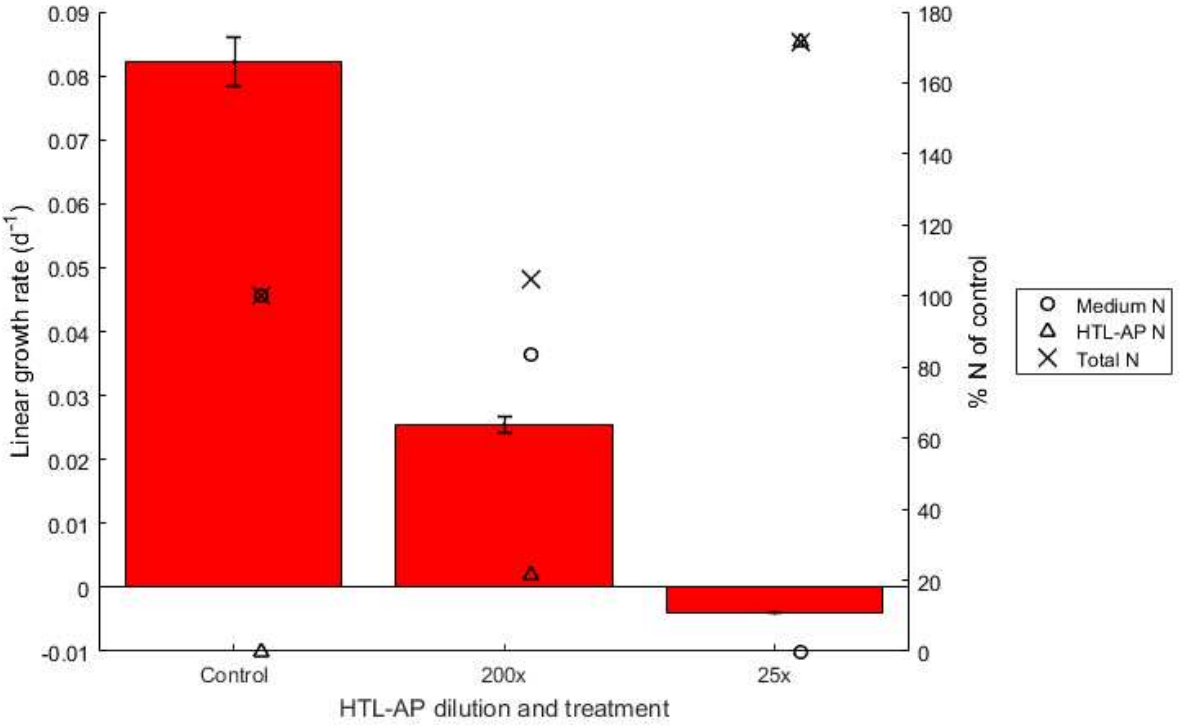

Figure 2. Linear growth rates of D. armatus on untreated hydrothermal liquefaction-aqueous phase (HTL-AP) in modified artificial seawater medium (MASM). Markers indicate the actual amount of nitrogen derived from medium, HTL-AP, and the total. All data for the growth conditions are shown as the average ± standard error of duplicate cultures (n = 2).

Based on the conclusion from several literature sources [20,47], a high amount of free ammonia from HTL-AP may inhibit growth in *Scenedesmus* (and *Desmodesmus* by close relation), but the inhibitory effect of free ammonia is diminished on the ammonia-tolerant *Chlorella*. In *Chlorella*, ammonia toxicity is not expected to be the primary factor in decreased growth with the introduction of diluted HTL-AP. In 10 mM NH_4Cl, 1.83 mM free ammonia is present at pH 8.6 (Table A - 3), where the 200x and 100x HTL-AP *C. vulgaris* cultures peak in the first few days of cultivation. According to other studies on ammonia tolerance in *Chlorella*, the NH_4-N concentration and pH in these studies should not be enough to inhibit *Chlorella* growth [43,44,48]. As seen further in Section 3.5, heterocyclic nitrogenous compounds are suspected as the largest cause of HTL-AP toxicity. However, future studies must address issues

that may arise from pH effects that result in ammonia toxicity, especially if less ammonia-tolerant strains are tested. Furthermore, it is possible that certain species of algae are more amenable to recycling HTL-AP from their own species compared with inter-species recycling, which may be due to a combination of either ammonia sensitivity or complex nitrogen component toxicity. Both of these hypotheses are critical to explore to expand the application of this study.

The growth studies indicated that *C. vulgaris* was more tolerant than *D. armatus* at higher concentrations of HTL-AP in medium; because of this, *D. armatus* was set aside in favor of *C. vulgaris* for subsequent experiments. It should be noted that a previous report [20] reached a similar conclusion in initial HTL-AP studies for *Scenedesmus obliquus* (closely related to algae in the *Desmodesmus* genus) when grown on HTL-AP derived from *Chlorella* sp., and reported growth results only for *Chlorella sorokiniana* after establishing the baseline tolerance.

2.3.3 Growth on treated HTL-AP

Growth on treated HTL-AP dilutions were tested only with *Chlorella vulgaris* UTEX 395 due to previously demonstrated higher tolerance to untreated HTL-AP. Along with control mBBM, media preparations of 200x and 100x dilutions of AC-, DX-, PVPP20-, and PVPP50-treated HTL-AP were used to test *C. vulgaris* for improved growth in HTL-AP after adsorbent treatment to remove targeted compounds (Figure 3).

In 200x and 100x dilutions, both the AC- and DX-treated HTL-AP supported higher growth rates than in untreated HTL-AP dilutions. Compared to the untreated HTL-AP, the AC-treated HTL-AP improved the linear growth rate by 17 ± 12% at 200x dilution and by 112 ± 22% at 100x dilution. The DX-treated HTL-AP improved growth even more, with a 40 ± 11% increase at 200x and a 197 ± 24% increase at 100x with respect to the untreated HTL-AP

medium. Based on Figure 3, it can be concluded that growth of *C. vulgaris* in the 100x DX treatment is slightly improved over the 200x DX treatment. Growth in the DX-treated HTL-AP medium was not significantly different from the control mBBM at both 200x and 100x dilutions. Similarly, there is no statistically significant difference between growth in 200x and 100x dilutions of AC-treated HTL-AP, though both treatments showed a lower growth rate than the control.

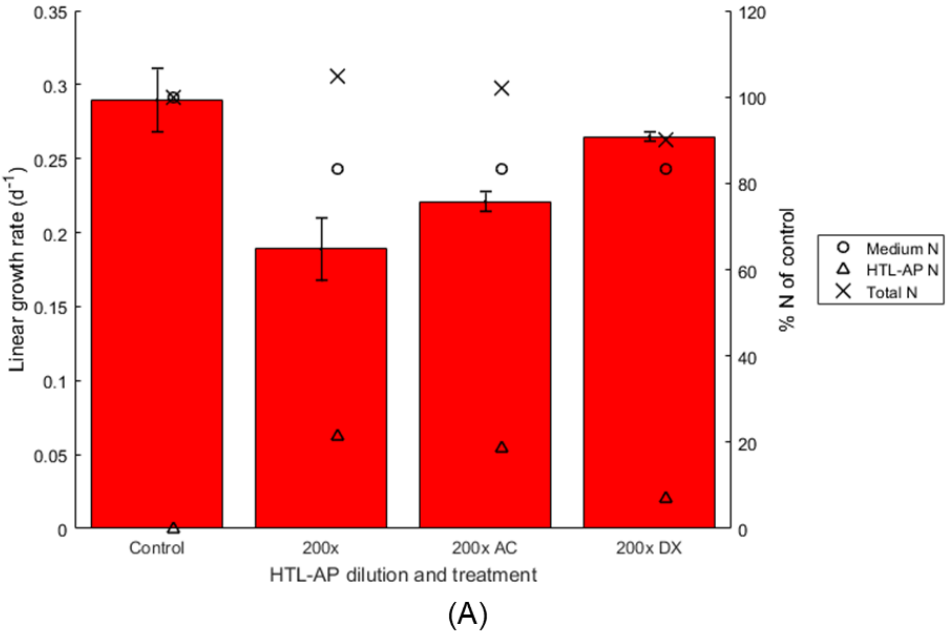

(A)

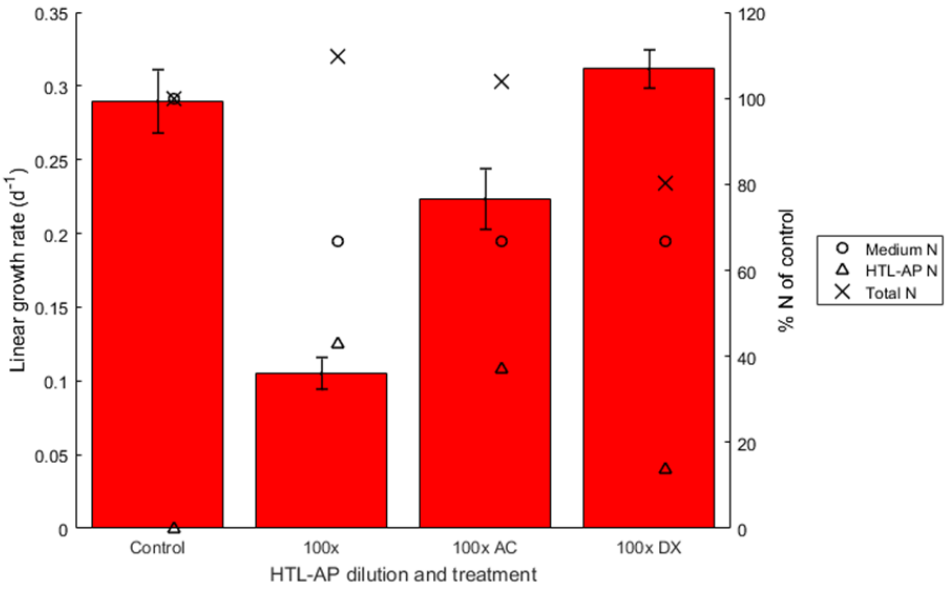

(B)

Figure 3. Linear growth rates of C. vulgaris in (A) 200x and (B) 100x dilutions of varying hydrothermal liquefaction-aqueous phase (HTL-AP) adsorption treatments (AC, activated carbon, DX, Dowex 50WX8). The same modified Bold's Basal Medium (mBBM) control was used between dilutions. Markers indicate the actual amount of nitrogen derived from medium, HTL-AP, and the total. All data for the growth conditions are shown as the average ± standard error of duplicate cultures (n = 2).

It is speculated that the presence of different compounds in HTL-AP would change the biomass composition [25], which could explain the differences in growth rates between untreated and treated HTL-AP due to the removal of some of these compounds. Table 4 outlines the ash-free biomass composition of untreated, AC, and DX treatments after completion of the last experiment. There is no notable difference in biomass composition between any of the treatments; this fails to support the idea that *C. vulgaris* changes composition when grown successfully on treated HTL-AP. The potential effect of mixotrophy in the presence of organic carbon was also considered. This is an area that is under investigation and will be reported on in future work.

Table 3. Ash-free compositional data comparison between treatments for lipids, measured as fatty acid methyl esters (FAMEs), proteins, carbohydrates, carbon, hydrogen, and nitrogen. All data shown as the average ± standard deviation of three replicate measurements (n = 3) with exception of 200x AC and 100x DX.

	FAME	**Protein**	**Carbohydrate**	**C**	**H**	**N**
Control	10.74 ± 0.03	32.83 ± 0.06	23.72 ± 0.35	49.17 ± 0.14	7.39 ± 0	6.87 ± 0.02
200x untreated	11.37 ± 0.16	31.68 ± 0.96	26.23	49.68 ± 0.31	7.49 ± 0.06	6.63 ± 0.2
100x untreated	10.35 ± 0.74	35.6 ± 0.69	-	49.98 ± 0.57	7.53 ± 0.07	7.45 ± 0.14
200x AC	10.5	30.88	32.49	48.79	7.41	6.47
100x AC	10.45 ± 0.22	31.4 ± 0.13	29.09 ± 0.67	49.21 ± 0.29	7.46 ± 0.04	6.57 ± 0.03
200x DX	11.09 ± 0.2	33.82 ± 0.13	24.53 ± 1.65	50.01 ± 0.06	7.46 ± 0.03	7.08 ± 0.03
100x DX	11	33.34	25.06	49.96	7.48	6.98

The difference in algal growth between the AC and DX treatments can rather be explained by the HTL-AP compositional analysis in Table 2. After AC treatment, the total organic carbon content in HTL-AP was reduced by 55% and the Kjeldahl nitrogen content was reduced by 26%. The DX treatment reduced the organic carbon content by 42% and the Kjeldahl nitrogen content by 56%. It is likely that while the DX treatment removed less organic carbon, many of the toxic compounds include ionic species like NH_4-N, as well as larger heterocyclic nitrogen containing components, were removed in much larger quantities than other treatments.

The deleterious effect of either the heterocyclic nitrogen or the NH_4-N content on the growth remains to be discerned and is not possible with the data currently available. Because there was no change in growth in DX-treated HTL-AP medium compared to the control, we are unable to draw the conclusion that mixotrophic growth is promoted by the presence of additional organic material in HTL-AP; the DX treatment only supports growth by remediation of toxicity.

Cultures in the DX-treated HTL-AP medium remained in the pH 6.5 – 7.0 range for approximately 5 days past inoculation, which other treatments did not experience (Figure A - 3 and Figure A - 4). The lower pH is more pronounced in the 100x treatment, as there is less NH_4^+-N present overall (Figure 3B), and estimated ammonium concentration based on Henderson-Hasselbalch equation as calculated following MATLAB code in Table A - 3. We believe that the DX resin removes primarily heterocyclic nitrogen products, in addition to a fraction of the ammonium. While the reduction in ammonium would need to be made up with additional HTL-AP, the reduced toxicity by elimination of the heterocyclic N components will make this more easily implemented. Recent work in our laboratory included a study of DX treatment of HTL-AP followed by GC analysis of the effluent, the original material, and desorbed products from the resin. Results illustrate the disappearance of heterocyclic nitrogen components (pyridine, pyrrolidone, imidazole derivatives), which are theorized to be selectively removed by the DX resin treatment (NREL unpublished work).

As a test of the extent of efficacy of DX as a toxicity adsorption treatment, *C. vulgaris* was further tested in medium containing the maximum strength of DX-treated HTL-AP required for full nitrogen replacement. The dilution factor required to supply full NH_4^+-N replacement (10 mM) was calculated based on the NH_4^+-N concentration from PNNL (Table 2). This dilution was determined to be 10x, or 136% nitrogen replacement when corrected for the updated nitrogen

analysis. Though the growth rate at the maximum HTL-AP concentration was severely inhibited, *C. vulgaris* still grew at a positive rate for the first 6 days of cultivation. The control culture in the first 6 days produced a linear growth rate of 0.194 ± 0.005 d^{-1}, while the 10x HTL-AP culture had a linear growth rate of 0.073 ± 0.001 d^{-1}. Although the growth rate was still severely inhibited (62%), *C. vulgaris* still established some degree of tolerance after the HTL-AP was treated. In contrast, the 50x dilution (71% N replacement) of untreated HTL-AP did not support any positive growth of *C. vulgaris*. It is possible that bacterial contamination contributed to spectrophotometric readings; however, the detection of surviving algal cells was a key difference between the maximum untreated and treated HTL-AP dilutions. As it is realistically infeasible to recycle an HTL-AP stream at a 1:10 dilution in large-scale algal cultivation, the benefit from this result arises from establishing the absolute limits of efficacy of this particular resin load as an adsorption treatment, rather than the operational limits.

As a third remediation strategy, we applied a poly(vinylpolypyrrolidone) resin to clean up the HTL-AP, because of its selective adsorption of polyphenols, initially thought to be a major culprit in HTL-AP toxicity. In contrast to AC- and DX-treated HTL-AP, both PVPP20 and PVPP50 treatments showed little beneficial effect on growth at 100x dilution (Figure 4). Compared to the 200x and 100x dilutions of untreated HTL-AP from the previous experiment, there was no change in growth; while the cultures in 200x PVPP-treated dilutions grew well, cultures in the 100x PVPP-treated dilutions were inhibited regardless of the PVPP loading. These growth rates demonstrate that PVPP was notably less effective as a remediation treatment compared to AC- and DX-treated HTL-AP. Although *C. vulgaris* growth remained similar to the control at 200x dilution, the 100x PVPP-treated cultures maintained a growth rate 50% less than the control, which is only comparable to the 100x dilution of untreated HTL-AP (47% less

growth vs. control). Compositional analysis on the HTL-AP indicated that neither of the PVPP treatments changed the carbon nor the nitrogen content by more than 9% (Table 3), which leads to the conclusion that PVPP has little to no remediation effect on toxic compounds in HTL-AP at the concentrations tested. It remains to be studied whether higher PVPP concentrations are able to remove some of the more complex heterocyclic products found, while leaving the ionized ammonium products intact. The protein-binding properties of PVPP were expected to remove heavier adducted organic components, such as phenols [34]. It is likely that despite its effect as a phenolic adsorbent, the HTL-AP used in this study did not contain enough phenolics to contribute to HTL-AP toxicity. As discussed earlier, an estimate of the phenolic content in *Chlorella* HTL-AP is in the range of 2% of the TOC, or about 500 ppm concentration. Thus, the success of the AC and DX treatments can be attributed to the removal of more prevalent heterocyclic nitrogen compounds.

Table 4. Number of molecular assignments (DX = Dowex 50WX8).

	Untreated extract	DX extract	% reduction from treatment
Total monoisotopic assignments	6,654	3,988	40.1
Number of peaks with H/C < 1	913	129	85.9
Number of peaks with H/C < 0.5	295	26	91.2
Percentage of total abundance with H/C < 1	8.4	1.7	79.8
Percentage of total abundance with H/C < 0.5	2.6	0.3	88.5

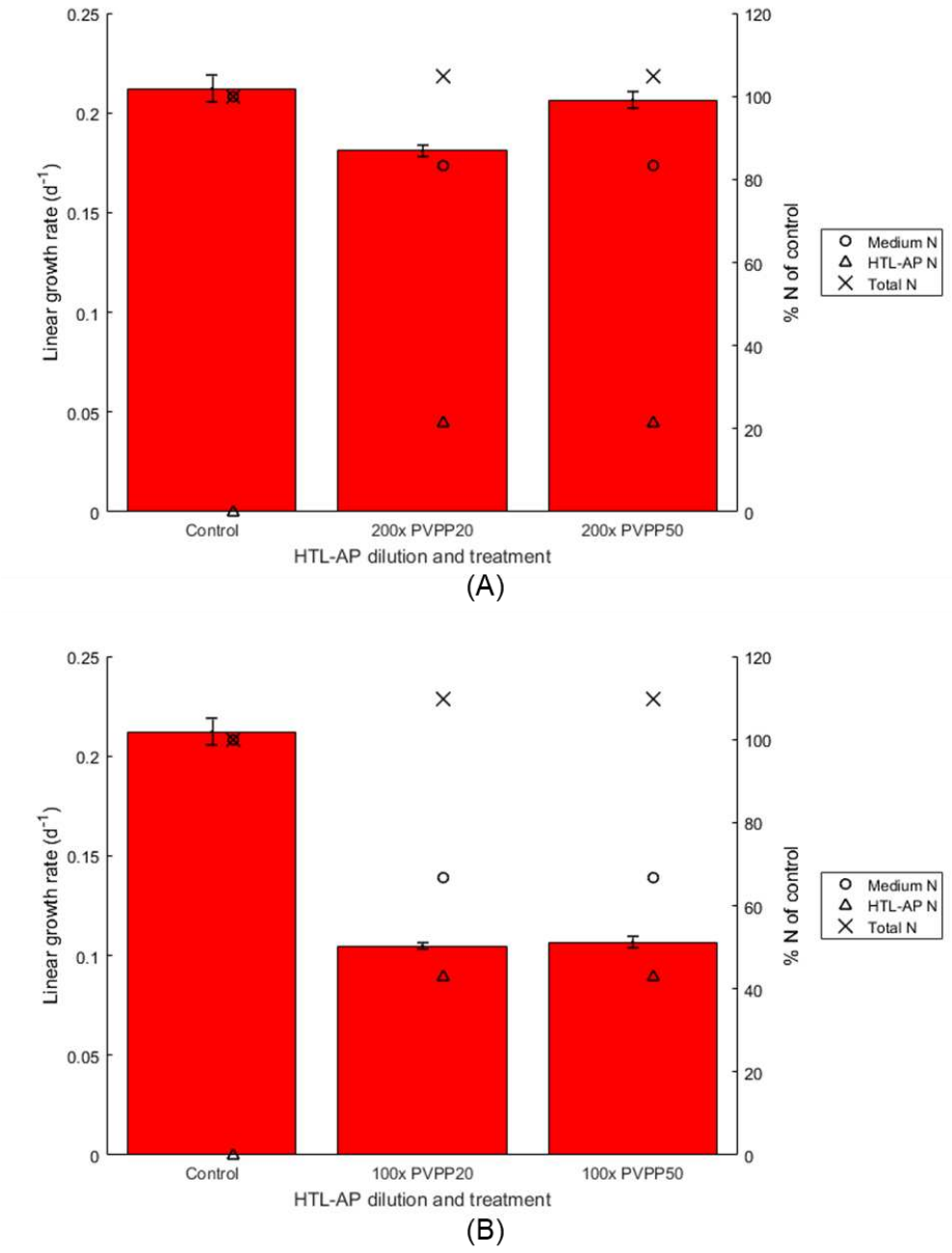

Figure 4. Linear growth rates of C. vulgaris in (A) 200x and (B) 100x dilutions of polyvinylpyrrolidone (PVPP)-treated hydrothermal liquefaction-aqueous phase (HTL-AP). All data for the growth conditions are shown as the average ± standard error of duplicate cultures (n = 2).

2.3.4 FT-ICR MS characterization of HTL-AP after treatment

Because the Dowex 50WX8 resin had the most effective toxicity removal effect of all treatments tested, we subjected these fractions to a more in-depth elemental analysis and molecular profiling. It is likely that as an ion-exchange resin, Dowex 50WX8 has desalting properties that remove inhibitory ionic components, which are ideal for rapid, high-resolution mass spectrometry profiling as has been described before [35].

To rapidly characterize the molecular composition of the HTL-AP, we analyzed the organics (isolated by extraction with DCM/IPA as described in the methods) by direct infusion mass spectrometry as described above. The ultra-high-resolution FT-ICR mass spectrometer is able to collect mass spectra at such high mass accuracy that one detected molecular ion can be matched to one elemental formula. Based on these formulae and the respective C, H, N, O, S composition, we are able to look for major changes in the spectra between the raw and the treated HTL-AP samples. In particular, we looked at the distribution of C, H, N, and O and the respective ratios using a Van Krevelen plot visualization, which explore the relationship between aromaticity (H/C) and heteroatom (N, O, or S) content. This relationship is most often explored with the ratio of O/C; however, in this work we also include N/C as nitrogen is a major contributor to the overall molecular formulas observed for HTL-AP. Figure 5 shows the Van Krevelen plots for the untreated and DX treated samples with O/C on the top row and N/C on the bottom. We observe that after DX treatment (Figure 5B and D) there are fewer compounds at low H/C ratio, which corresponds to the removal of a large fraction of the aromatic compounds. Table 4 reveals that the number of monoisotopic assignments with H/C < 1 drops from 913 without treatment to 129 after DX treatment. This trend is observed in the polyaromatic hydrocarbon and polyaromatic heterocycle region as well (*i.e.*, H/C < 0.5) with a decrease from

295 assignments to only 26 assignments after DX treatment. This shows a clear specificity in the removal of the most aromatic components by DX treatment.

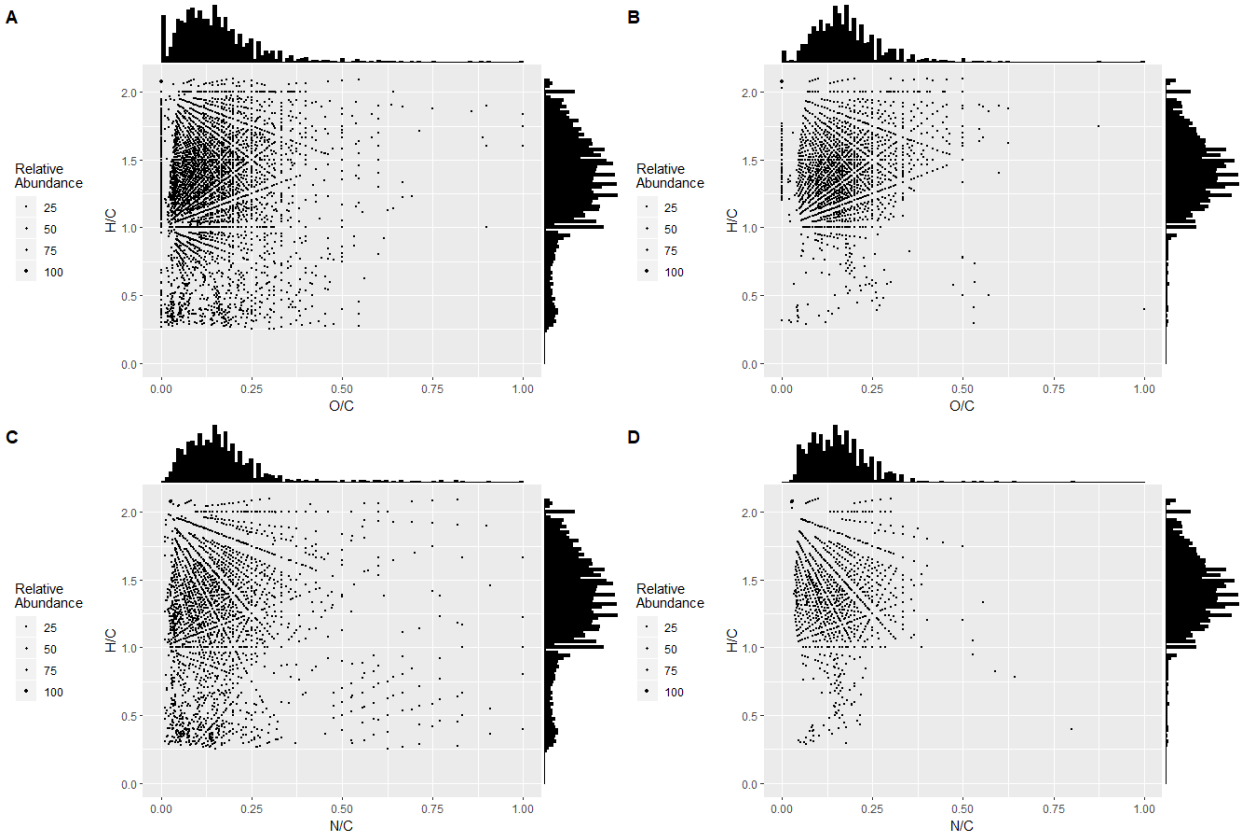

Figure 5. Van Krevelen plots for untreated (left column) and Dowex 50WX8 (DX) treated (right column) hydrothermal liquefaction-aqueous phase (HTL-AP). A) H/C vs. O/C for untreated HTL-AP, B) H/C vs. O/C for DX treated HTL-AP, C) H/C vs. N/C for untreated HTL-AP, D) H/C vs. N/C for DX treated HTL-AP.

Based on the elemental composition assignments of the between 4,000 and 6,000 uniquely identified molecular ions for the respective DX treatment and the raw HTL-AP respectively (Table 3), grouping in terms of heteroatom class is possible and informative to rapidly assess differences in molecular composition. Changes in the heteroatom class composition were observed for the DX treated samples, with summarized data shown in Figure 6. The untreated sample shows that the N_2O_x, N_3O_x, and N_4O_x heteroatom groups are the most abundant initially; however, after DX treatment there is a shift to lower overall nitrogen content,

and N_1O_x, N_2O_x, and N_3O_x heteroatom groups become the most abundant groups. We also observe the loss of N_6O_x compounds and the reduction in N_4O_x and N_5O_x heteroatom groups after DX treatment. This reduction in higher-order nitrogen compounds is also indicative of the reduction of aromaticity, since higher-order nitrogen compounds likely consist of pyrrole-, pyridine-, and imidazole-type structures [49]. In fact, when we compare the changes in nitrogen content to changes in oxygen content, we see that although the overall nitrogen content decreases, little or no change is observed for the oxygen distribution within N_yO_x families. The removal of polyaromatic nitrogen-containing compounds coincides with an observed reduction in toxicity and suggests that nitrogen-containing poly-aromatic hydrocarbon (PAH)-type molecules that are present in the HTL-AP samples contribute to toxicity in these algal species. Further, the increased growth rate observed from DX-treated HTL-AP in combination with remaining aliphatic N_yO_x compounds suggests that these compounds may play a role in the nutrient cycle of the algae. Recent experiments in our laboratory provide support for the presence and selected adsorption of heterocyclic nitrogen components, as identified by GC-MS (data not shown).

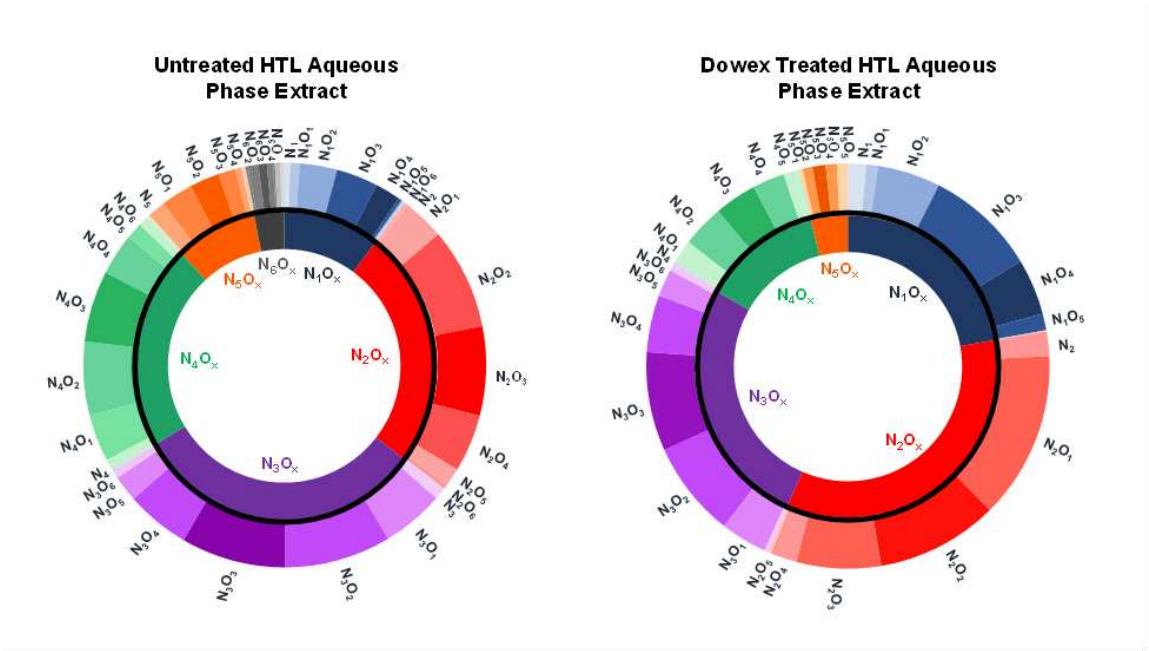

Figure 6. Heteroatom class / heteroatom group graphs for untreated and Dowex 50WX8 (DX) treated hydrothermal liquefaction-aqueous phase (HTL-AP). The outer annuli represent the distribution of heteroatomic classes from Fourier Transform Ion Cyclotron Resonance Mass Spectrometer (FT-ICR MS) analysis, where the size of the band is indicative of the relative abundance of the corresponding class. The inner annuli represent the heteroatom groups based on nitrogen content.

Our data and conclusions here are consistent with reported results in the literature [49]. Alimoradi et al. (2019) reported 50% effective concentration (EC_{50}) values causing growth inhibition in *Bacillus subtilis* from HTL-AP produced under varying reaction temperatures (270 – 345 °C). The EC_{50} ranged from 6.8 v/v% to as low as 1.0 v/v% HTL-AP at 345 °C. The authors concluded that mixes of pyrrolidinones, pyrazines, pyrroles, and melanoidin-like compounds were the driving force behind HTL-AP toxicity. Our preliminary results from FT-ICR MS data indicate that Dowex 50WX8 is responsible for removing high nitrogen-containing components, such as those that cause toxicity in HTL-AP as reported in Alimoradi et al. [49]. However, further work is needed and is currently ongoing to demonstrate the effect of recycling the DX adsorbed products to experimental cultivation work and to correct for the ammonium concentration. The respective impact of ammonia toxicity versus the presence of high-nitrogen

containing heterocyclic components needs to be decoupled to fully understand the toxicity aspect of the nutrient recycling conundrum after processing algal biomass. In future studies, it may be possible to elute adsorbed components through chromatographic methods and focus on the biological activity and toxic effect of specific components in the adsorbed fraction. A deeper exploration of the chemical interactions in HTL-AP would be a beneficial supplement or follow-up to this study to determine alternative, and likely cheaper, treatments with similar chemical functions.

2.4 Conclusions

Remediation of HTL-AP toxicity may be a key factor in the techno-economic viability and sustainability of hydrothermal liquefaction as a downstream biofuel process. Nutrient recycle from HTL-AP may be able to recover up to 40 – 70% of biomass and 90% of nitrogen that would otherwise be lost to waste. Incorporating data from this study into techno-economic and life-cycle modeling can help determine the utility of remediation treatments. It is noted that AC and resin treatment loading factors could be optimized in further studies to reduce material consumption.

This study concludes that direct integration of nutrient recycle from untreated HTL-AP is infeasible with current benchmark algae strains without a major loss in productivity under the tested conditions. The apparent toxic effect of HTL-AP on algae depends on the HTL-AP dilution and the algal species cultivated. Wild-type *Desmodesmus armatus* struggled to grow in even dilute (200x) HTL-AP. Even a tolerant strain such as *Chlorella vulgaris* UTEX 395 was unable to sustain healthy growth at an HTL-AP dilution factor of only 100x at the bench scale.

Treatment with the ion-exchange resin Dowex 50WX8 provided the greatest positive effect on algal growth of the adsorbents tested. Activated carbon was a fairly effective treatment,

but to a lesser degree than Dowex 50WX8. Polyvinylpolypyrrolidone (PVPP), while reportedly selective for toxic polyphenolic components, was not an effective adsorbent to remove the toxic compounds under tested conditions, suggesting that toxicity may be exhibited by other components in the HTL-AP, or the PVPP loading was not sufficient to adsorb the higher than anticipated phenolics concentrations. The success of Dowex 50WX8 in remediating HTL-AP toxicity leads to further questions in the chemical interactions between resins and the toxic components in HTL-AP. A detailed molecular analysis of further purified fractions after HTL-AP treatment will be a subject of future research.

CH. 3: LIMITS OF UNCERTAINTY IN COMMERCIAL-SCALE HYDROTHERMAL LIQUEFACTION OF ALGAE [b]

3.1 Introduction

Algae have shown promise as a potential feedstock for renewable fuels due to their high biomass productivity and ability to capture waste carbon dioxide (CO_2) from co-located industrial facilities. Algae facilities also offer opportunities to integrate with other waste streams (i.e. wastewater) and can use non-arable land. Once harvested, algae biomass can be converted to fuels and products through a variety of different pathways. Renewable liquid fuels, such as those derived from algae, are a major focus for achieving climate goals and independence from fossil fuels. In the European Union, the Renewable Energy Directive 2009/28/EC mandated a share of 10% biofuels in Europe's transportation fuel consumption by 2020 [50]. The Renewable Fuel Standard (RFS) includes mandates that are intended to promote and increase biomass-based fuel production in the United States (U.S.). One of the requirements for this fuel category is a minimum 50% reduction in well-to-wheels greenhouse gas (GHG) emissions from the 2005 petroleum baseline [5]. According to the International Energy Agency, the global transportation sector accounted for 24% of total fuel combustion CO_2 emissions with three-quarters were attributed to road vehicles in 2019 [51]. If energy demand – particularly from transportation – increases as projected with a growing population, it is imperative to develop cost-effective and sustainable liquid fuels from renewable sources that do not compete with food. Quinn et al. (2012) has noted that in the U.S., approximately 60 million hectares of land could be available

[b] This chapter was published as a peer-reviewed journal article: Chen, P.H., Quinn, J.C., 2021. Microalgae to biofuels through hydrothermal liquefaction: Open-source techno-economic analysis and life cycle assessment. Appl. Energy 289. https://doi.org/10.1016/j.apenergy.2021.116613

for near-future microalgae fuel production. This amount of microalgae would produce between 2.6 to 13.3 times the U.S. Department of Energy (DOE) renewable fuel goal of 1 billion barrels of oil by 2030 [52]. Even when considering CO_2 transportation limitations, the U.S. microalgae production potential surpasses the DOE goal by 1.8 times; however, severe economic challenges would arise [53]. Beyond the southern U.S., studies have been performed illustrating the potential of microalgae to address a transition from conventional petroleum to renewable fuels. Between 13 and 15 g m^{-2} d^{-1} of annual productivity could be produced in Australia, Brazil, Colombia, Egypt, Ethiopia, India, Kenya, and Saudi Arabia [54]. Microalgae, while promising, must overcome a variety of challenges to become economically competitive with conventional fuels including, but not limited to energy yields, byproduct recyclability, valuable co-product development, and resource availability [55].

Hydrothermal liquefaction (HTL) is a particularly interesting thermochemical process for converting algae feedstocks to fuel. The HTL process converts a wet biomass feed into biocrude, a petroleum crude oil analog, on the order of minutes. The reaction is defined by subcritical conditions (250 – 375 °C, up to 22 MPa) in which water acts as a highly reactive liquid medium. One major advantage to HTL is its ability to convert all major biomass fractions – lipids, carbohydrates, and proteins – into fuel, whereas other conversion technologies typically can only focus on one (*i.e.* solvent extraction for lipids and fermentation for carbohydrates) [11]. Beyond biocrude, aqueous phase and gas phase byproducts have potential to be recycled back into the algae cultivation system, which can reduce fresh resource demand as demonstrated from studies such as Chen et al. (2017) [56], Selvaratnam et al. (2015) [57], and Martinez-Fernandez et al. (2017) [58]. Char solids are usually produced in small quantities but can provide carbon sequestration credits [59].

Despite the technical advantages, HTL has not yet achieved commercial-scale adoption. The economic and environmental merits are key factors in determining the viability of the technology. Even if biomass costs are favorable, the high cost of HTL conversion is a major obstacle in achieving parity with conventional fuels. Several factors are critical for cost-competitive algae fuels. Biomass price and fuel yield have the greatest effect on the minimum fuel selling price (MFSP); higher yields of biocrude and lower feedstock costs drive down the MFSP considerably, as demonstrated in sensitivity analyses of HTL in Jones et al. (2014) [21], Zhu et al. (2019) [60], and Gu et al. (2020) [61]. Jones et al. (2014) reports techno-economic assessment (TEA) results based on optimistic cost targets, where biomass is optimistically purchased at $474 per dry metric ton and the continuous HTL process produces a 51% biocrude yield to achieve an MFSP of $1.26 per liter gasoline equivalent (LGE) ($4.77 per gallon gasoline equivalent (GGE)) [21]. The Davis et al. (2016) open raceway pond (ORP) assessment optimistically assumes a minimum biomass purchase price of $541 metric ton^{-1} ($491 US ton^{-1}), which requires an annual average biomass production rate of 25 g m^{-2} d^{-1} to break even [62]. However, the current state of cultivation technology has only justified average annual productivity up to about 13 g m^{-2} d^{-1}, half that required for biomass cost targets [63]. Other operating assumptions can also add cost uncertainty. The HTL conversion cost ranges from $0.47 LGE^{-1} ($1.77 GGE^{-1}) for direct HTL aqueous recycle to cultivation to $0.81 LGE^{-1} ($3.08 GGE^{-1}) if catalytic hydrothermal gasification (CHG) is integrated to treat aqueous waste and produce natural gas for internal hydrogen production [60]. A wide range of economic assumptions in current HTL literature makes it difficult to attribute the burden of upstream or downstream costs in biofuel production. There is a need to focus on accurately modeling the

downstream conversion of algal biomass without upstream cost assumptions distracting from key results about HTL technology.

Modeling assessments of algae-to-fuel pathways often focus on economic challenges, but the life-cycle assessment (LCA) of fuel systems must also be factored into sustainability targets. Environmental emissions and energy use are tightly coupled to the production system's energy requirements. Therefore, it is critical for an algae production system to take advantage of any opportunity to recover and reduce energy duties. Several studies have performed LCAs of algae HTL systems, typically focusing on global warming potential (GWP) and net energy ratios (NER)[c]. Results range from favorable in Batan et al. (2010) [64] and Ponnusamy et al. (2014) [65] (GWP below RFS mandates; NER < 1), highly unfavorable in Mu et al. (2017) [66], or mixed answers in Bennion et al. (2015) [67], Liu et al. (2013) [68], and Sun et al. (2019) [69]. System boundaries and operating assumptions vary greatly between these studies, which can make it difficult to define the state of algae HTL from an LCA perspective. Moreover, recent efforts in the greater LCA field have expanded to other environmental impacts beyond GWP and NER to include other impact categories, such as eutrophication, air quality, and resource depletion [63]. While the primary goal of algae biofuels is to produce energy with fewer GHG emissions than conventional fuels, these other environmental impacts should not be ignored in LCA comparisons.

The HTL reactor temperature is a key operating specification that directly impacts the system's operational requirements, which in turn influences TEA and LCA metrics. HTL operation requires high-temperature water as a subcritical liquid medium. At this range of

[c] NER differs from other common metrics like energy return on investment (EROI) and fossil energy use. NER does not differentiate between energy sources or account for embodied energy in the system, so the reporting is simple and transparent.

operating conditions, the physical properties of liquid water change in an increasingly nonlinear fashion. Some of the most detailed HTL model assessments to date in Jones et al. (2014) [21] and Knorr et al. (2013) [70] have not yet developed a sensitivity analysis for varying reaction temperature. These studies assume a fixed reaction temperature of 350 °C, as current convention dictates that higher HTL temperatures generally result in higher biocrude yield. Due to the countless possible interactions between components in the HTL system, there are numerous viable property estimation models that can predict deviations in thermodynamic properties at HTL conditions. Models tend to capture real properties more or less accurately depending on the components present in a mixture. For example, the non-random two-liquid (NRTL) model predicts interactions between two liquid components fairly well, but does poorly with pure compounds [71], while the Peng-Robinson equation of state can show non-idealities in nonpolar liquid compounds [72]. The complex mix of components and extreme operating conditions of HTL can make it difficult to choose a model that accurately captures thermodynamic interactions. This modeling challenge emphasizes the importance of different thermodynamic assumptions on HTL system energy requirements.

There is limited HTL literature focused on the effect of varying HTL conditions for algal feedstocks, especially at commercial scales. Jena et al. (2011) is one of the few studies that has correlated HTL yields with temperature, residence time, and solids loading [73]. Studies such as Yang et al. (2019) [74] and Valdez et al. (2012) [75] have attempted predictive yield models based on experimental data, but it is difficult to translate their application to general feedstocks. Lower operating temperatures have been shown to produce high biocrude yields in Li et al. (2014) [76] and López Barreiro et al. (2013) [77], but these results were subject to variations in other operating conditions like residence time and feed concentration. The wide uncertainty of

operating conditions and unclear assumptions in literature indicate that an updated assessment on algal HTL is needed. This study offers new insight on thermodynamic parameters that have gone relatively untouched in HTL modeling and explores their effects on economic and life-cycle metrics.

This work leverages a flexible HTL process model to develop a robust TEA and LCA and explore the effect that model uncertainties have on economic and environmental metrics. Novel contributions to HTL research include an analysis of the effect of temperature and property methods on simulation models, a full LCA on environmental impacts beyond GWP and NER, a scenario analysis on critical performance metrics, and a new TEA approach to determine HTL's burden on upstream costs. Results highlight hotspots for further research and improvements in this technology and identify performance targets for HTL to achieve economic and environmental viability. An open-source *Aspen Plus* (AspenTech, Inc., MA, USA) model and *Excel* (Microsoft, WA, USA) interface are included with this work to provide transparency in methods and results and support future modeling efforts in the research community.

3.2 Methodology

The HTL model was developed in *Aspen Plus* based on supporting information from commonly cited literature assessments [21,70]. The key economic performance indicator in this work was the minimum fuel selling price (MFSP) contribution of HTL. The key environmental performance indicators were the net energy ratio (NER) and the ten impact categories from the Tool for the Reduction and Assessment of Chemical and Other Environmental Impacts (TRACI) version 2.1. The TEA system boundary included the HTL reactor, the fuel upgrading process, utilities, and fuel transportation and distribution. One major difference in this work from other assessments is that a baseline biomass purchase price was not established beforehand. By

isolating the TEA boundary to the HTL process, the maximum allowed biomass price was calculated for selected final fuel cost benchmarks (*i.e.*, \$3, \$5, and \$7 GGE^{-1}). Life-cycle accounting included the emissions from algae pond cultivation, harvesting, the HTL reactor, fuel transportation and distribution, and fuel end use. The expansion of the system boundary to a well-to-wheels basis was required to make LCA comparison with other similar fuels. However, a detailed cultivation model was not included in the scope of this work. Process flows for cultivation (*e.g.* nutrients, electricity) were scaled from previous literature reviews and modeling efforts in Laurens et al. (2017) [63] and Davis et al. (2012) [78] and added as LCA inputs. A process flow diagram of the HTL system boundary is detailed in Figure 7, with greater details included in Figure B - 1 and Figure B - 2.

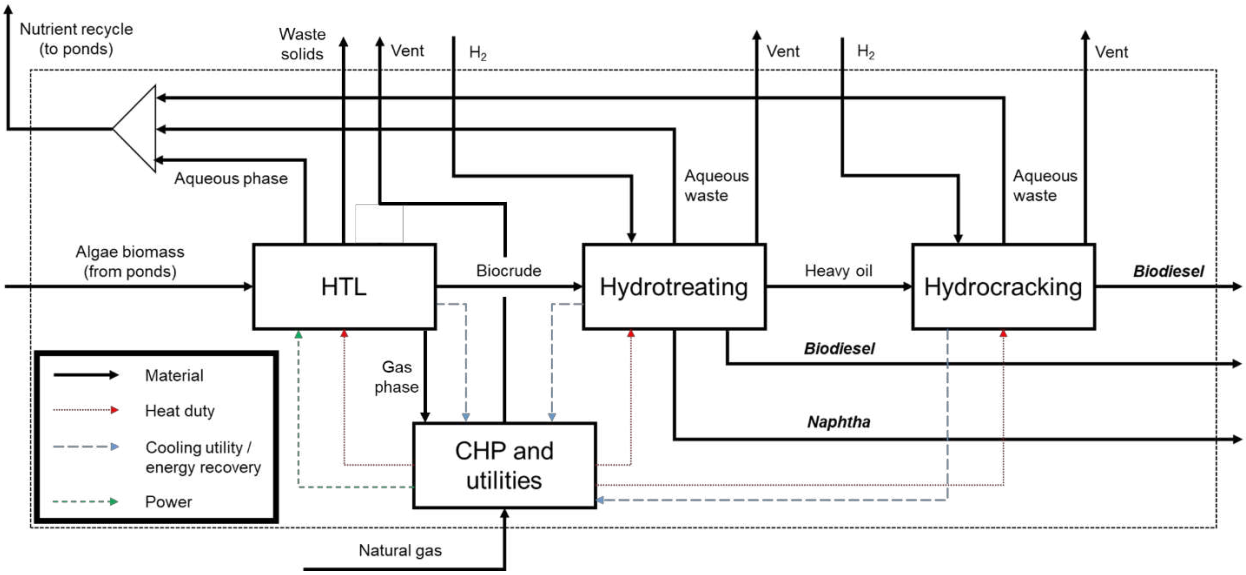

Figure 7. Process flow diagram of the hydrothermal liquefaction system boundary (indicated by the dotted box). The process includes the reactor, hydrotreating, and hydrocracking to process algal biomass into biodiesel and naphtha. Heating, cooling, and electrical power are supplied from a centralized combined heat and power system or external utilities.

3.2.1 Operating parameter selection

The baseline conversion system was intended to represent an algae production facility that supports a 5,000-acre ORP farm and converts all algal biomass to fuel through HTL. The

baseline parameters of this study were based on a literature survey of algae HTL data as displayed in Table 5. Studies were included if the HTL data was based on a microalgae feedstock and met criteria for reasonable continuous, large-scale operating conditions. Temperature, residence time, and feed solids loading were considered the most important parameters.

Table 5. Parameters sampled from algae hydrothermal liquefaction literature to develop the baseline for this work. These studies were considered the most representative of viable operating conditions in the current state of technology. The mean biocrude yield was 45% and the sample standard deviation was 6.6%. A 95% confidence interval for the mean was constructed using the student t-distribution to determine optimistic and conservative bounds on the biocrude yield.

Reference	Reaction temperature [°C]	Residence time [min]	Solids loading	Biocrude yield
[19]	350	30	17%	53%
[19]	350	30	20%	38%
[73]	350	30	20%	35%
[73]	350	60	20%	40%
[77]	350	15	18%	55%
[75]	300	20	15%	50%
[75]	350	40	15%	43%
[75]	350	60	20%	40%
[79]	350	20	19%	47%
[80]	350	40	17%	51%
[60]	350	15	20%	43%
Mean	*346*	*32*	*18%*	*45%*
Standard deviation	*15.1*	*16*	*2.0%*	*6.6%*
This study (baseline)	*350*	*30*	*20%*	*45%*
This study (optimistic)	*320*	*15*	*25%*	*60%*
This study (conservative)	*350*	*60*	*15%*	*30%*

In most studies, the default reaction temperature was 350 °C and thus this temperature was selected as the baseline. Several surveyed studies deviated strongly from the baseline temperature and one or more other typical operating conditions [76,77,81]. The impact of deviating from baseline conditions was examined as a part of the scenario analysis in this work. However, some algae HTL studies deviated too far from representative conditions; justification for excluding studies is explained in Appendix B. Operating conditions and yields from the eleven scenarios in Table 5 were considered as a basis for the baseline scenario and conservative

and optimistic bounds [19,60,73,75,79,80,82]. Catalysts were not mentioned in any of the surveyed studies. All were based on experimental data except Zhu et al. (2019), which was model-based.

The statistical mean (45%) and standard deviation (6.6%) of biocrude yields from Table 5 were calculated from the student *t*-distribution to establish the baseline scenario. Low ("conservative") and high ("optimistic") yields for the scenario analysis were determined by bounding the *t*-distribution on both ends with 95% probability, centered on the mean. The lower bound was 30% and the upper bound was 60%. The median residence time was selected for the baseline case and the minimum / maximum were used in the optimistic and conservative scenarios, respectively. The baseline reaction temperature was 350 °C and the solids loading was assumed 20 wt%.

The TEA and LCA scenario analyses required operational parameters to be defined for the cultivation system. Davis et al. (2016) outlined an annual average biomass productivity scenario of 25 g m^{-2} d^{-1} in an ORP facility to meet future U.S. Department of Energy (DOE) cost targets [62]. The current state of technology places this figure closer to 13 g m^{-2} d^{-1}, and can be as low as 10 g m^{-2} d^{-1} or less [63]. Global annual productivity yields have been predicted to potentially reach 13 to 15 g m^{-2} d^{-1} [54]. The baseline productivity scenario was assumed to be 17.5 g m^{-2} d^{-1}, the average of the 10 and 25 g m^{-2} d^{-1} cases, representing a near-future state of technology scenario.

3.2.2 Thermodynamic properties

Though there were studies that were excluded from Table 5 for not meeting baseline screening criteria, algae HTL literature as a whole represented a wide range of HTL operating temperatures. The HTL feed stream is mostly composed of water, but interactions between

stream components (carbohydrates, lipids, proteins, and ash) and the solvent (water) were expected to create deviations from pure water properties. Additionally, the thermodynamic properties of streams are highly dependent on operating temperature. The Soave-Redlich-Kwong (SRK) equation of state has been used in wood HTL literature, as described in Lozano et al. (2019) [83] and Castello et al. (2018) [14]. A derivative of SRK, the predictive Soave-Redlich Kwong (PSRK) equation of state has seen precedence in algal HTL literature from Jones et al. (2014) [21][d]. However, other property models – the Peng-Robinson equation of state and the NRTL model – were also included to highlight the importance of selecting an appropriate method for simulations. All property method variations were limited to calculations in the *Aspen Plus* V10 simulation. Key properties affected by *Aspen Plus* calculations included (but were not limited to) enthalpy and heat capacity.

For the baseline scenarios, the goal was to minimize the natural gas heat utility by maximizing the main heat exchanger area. To do this, the hot outlet temperature was set to 115 °C to prevent temperature crossover and the heat transfer coefficient was fixed at 0.818 kW m^{-2} K^{-1} (144 BTU hr^{-1} ft^{-2} R^{-1}) based on the "Case B: Preheater, low viscosity" scenario [e] from Knorr et al. (2013). An explanation of the "Case B" configuration can be found in Appendix B.

3.2.3 *Aspen Plus* model and simulation

The software *Aspen Plus* V10 was used to develop the HTL reactor simulation described in this work. The process model was based on heavily on previous HTL models in Jones et al. (2014) and Knorr et al. (2013) [21,70], each of which focused on different feedstocks and

[d] Jones et al. (2014) uses the PSRK equation of state, but this information is not explicitly mentioned in the report. The model was confirmed by correspondence with a co-author.
[e] Knorr et al. (2013) notes that this may not be the case for woody feedstocks, but will work for slurries with properties similar to water, like algae.

configurations of the HTL reactor system. An *Aspen Plus* chemical component list is included in Appendix B (Tables B – 1 through B – 4) [21]. An open-source *Aspen Plus* model is also included as a part of this publication.

At the HTL pre-heater, the hot outlet stream was constrained to 115 °C in the *Aspen Plus* simulation to determine the minimum natural gas heat duty. Further cooling utility was required to cool the hot stream from 115 to 80 °C. The calculated energy balance is dependent on the property estimation method and HTL reaction temperature. A hot oil circulation system was assumed to be necessary to effectively transfer heat to the primary heater [70]. However, this hot oil system was not directly modeled in this work; instead, *Aspen Plus* determined the required heat duty to the HTL system and the oil circulation system was included through capital cost estimations as described in Table B - 5.

The HTL reactor was built in *Aspen Plus* as an RYield block. Though product yields in this study differed from other model references, individual component yields were kept proportional within their product phase (*e.g.*, naphthalene mass fraction of 0.051 in the biocrude phase, regardless of biocrude yield). For the sake of simplicity, all feed components except for water, ash, and dissolved salts (modeled as $(NH_4)_2SO_4$) were converted into products. The Ryield block was isothermal and the heat of reaction was assumed negligible compared to the sensible heat duty.

Though there are methods to predict the yields and compositions of different algae feedstocks as seen in Valdez et al. (2014) [84] and Leow et al. (2015) [85], it was difficult to validate these models for an arbitrary algae feedstock. Total product yields varied between scenarios, but the compositions of the feed and product streams were always assumed the same as Jones et al. (2014) to simplify the upgrading model downstream [21]. An upgrading block was

attached downstream of the HTL biocrude outflow. This system included hydrotreating (HT) and hydrocracking (HC) and was scaled directly from Jones et al. (2014) [21]. The upgrading step has been validated with experimental distillation data for specific algae feedstocks, but it is assumed here that the reference model is applicable to a general algae composition. Previous HTL studies in Jena et al. (2011) [73], Xu & Savage (2015) [79], and Elliott et al. (2015) [12] have analyzed the heating value of biocrude produced under various conditions. However, to simplify this work, the final fuel products (biodiesel and naphtha) were assumed to have constant specific energy regardless of the simulated HTL conditions. The higher heating values of conventional diesel and petroleum naphtha, respectively, were assumed to be 38.3 and 34.7 MJ L^{-1} [86]. Fuel outputs were reported on an LGE basis *i.e.* the volume of fuel containing the same amount of energy as one liter of petroleum-based gasoline. Conversions to GGE are included in parentheses in the results to compare with DOE assessments and cost targets.

Hydrogen for biocrude upgrading was assumed to be purchased from a nearby off-site facility. This eliminated the need for an additional facility for hydrogen generation. Biogas produced from the HTL gas phase and biocrude upgrading was routed to a water scrubber to remove excess CO_2 and NH_3, validated experimentally in Rotunno et al. (2017) [87] and modeled in Jones et al. (2014) [21], then fed back into the heating utility to reduce the natural gas duty entering the HTL system boundary. Nutrient recycle was assumed to directly feed back as an algae cultivation credit without additional aqueous waste treatment, which can be justified by recent work suggesting that a majority of aqueous phase nitrogen and phosphorus can be directly recycled back into adapted algae cultures [20].

3.2.4 Techno-economic analysis (TEA)

The MFSP contribution of the HTL system boundary was determined from "N^{th}-of-a-kind" (NOAK) plant assumptions, as outlined by Bioenergy Technologies Office (BETO) economic assessment standards (Table 6) [88]. These parameters reflect a theoretical commercial-scale plant that has reached technological maturity. With these assumptions fixed (Table 6), a *Microsoft Excel* iterative solver was used to calculate the product revenue required to achieve a net present value (NPV) of $0 for the plant's full 30-year lifetime. All liquid fuel products were lumped into a single cost on an energy equivalent (LGE or GGE) basis. The cost year of analysis was 2019, the most recent year available in the Chemical Engineering Plant Index [89].

Table 6. Baseline "N^{th}-of-a-kind plant" economic assumptions. With these assumptions applied over the life of the plant, the objective is to find the minimum fuel selling price (MFSP) contribution such that the plant breaks even.

Parameter	**Standard value**
Internal rate of return	10%
Plant financing debt / equity	60% / 40% total capital
Plant life	30 years
Income tax rate	35%
Interest rate	8.0% annual
Debt financing term	10 years
Working capital	5% fixed capital (excl. land)
Depreciation schedule	7-year modified accelerated cost recovery system (MACRS)
Construction period	8% year 1 60% year 2 32% year 3
Plant salvage value	None
Start-up time	6 months
Start-up revenue and costs	50% revenue 75% variable costs 100% fixed costs
On-stream factor	90% (330 days per year)
Indirect capital	60% total installed capital
Base cost year	2019 [89–92]

Capital cost estimation for the HTL system was based on individual equipment scaled from Knorr et al. (2013), Case B [70] (explanation in Appendix B). The scaling variable depended on the equipment; for example, heat exchanger costs were based on area, while the HTL reactor cost was scaled by length. Contrary to the HTL reactor system, the capital cost of upgrading equipment was scaled by flow rate as a lumped system [21]. Variable operating costs were similarly derived from a combination of literature sources. Electricity costs were obtained from U.S. Energy Information Administration data [92], natural gas costs were sourced from Dutta et al. (2011) [93], and purchased hydrogen costs were assumed from Dillich et al. (2012) [94]. This work excluded the implementation of an on-site hydrogen generation plant, instead applying hydrogen duty purely as an operational cost. Excluding the biomass cost from the TEA system boundary allows for this work to focus on the contribution of the HTL conversion process. The maximum allowable biomass price was back-calculated to determine the burden on the cultivation stage to meet selected total fuel cost targets ($3, $5, and $7 GGE^{-1}). Because of these assumptions, variable operating costs were not directly comparable with the primary reference literature in Jones et al. (2014) [21]. Unit costs and cost indices were based on typical values for the U.S.; however, it should be noted that the included open-source model can be adapted for cost indices in any global region. Detailed capital estimation parameters and operating costs are listed in Table B - 5 and Table B - 6.

3.2.5 Life-cycle assessment (LCA)

The LCA functional unit was 1 MJ fuel produced. Unlike the TEA system boundary, which included only the HTL and upgrading units, a well-to-wheels boundary for LCA was deemed necessary to compare with impacts of other transportation fuels. The LCA system boundary was expanded to include an algae cultivation facility, a harvesting stage, fuel

transportation and distribution, and the fuel product end use (combustion). Upstream facilities (cultivation and harvesting) were assumed to be co-located with the HTL plant, so feedstock transportation was negligible. The expanded boundary accounts for nutrient recycling, CO_2 absorption, and end use emissions. All impacts were evaluated with an attributional LCA approach. Consequential LCA factors, such as indirect land use change and market effects, were not considered in this work.

Most life-cycle inventory data was collected from the *ecoinvent Version 3.4* database [95]. Outputs from the *ecoinvent* "cutoff" model were applied wherever possible. In this paper, geographically dependent impacts were centered on the southern United States as a case study representing a promising algae cultivation location; however, the open-source model can be adapted to accommodate inventory data from other areas of the world. The Tool for Reduction and Assessment of Chemicals and Other Environmental Impacts (TRACI) version 2.1 assessment method was used, which includes ten different impact categories: GWP (100-year horizon), acidification, ecotoxicity, human health (carcinogenic and non-carcinogenic), ozone depletion, photochemical ozone formation, fossil fuel depletion, and respiratory effects. The other relevant life-cycle metric in this assessment was the NER, which is the ratio of total energy input to total fuel higher heating value (HHV). An NER less than 1 is desirable as defined here.

Life-cycle impacts of algae biomass feedstock were derived from the Davis et al. (2016) algae ORP model, with energy requirements scaled from Davis et al. (2012) [62,78]. Geographical differences in upstream life cycle inventory were not accounted for in this work. Variation in life cycle impacts of harvesting and dewatering technologies was assumed to be negligible, as supported by Cruce et al. (2021) [55]. Hydrogen life-cycle data were retrieved from a hydrogen production assessment, which included natural gas steam reforming [96], and

life-cycle impacts were converted from the ReCiPe method to TRACI equivalents. The HHV of hydrogen was included as an energy input for the NER [86], as it was considered necessary in the upgrading stage to increase the energy value of the fuel product. Energy required for fuel transportation and distribution was considered negligible, but still included for the LCA system boundary [67]. A standard +75.7 g CO_2 eq MJ^{-1} from fuel end use was included in the final GWP in all cases [97]. Total HTL fuel impacts were compared with the well-to-wheel impacts of soy-based biodiesel and conventional low-sulfur diesel [64,95,97].

3.2.6 Scenario analysis

As described earlier in Section 2.1, HTL literature assumptions varied greatly. To avoid presenting a deterministic answer from only the baseline scenario, each of these assumptions were bounded to understand changes in fuel cost and LCA metrics if other values from literature were used. Conservative and optimistic bounds for some operating parameters were determined from literature and are outlined in Table 7. Each parameter was varied, one at a time, toward either the conservative or optimistic bound. An overall conservative scenario and an overall optimistic scenario were also defined through this method. These overall scenarios combined all parameter variations in their respective direction and are referred to as the "All parameters" scenario in the results. An additional conservative scenario was included to contrast technological maturity assumptions for an NOAK plant model against a "first-of-a-kind" (FOAK) plant, which accounts for additional contingency costs and reduced performance associated with new technologies [98]. More details about FOAK assumptions and methodology are found in Appendix B. The FOAK scenario was excluded from the "All parameters" scenario.

Table 7. Parameters chosen for the techno-economic analysis and life cycle assessment scenario analysis. Scenarios marked with an asterisk (*) are exclusive to economic scenarios. Optimistic and conservative bounds were developed from representative literature sources listed in the "Scenario basis" column.

Scenario	Scenario basis	Optimistic	Baseline	Conservative
HTL temperature	Temperature analysis	320 °C	350 °C	*N/A*
Biocrude yield	95% *t*-distribution bound around mean (Table 5)	60%	45%	30%
Feed solids loading	[99]	15%	20%	25%
Algae cultivation productivity [g m^{-2} d^{-1}]	[62,63]	25	17.5	10
Heat exchanger *U [kW m^{-2} K^{-1}]**	[70,100,101]	1.26	0.818	0.50
Heat of reaction	[83]	-400 kJ kg^{-1}	0	+400 kJ kg^{-1}
Reactor residence time*	Minimum / median / maximum (Table 5)	15 min	30 min	60 min
Nutrient recycle	±30% from baseline	90%	60%	30%
Natural gas and hydrogen cost*	[94], ±20% from baseline	\$0.14 m^{-3} NG \$1.26 kg^{-1} H_2	\$0.18 m^{-3} NG \$1.57 kg^{-1} H_2	\$0.22 m^{-3} NG \$1.88 kg^{-1} H_2
Technological maturity*	[98]	*N/A*	NOAK	FOAK

The importance of heat exchanger areas draws particular attention toward calculating appropriate overall heat transfer coefficients (U). Knorr et al. (2013) detailed several scenarios for U, including low-viscosity and high-viscosity scenarios for heat exchangers in the study's "Case B" configuration (explanation in Appendix B). The baseline values for these two scenarios were 0.818 and 0.079 kW m^{-2} K^{-1} (144 and 14 BTU hr^{-1} ft^{-2} $°F^{-1}$ as reported in the original source), respectively – an order of magnitude apart. The low-viscosity case was determined to be more representative of an algae feed slurry. The range of uncertainty was still very high, with a lower bound of 0.11 kW m^{-2} K^{-1} and an upper bound of 2.16 kW m^{-2} K^{-1} (20 to 380 BTU hr^{-1} ft^{-2} $°F^{-1}$). As a result, the total capital investment range fell between \$267M and \$1,703M from varying U alone, which highlights the impact of heat exchanger assumptions [70]. Similar U calculation methods were used in the current work to narrow the uncertainty of this critical parameter in the scenario analysis (2.7 Calculations). Rheological studies on algal slurries have determined viscosity to be a function of temperature and solids loading. A wide range of

viscosity values ranging from 2.4×10^{-4} to 1 Pa·s were considered based on literature of algae feeds around 20 wt% solids [70,100–102]. Fouling resistance was also varied from 0.710 to 1.89 kW m^{-2} K^{-1} (125 to 333 BTU hr^{-1} ft^{-2} $°F^{-1}$), expressed as the inverse of the fouling factor [70]. As seen in Figure B - 3 and Figure B - 4, U decreases nonlinearly with increasing viscosity, but sees a near-linear trend with respect to fouling factor. Viscosity was determined to be a much more uncertain factor in determining U, and therefore heat exchanger areas. Fouling resistance was excluded from this scenario analysis. The low-viscosity baseline U of 0.818 kW m^{-2} K^{-1} (144 BTU hr^{-1} ft^{-2} $°F^{-1}$) from Knorr et al. (2013) was set as the baseline in this work [70]. With parameters from other literature entered into Eqs. 1, 2, and 3, 0.50 and 1.26 kW m^{-2} K^{-1} (88 and 222 BTU hr^{-1} ft^{-2} $°F^{-1}$) were considered reasonable lower and upper bounds of U.

Sensible heat duty was provided by the heat exchanger and hot oil heater to bring the HTL feed up to reaction temperature. Though the reactor was considered isothermal but not adiabatic, the heat of reaction was not accounted for in *Aspen Plus* because of the uncertainty in stream compositions and properties. The baseline scenario in this work assumed that the heat of reaction (ΔH_r) was negligible, but this is likely not the case in real operation. Thus, an additional scenario was included to account for an exothermic (optimistic) or an endothermic reaction (conservative) with a magnitude of ±400 kJ kg^{-1} dry feed [83].

3.2.7 Calculations

Equations from the Methodology section are explained here.

The Colburn equation was used to calculate convective heat transfer coefficients h (Eq. 1), which were then used to estimate U (Eq. 2).

$$\left(\frac{h}{C_p G}\right)\left(\frac{\mu C_p}{k}\right)^{\frac{2}{3}} = 0.023\left(\frac{\mu}{DG}\right)^{\frac{1}{5}} \quad (1)$$

$$\frac{1}{UA_s} = \frac{1}{(hA_s)_{cold}} + \frac{R''_{f,cold}}{A_s} + \frac{\ln\left(\frac{D_{outer}}{D_{inner}}\right)}{2\pi kL} + \frac{R''_{f,hot}}{A_s} + \frac{1}{(hA_s)_{hot}} \quad (2)$$

Assuming the conductive resistance and hot stream fouling factor are both negligible, Eq. 2 simplifies to the form in Eq. 3:

$$\frac{1}{U} = \frac{1}{h_{cold}} + R''_{f,slurry} + \frac{1}{h_{hot}} \quad (3)$$

Thus, necessary parameters to determine U include fluid heat capacity (C_p), viscosity (μ), thermal conductivity (k), mass velocity (G), pipe diameters (D), and algae feed fouling factor ($R''_{f,slurry}$).

For a tubular flow reactor with diameter D, mass flow rate $\dot{m}$, residence time τ, and density ρ, the length L of the HTL reactor was calculated via Eq. 4.

$$L = \frac{4\dot{m}\tau}{\pi\rho D^2} \quad (4)$$

3.3 Results and discussion

A representative set of HTL operating conditions was established as the baseline scenario. This work provides a detailed breakdown of baseline TEA and LCA results. To date, this work is the first of its kind to perform a full spectrum of LCA impacts that goes beyond GWP and NER. These baseline results are presented and followed by a sensitivity analysis to temperature and property estimation methods on equipment design and corresponding capital cost estimation and operational costs. The objective of the thermodynamic analysis is to establish the most appropriate standard property model for algal HTL process modeling. Flaws in choosing inappropriate property methods are highlighted.

The scenario analysis explores the effect on HTL performance from varying other parameters from the baseline, such as biocrude yield and nutrient recycle. Discussion centers on comparisons with current HTL literature and conventional transportation fuels. Other

engineering considerations that are not applied to the current work, such as post-HTL separations and nutrient recovery methods, are briefly discussed as potential modeling additions.

3.3.1 Baseline TEA

The model developed in this work was first validated against the original work in Jones et al. (2014), which reported an MFSP (in 2011$) of $1.19 LGE^{-1} ($4.49 GGE^{-1}) assuming a biomass purchase price of $430 dry ton^{-1} [21]. Replicating the input parameters in the reference work produced an MFSP of $1.17 LGE^{-1} ($4.44 GGE^{-1}), or an error of 1.11% from the original work. The only major difference between the two efforts was the replacement of the onsite hydrogen plant in the original reference with a variable operating cost for purchased offsite hydrogen.

Based on the literature analysis described in Section 2.1, the baseline conditions are 350 °C operating temperature, 30 min residence time, and 20 wt% feed solids to achieve a mean biocrude yield of 45%. The baseline property estimation method is PSRK. The baseline MFSP

contribution of HTL is \$0.45 LGE^{-1} (\$1.69 GGE^{-1}). The HTL cost is further broken down by major areas in Figure 8, with results excluding the algae feedstock cost.

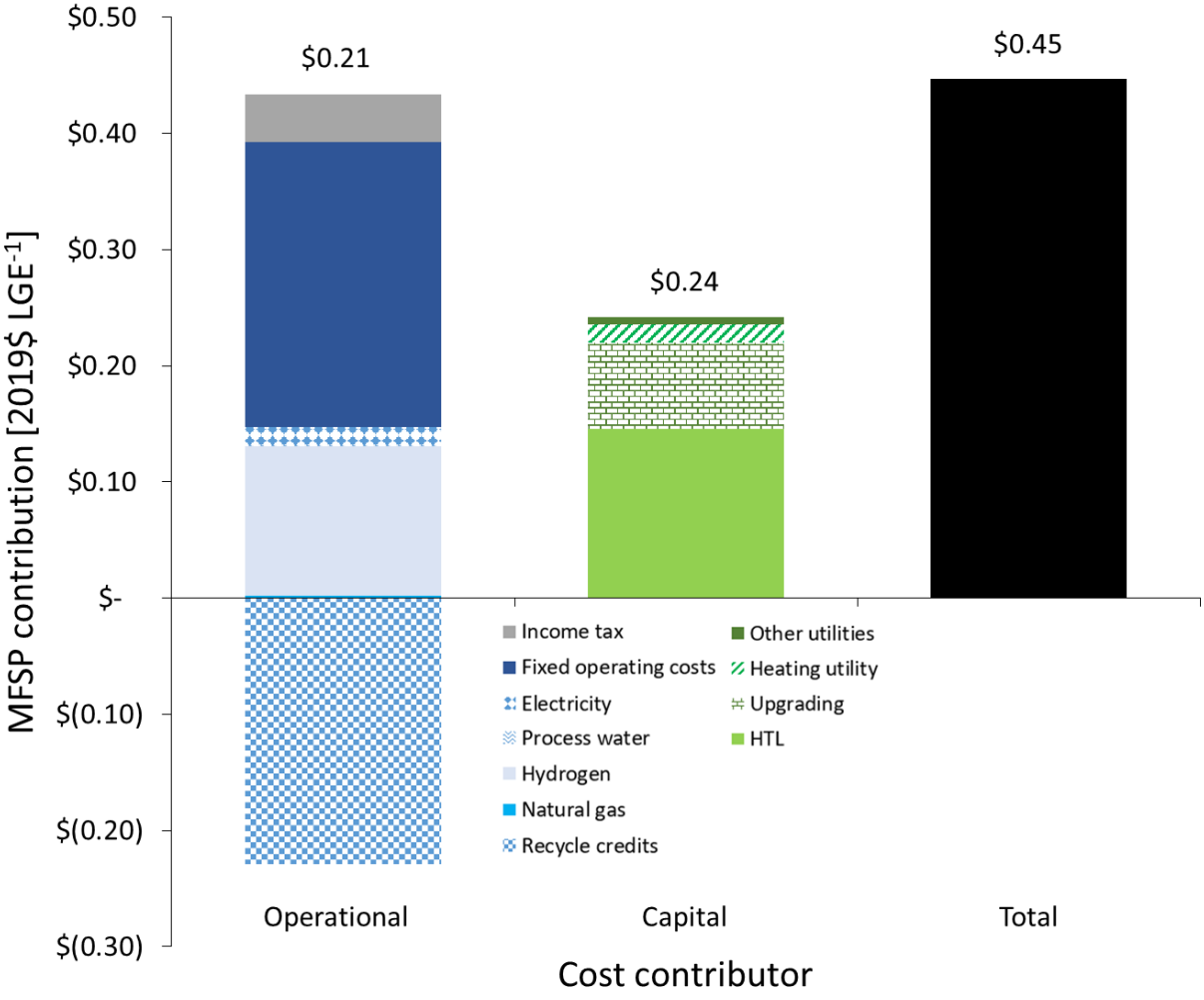

Figure 8. Breakdown of HTL contribution to MFSP. Blue bar represents operational costs and green bar represents capital costs. Net total (\$0.45 LGE^{-1}) is reported as the solid black bar. Results do not include the cost of the algae feedstock.

The baseline capital cost contributes \$0.24 LGE^{-1} (\$0.92 GGE^{-1}), making up 54% of the HTL system cost. Of that capital cost, the heat exchanger comprises 14% and the HTL reactor contributes 6%. Thus, it is expected that uncertainties in heat exchanger area calculations will produce a moderate effect on the HTL cost. Out of the variable operating costs, nutrient recycle contributes the greatest impact to MFSP. The baseline assumption of recycling 60% nutrients

provides a \$0.23 LGE^{-1} (\$0.87 GGE^{-1}; 51%) credit. In other HTL literature, the conversion cost has been noted to be sensitive to the recycle treatment method. With 90% nutrient recycle in Zhu et al. (2019), direct (untreated) recycle resulted in a \$0.27 LGE^{-1} (\$1.02 GGE^{-1}) credit toward a \$0.47 LGE^{-1} (\$1.77 GGE^{-1}) total HTL cost. Zhu et al. also evaluated a recycle pathway with CHG integrated after the HTL unit, resulting in a \$0.25 LGE^{-1} (\$0.94 GGE^{-1}) nutrient credit for a greater total of \$0.80 LGE^{-1} (\$3.04 GGE^{-1}) [60], more than triple the cost without CHG. Thus, the exclusion of CHG, as assumed in this work, is an economic requirement to reduce HTL costs and justifies direct nutrient recycle. It should be noted that one of the foundations of this work integrates CHG with the HTL system [21], but cannot achieve its \$3 GGE^{-1} MFSP target, as the cost of HTL with CHG already surpasses \$3 GGE^{-1} without even factoring in the cost of biomass.

Because natural gas is not reclaimed from CHG and routed to an on-site hydrogen plant, purchased hydrogen is the next greatest variable operating cost with a baseline of \$0.13 LGE^{-1} (\$0.49 GGE^{-1}, 29%). Outside the HTL system boundary, the levelized cost of hydrogen is inexorably linked to the cost of natural gas when produced from steam-methane reforming [94]. The direct natural gas cost contribution, however, is negligible. Low natural gas duties are attributed to the upgrading stage, where volatile gases can be recovered and fed back to the heating utility. Though natural gas contributes negligible costs in the baseline configuration, the impact of natural gas consumption on HTL performance is emphasized in the thermodynamic analysis.

3.3.2 Baseline LCA

LCA results from the initial validation work were compared to Frank et al. (2013), which calculated a well-to-wheels GWP of 29 g CO2eq MJ-1 [60]. The validation results produced a

GWP of 46 CO2eq MJ-1. Though there is a 59% error between these calculations, the results can still be considered comparable, as there are critical differences in assumptions between the two models, such as temperature and biocrude yield. The difference further highlights a need to better understand the effect of these parameters on HTL performance.

The breakdowns of baseline TRACI life-cycle impacts and NER are shown in Figure 9, with total impacts of HTL fuel, soy biodiesel, and conventional diesel compiled in Table 8. Each impact is discussed with greater detail in individual sections.

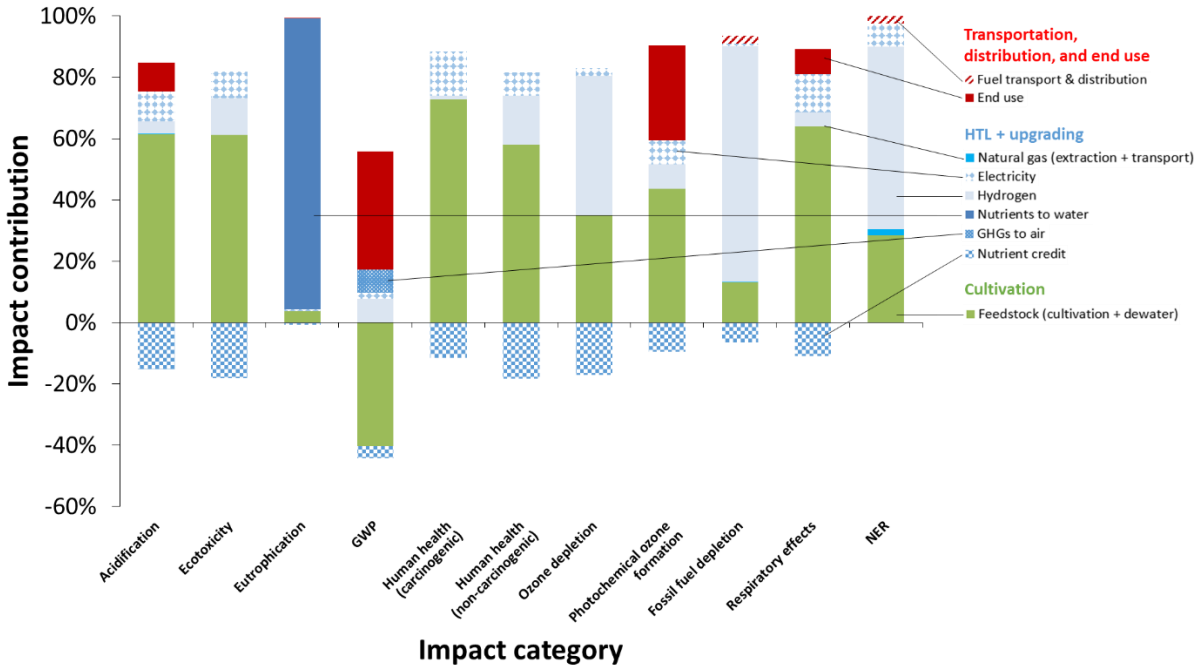

Figure 9. Environmental impacts of the baseline scenario broken down by resource consumption and normalized by percent contribution. All bars sum up to a magnitude of 100%. The functional unit is 1 MJ of liquid fuel product.

Table 8. Summary of total environmental impacts of the baseline scenario compared to soy-based biodiesel and conventional diesel. The system boundary is well-to-wheels.

Impact category	Algal HTL fuel	Soy biodiesel [95,97]	Conventional diesel [95,97]	Units [per MJ fuel]
Acidification	1.9×10^{-4}	1.19×10^{-4}	1.44×10^{-4}	kg SO_2 eq
Ecotoxicity	1.4×10^{-1}	7.11×10^{-2}	1.94×10^{-2}	CTUe
Eutrophication	3.5×10^{-3}	7.13×10^{-5}	4.05×10^{-5}	kg N eq
Global warming potential (GWP)	2.3×10^{-2}	1.01×10^{-1}	8.83×10^{-2}	kg CO_2 eq
Human health (carcinogenic)	1.5×10^{-9}	7.52×10^{-10}	3.67×10^{-10}	CTUh
Human health (non-carcinogenic)	6.7×10^{-9}	2.84×10^{-9}	7.71×10^{-10}	CTUh
Ozone depletion	5.4×10^{-9}	2.84×10^{-9}	2.01×10^{-8}	kg CFC-11 eq
Photochemical ozone formation	2.7×10^{-3}	2.62×10^{-3}	2.02×10^{-3}	kg O_3 eq
Fossil fuel depletion	2.6×10^{-1}	2.57×10^{-2}	1.67×10^{-1}	MJ
Respiratory effects	4.3×10^{-5}	2.29×10^{-5}	1.62×10^{-5}	kg PM2.5 eq
Net energy ratio (NER)	3.0×10^{-1}	1.64×10^{0} [64]	1.9×10^{-1} [64]	MJ

3.3.2.1 GWP (100-year horizon)

The well-to-wheels GWP with baseline parameters is +23 g CO_2 eq MJ^{-1}, well below the 2005 RFS diesel mandate of 46 g CO_2 eq MJ^{-1} [103]. The HTL GWP also compares favorably against soy biodiesel, which has touted as a renewable alternative to petroleum fuel despite having a larger GWP impact. Most GWP credits are attributed to the carbon captured from the algae feedstock, but they are offset by the end use emissions. The GWP inside the HTL system boundary is +26 g CO_2 eq MJ^{-1}. The HTL system boundary contribution to GWP in Jones et al. (2014) varies between +9.1 and +20.5 g CO_2 eq MJ^{-1} depending on system boundary assumptions [21]; however, differences in certain assumptions like fuel yield and nutrient recycle are not accounted for. The baseline GWP in this work is comparable with the reference model despite these differences in assumptions.

3.3.2.2 Acidification

With an impact of 1.8×10^{-4} kg SO_2 eq MJ^{-1}, HTL fuel performs worse than soy biodiesel (1.6×) and conventional diesel (1.3×). It should be noted that 88% of this impact in algae HTL comes from the feedstock, where high power demand is required for cultivation and harvesting. This trend can be observed in other LCA categories where feedstock comprises the majority of the impact, which places the environmental burden on cultivation and harvesting, not the HTL system.

3.3.2.3 Ecotoxicity

The total HTL fuel ecotoxicity impact is 1.4×10^{-1} CTUe MJ^{-1}. Relative to soy and conventional diesel, algal HTL fuel performs much worse in this category, with a 1.9× impact over soy biodiesel and a 7.0× impact over conventional diesel. Similar to the acidification category, the feedstock is the major cause of the large ecotoxicity impact, as it contributes a majority (96%) to this category.

3.3.2.4 Eutrophication

Eutrophication is singled out as the impact category most affected by assumptions made inside the HTL system boundary. The total impact is particularly sensitive to the proportion of non-recycled nutrients; the baseline impact is 3.5×10^{-3} kg N eq MJ^{-1}, which is two orders of magnitude greater than the impacts of soy and conventional diesel [95]. Improving the nutrient recycle to 90% decreases the eutrophication impact to 9.6×10^{-4} kg N eq MJ^{-1} (0.27× baseline), while decreasing to 30% recycle increases eutrophication to 6.1×10^{-3} kg N eq MJ^{-1} (1.7× baseline). While the eutrophication impact can potentially reach a fraction of the baseline with recycling improvements, any nutrient waste in the algae production process introduces an

exceptionally large eutrophication potential that dominates the impacts of soy or conventional diesel.

3.3.2.5 Human health (carcinogenic and non-carcinogenic)

Both human health categories compare considerably worse against soy and conventional diesel. The HTL impacts are 1.54×10^{-9} and 6.72×10^{-9} CTUh MJ^{-1} in the carcinogenic and non-carcinogenic categories, respectively. HTL fuel impacts are more than double that of soy biodiesel in both human health categories. In the carcinogenic category, algal HTL fuel has a 4.2× impact relative to conventional diesel, while in the non-carcinogenic category, HTL fuel has an even greater impact over conventional diesel by a factor of 8.7×. The large relative magnitudes are not attributed to the HTL system; the feedstock contributes 95% and 92% to the respective categories.

3.3.2.6 Ozone depletion

The total magnitude of ozone depletion from HTL biodiesel is 5.4×10^{-9} kg CFC-11 eq MJ^{-1}. Ozone depletion is one of the only TRACI categories where hydrogen has a greater impact than the feedstock, allowing HTL fuel to perform better than conventional diesel with an impact factor of 0.27×. However, the HTL fuel impact is 1.9× greater than soy biodiesel, likely because the transesterification of crude soy oil does not require a hydrogen upgrading step.

3.3.2.7 Photochemical ozone formation

HTL fuel has a baseline impact of 2.7×10^{-3} kg O_3 eq MJ^{-1} in the photochemical ozone formation category. The HTL fuel impact is near the same as soy biodiesel and 1.3× greater than conventional diesel. Though the feedstock comprises a majority of this impact, the end use stage has a 38% contribution, more than in any other category except GWP.

3.3.2.8 Fossil fuel depletion

The other TRACI category in HTL that is not dominated by feedstock impacts is fossil fuel depletion. Hydrogen contributes 89% of the HTL fossil fuel depletion impact (0.26 $MJ_{surplus}$ MJ_{fuel}^{-1}) because of its high requirement for natural gas as a feedstock in steam-methane reforming. The total impact is comparable in magnitude to conventional diesel (1.9×), but is an order of magnitude higher than soy biodiesel. Similar to ozone depletion, it can be concluded that soy biodiesel has an advantage in the fossil fuel depletion category because it does not consume hydrogen in the conversion process.

3.3.2.9 Respiratory effects

The total respiratory effects impact for HTL fuel is 4.3×10^{-5} kg PM2.5 eq MJ^{-1}. Like several other categories, the algae feedstock dominates the total impact with a contribution of 82%. As expected from trends in other impacts, the respiratory effects category has a worse impact compared to other fuels, with a 1.9× factor over soy biodiesel and a 2.7× factor over conventional diesel.

3.3.2.10 NER

Within the HTL system boundary, the NER is 0.21. The NER equivalent of the HTL plant system boundary is 0.14 in the reference model, reported as fossil energy consumption [21]. Because the current model diverts HTL-generated gases to heating utility instead of an on-site hydrogen plant, the net natural gas requirement is much lower than the reference model. In place of natural gas feedstock for a hydrogen plant, purchased hydrogen is used as the product flow entering the system boundary. Hydrogen is not directly combusted in the biocrude upgrading step, but it must be considered an energy input because it adds energy value to the final fuel products. Hence, hydrogen contributes the most to the NER with an impact of 0.18. If

the system boundary is expanded to include growth, dewatering, and fuel transportation and distribution, the total NER is 0.30. With the given baseline assumptions, the total NER of HTL is 58% higher than the conventional diesel baseline of 0.19, but still favorable compared to the NER of 1.64 for soy biodiesel [64]. Other HTL studies report NER equivalents from a range of 0.34 to 1.25; however, biocrude yield assumptions varied greatly from 22% to 60% [65–69,104,105]. The gas recovery configuration in this work lowers the NER below the typical literature range and shows that energy recovery is critical for reducing this metric.

3.3.2.11 LCA interpretation

Baseline GWP and NER results validate algae HTL as a GHG- and energy-friendly alternative to other diesel products, but other environmental impacts should also be respected before considering algae HTL as a renewable fuel pathway. Beyond GWP and NER, other LCA metrics show a wide range of trends. As evident in the NER breakdown, algae cultivation requires high electricity use due to ORP paddlewheel power requirements. Feedstock-dominated impact categories are especially dependent on the electricity grid mix. A higher mix of clean, renewable power would drive well-to-wheel life-cycle impacts down, but would have little effect on impacts within the HTL system boundary. By contrast, eutrophication, ozone depletion, and fossil fuel depletion are impact categories that deserve more attention inside the HTL system boundary. It is imperative for algae fuels to find ways to reduce environmental impacts below conventional fuel levels through all life-cycle metrics, instead of focusing only on GWP and NER.

3.3.3 HTL model performance as a function of thermodynamic properties

Since water composes most of the mass balance through the HTL heat exchanger, the properties of water dominate heat exchanger calculations, including stream enthalpies and heat

capacities. The heat capacity of liquid water below the normal boiling point (100 °C) is near-constant at 4.2 kJ kg^{-1} K^{-1}. At 350 °C, this increases to 6.4 kJ kg^{-1} K^{-1} based on thermodynamic properties derived from the National Institute of Standards and Technology (NIST) [106]. Model estimations of enthalpy and heat capacity of compressed liquid water are compared in Figure 10. The comparison includes NIST data (tabulated and Shomate curve-fit) and select property model outputs from *Aspen Plus* Pure Analysis. The reference state was assumed to be 0 °C and 20 MPa. Based on NIST properties, the heat duty required to increase the temperature of subcritical water from 290 °C to 320 °C is 163 kJ kg^{-1}, whereas the same temperature increase from 320 °C to 350 °C requires 201 kJ kg^{-1}. The latter case requires 23% more energy input for the same temperature change. Of the selected methods, PSRK predicted water properties to be closest to steam tables and the Shomate equation, even at the high range of HTL temperatures. Meanwhile, water properties estimated by SRK deviated from NIST data by 16% at temperatures as low as 100 °C. At 350 °C, the NIST-calculated specific enthalpy of water was 1,626 kJ kg^{-1}, while the enthalpy calculated by PSRK and SRK were 1,738 and 1,966 kJ kg^{-1}, respectively, representing 7% and 21% deviations from NIST properties.

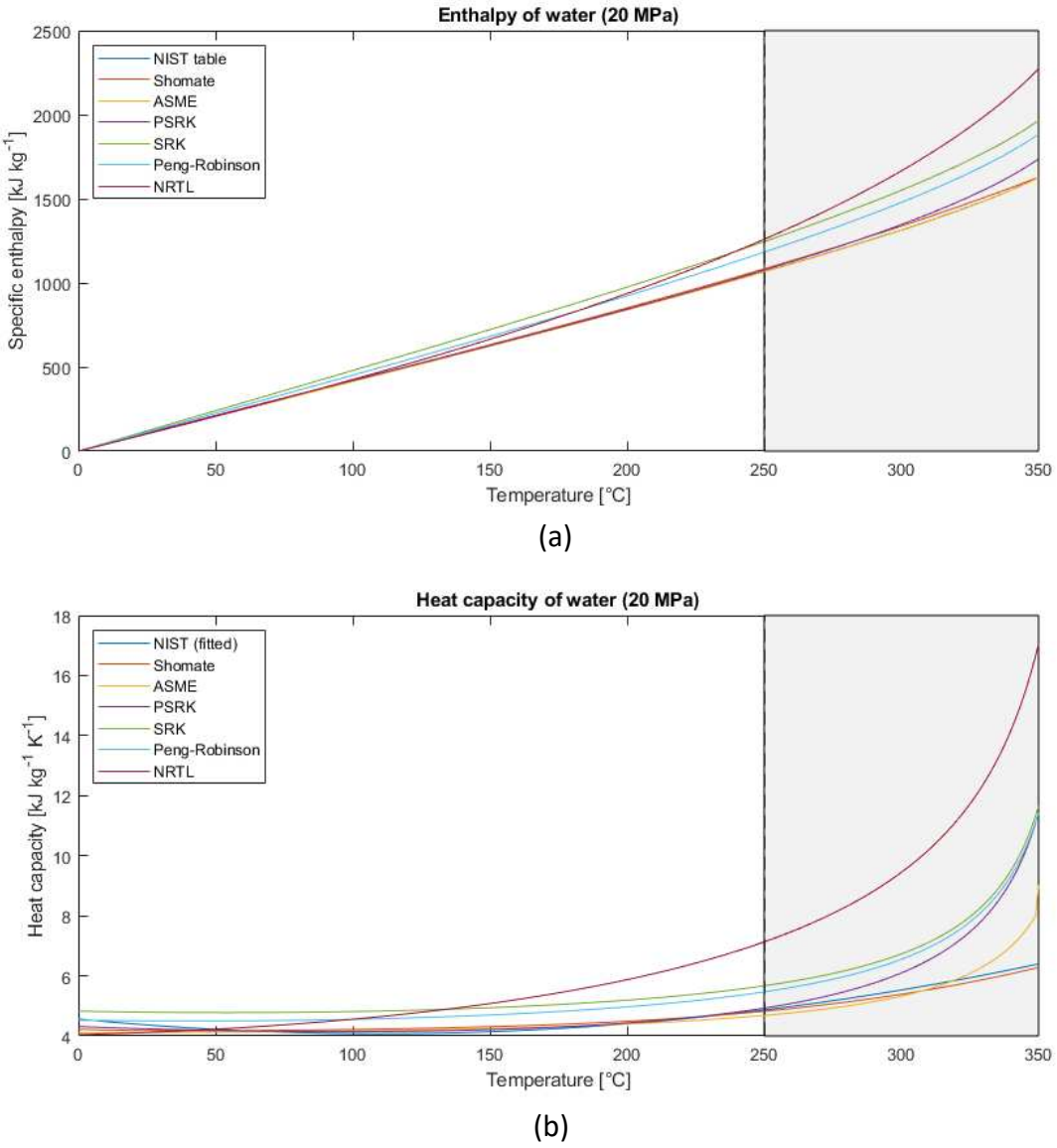

Figure 10. (a) Enthalpy and (b) heat capacity of subcritical / liquid water at 20 Mpa from 0 to 350 °C. Property estimates from the following methods are compared: NIST steam tables, Shomate equation, ASME steam tables, predictive Soave-Redlich Kwong (PSRK) equation of state (EoS), SRK EoS, Peng-Robinson EoS, and non-random two-liquid (NRTL) model. The shaded temperature range represents typical hydrothermal liquefaction operating conditions, where relevant properties deviate heavily between property estimation methods.

The impact of property estimation models is best exemplified through a comparison of calculated heat exchanger areas. Figure 11a outlines the required changes in heat exchanger design for HTL temperatures between 260 and 350 °C. As the reaction temperature increases, the

required area naturally increases. Because of the non-linear increase in thermodynamic properties, the required change in heat exchanger area from 320 to 350 °C based on PSRK calculations, for example, is 32%. The area change from 260 to 290 °C, by contrast, is only 25%. All heat exchanger areas are impacted heavily if an unsuitable property estimation method is selected. The heat exchanger area calculated by the NRTL model for a 350 °C reaction has a 76% error relative to the PSRK equation of state. Even SRK produces a 7% error from the PSRK area despite being derived from similar models.

Natural gas duty varies between temperatures and property estimation methods, as compared in Figure 11b. Heat duty was minimized in all cases with the given heat exchanger constraint of 115 °C at the hot stream exit. As a result, little variation in natural gas consumption is expected if the operating temperature decreases, as the heater only needs to make up for the temperature difference between the heat exchanger exit and the final operating temperature. Minimal errors in natural gas duty occur between temperatures in baseline PSRK simulations. Other property methods change the calculations of some feed component properties in *Aspen Plus*, leading to inherent simulation errors. Vapor-liquid equilibrium (VLE) calculations return convergence errors when the simulation is run with SRK or Peng-Robinson methods, which lead to the partial vaporization of feed streams. Hence, the calculated natural gas duties of these two methods have large relative errors compared to the baseline; Peng-Robinson simulations return zero natural gas duty except at 260 °C. The NRTL method, while free of VLE errors, also dictates zero natural gas duty across all operating temperatures. Water properties calculated by the NRTL method deviate greatly from other property methods, especially at temperatures in the HTL operating range. This phenomenon also explains the much higher heat exchanger areas required in the NRTL calculations. With the gas recycle configuration in this work, supplemental

natural gas duties are demonstrated to be especially sensitive due to their low magnitudes and are critical to accurately model. It is important to gain from this analysis that an appropriate property estimation method should result in consistent thermodynamic properties and converge on VLE calculations. The PSRK method meets these criteria and is justified here as the baseline; there is also precedence in algae HTL literature [21]. Caution is advised for other methods like SRK, which is widely used in lignocellulosic feed-based HTL models [70,83,107,108], but can cause VLE convergence errors with algae components.

Property estimation methods also change stream density, which impacts the cost of the HTL reactor. The cost of a flow reactor is typically scaled by length, which requires a calculation of volumetric flow from the estimated stream density (Eq. 4). However, as demonstrated in the baseline analysis, the cost contribution of the reactor is less than half of the heat exchanger in the given conditions. Thus, simulation errors on stream density do not dramatically affect the overall cost and reactor design is not discussed in detail.

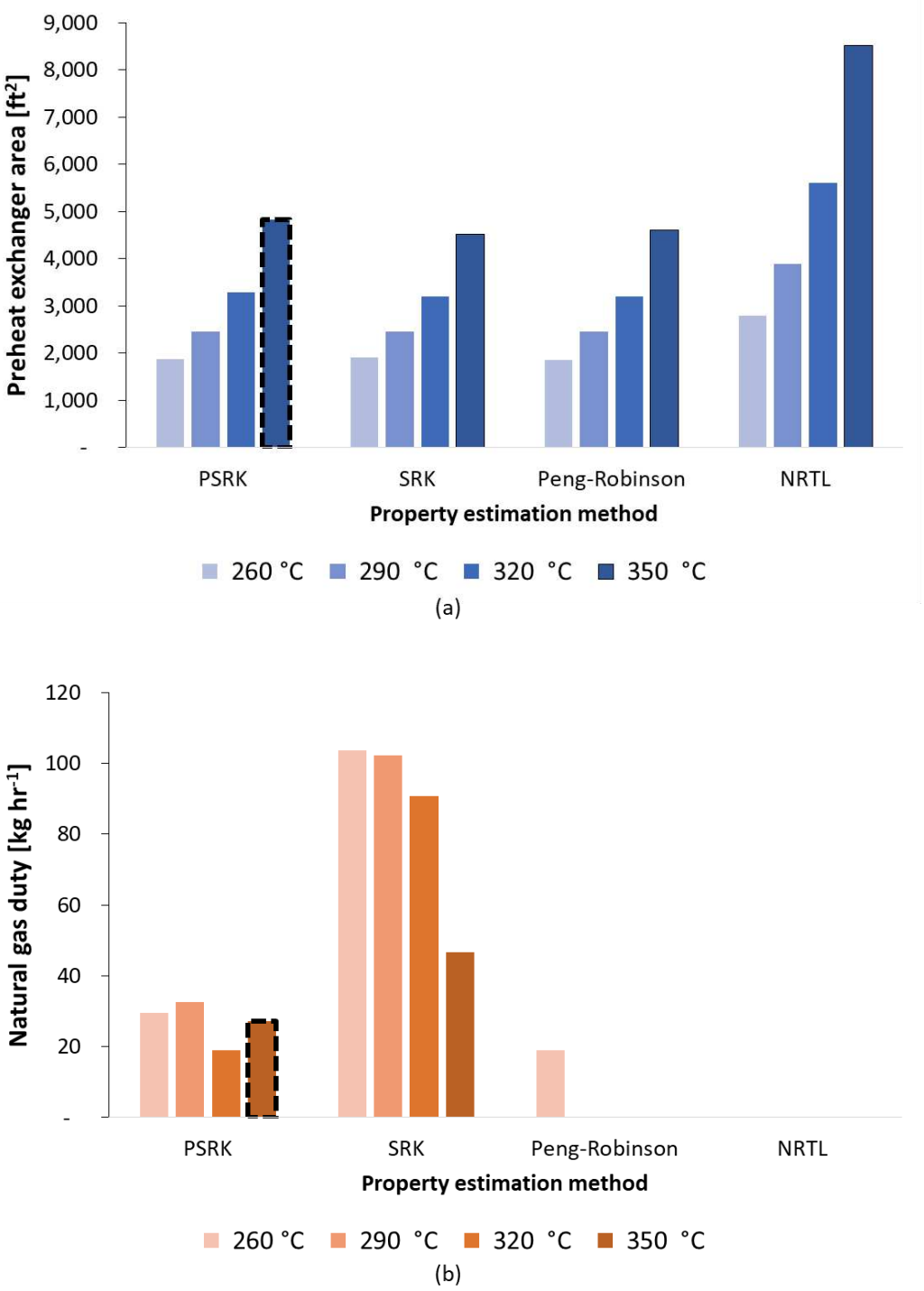

Figure 11. (a) Heat exchanger areas based on optimization around the pre-heat exchanger with the hot waste stream outlet constrained to 115 °C. (b) Natural gas duty as a function of temperature and property estimation method. Model was based on Knorr et al. (2013) "Case B". The feed inlet temperature is 25 °C. Baseline case is highlighted by dashed outline.

The impact of varying temperature and simulation properties on the MFSP contribution of HTL is demonstrated in Figure 12. The baseline (PSRK, 350 °C) HTL cost is \$0.45 LGE^{-1} (\$1.69 GGE^{-1}). If the temperature is fixed at 350 °C, the greatest cost difference between property methods is between Peng-Robinson and NRTL, a \$0.07 LGE^{-1} (\$0.26 GGE^{-1}) range. Poor selection of property method is reflected by relatively large deviations in HTL cost. For example, the error in HTL cost between the PSRK baseline and NRTL is 8%. When focusing on temperature in the PSRK results, the HTL cost decreases by 9% from 350 °C to 320 °C, but the same temperature decrease from 320 °C to 290 °C diminishes the benefit to a 6% cost difference. These nonlinear differences in HTL cost reflect the nonlinear impact of temperature on thermodynamic properties. In conclusion, Figure 11a and Figure 12 demonstrate the importance of heat exchanger design, as the capital expenses make up a heavy portion of the HTL cost. Though operating costs have a smaller effect on MFSP, Figure 11b clearly highlights the significance of appropriate property method selection on energy requirements. Deviations in equipment design calculations can cause moderate errors in HTL cost, but the effect is likely less impactful than other parameters like product yield and recycle credits.

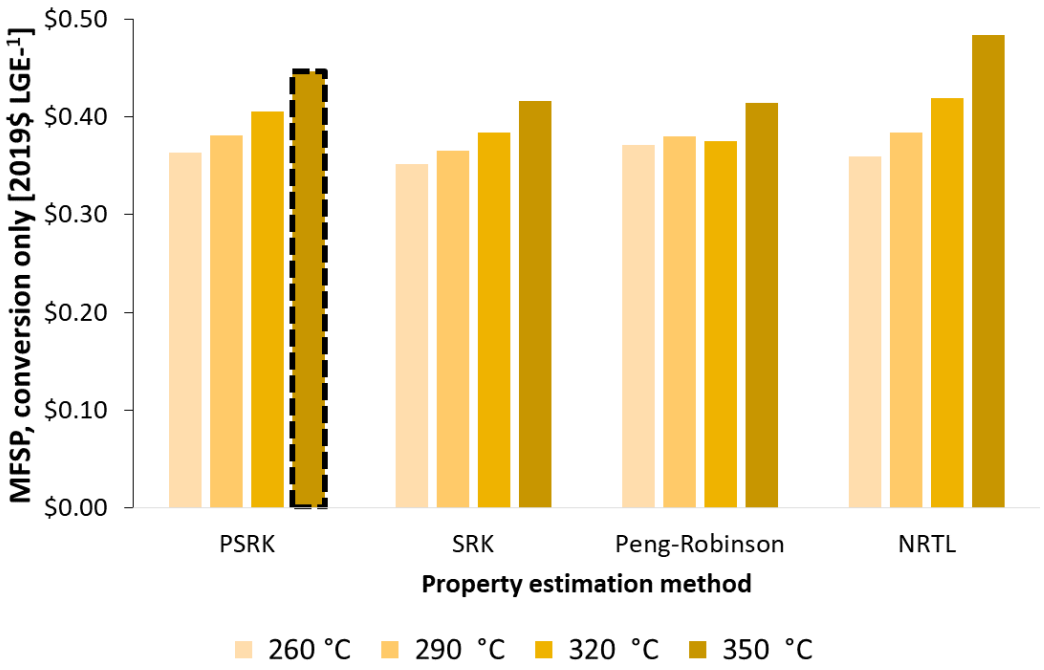

Figure 12. Minimum fuel selling price contribution from conversion and upgrading based on varying property estimation method and reaction temperature. Baseline case is highlighted by dashed outline. Results do not include the cost of the algae feedstock.

Temperature constraints in the HTL heat exchanger force the LCA metrics of this study to be approximately the same throughout all conditions. The heat duty, and therefore natural gas duty, are minimized by transferring as much energy as possible from the aqueous waste stream to the feed. The biogas recycle configuration and large hydrogen LCA impacts dilute any variation in GWP and NER between varying reaction temperatures. The scenario analysis in Section 3.4 explores the impact of these minor changes with more detail. If the constraint is changed such that heat exchanger areas are constant, then natural gas duties would increase. Without the natural gas minimization constraint in this study, the reduction in heat exchanger capital costs would be met by more unfavorable operational costs, GWP, and NER.

3.3.4 Scenario analysis

The wide uncertainty in HTL performance must be addressed to capture the limits of its viability. Critical operating conditions beyond temperature (Table 7) were varied in this scenario analysis. The tornado plots in Figure 13 compare the individual impact of each variable on TEA and LCA metrics in the conservative and optimistic scenarios, as well as the combination of all conservative and optimistic bounds.

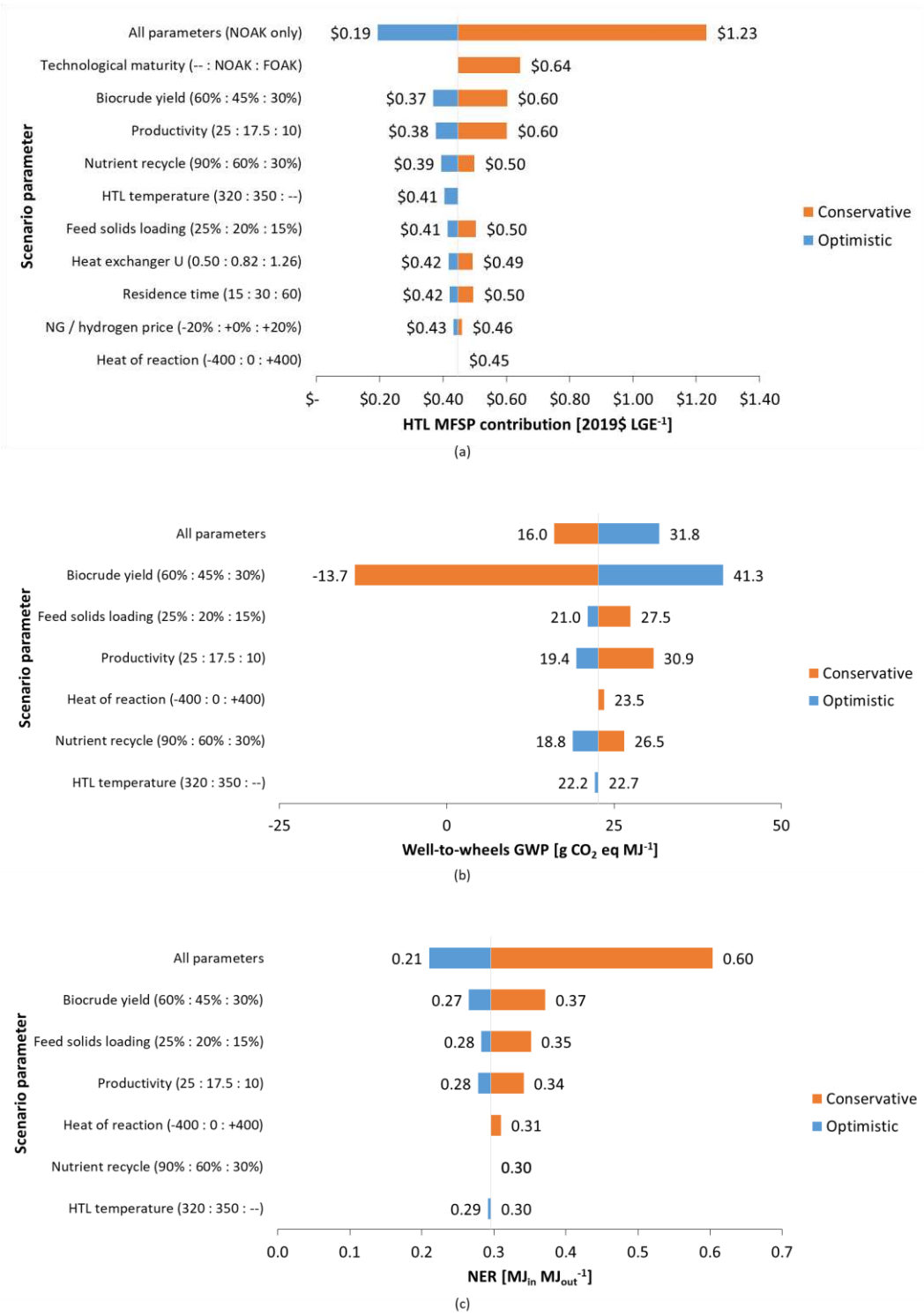

Figure 13. Tornado plots of (a) minimum fuel selling price, (b) global warming potential, and (c) net energy ratio scenarios in Table 7. "All parameters" are the combination of scenarios (except for technological maturity) that produce the absolute minimum or maximum fuel price if every sensitivity (optimistic or conservative from Table 7, respectively) is taken into effect.

As expected, the biocrude yield has the highest impact on the MFSP contribution. A conservative yield of 30% increases the cost contribution by 35%. There is a diminished return in the opposite direction as the cost contribution decreases by only 18% with an optimistically high yield of 60%. Biomass productivity influences the feed flow rate to the HTL system, which creates similar magnitudes of effect on cost due to economies of scale in capital cost estimation. The conservative and optimistic productivity scenarios produce respective +35% and -16% changes in the MFSP contribution compared to the baseline. Nutrient recycle scenarios have the next greatest effect on MFSP contribution (±12% both directions), followed by HTL temperature, feed solids loading, heat exchanger coefficient, residence time, natural gas cost, and lastly, heat of reaction. If all parameter changes (excluding FOAK) are considered at the same time, the lumped conservative scenario increases the HTL cost by 176% and the lumped optimistic scenario decreases the MFSP contribution by 57%.

To maintain an isothermal process, the HTL reactor requires additional energy duty equal to ΔH_r. An endothermic reaction would require additional natural gas duty to the reactor, while the heat released from an exothermic reaction could provide an opportunity for energy recovery. Data on ΔH_f for algae HTL systems is scarce, and even more so for continuous reactor systems [18]. A data fitting method for wood-fed HTL was developed in Lozano et al. (2019), but even within the same study, results varied in magnitude and whether the reaction is exothermic or endothermic [83]. However, in the current scenario analysis, the heat of reaction has little effect on both TEA and LCA metrics, demonstrating that sensible heat dominates the HTL system's energy requirements.

A TEA scenario is included to determine the impact of technological maturity via a theoretical FOAK plant, as opposed to standard NOAK assumptions. To date, HTL is an

unestablished technology, so additional assumptions are required to capture commercial adoption challenges, such as decreased product yield at start-up and capital cost contingencies. "Pioneer plant" assumptions were derived from Merrow et al. (1981) [98]. Largely owing to an increase in capital cost, the FOAK scenario has a greater effect on MFSP contribution than any individual conservative parameter, with a 48% increase from the baseline to \$0.66 LGE^{-1} (\$2.50 GGE^{-1}). Though the FOAK scenario is difficult to compare with other NOAK parameters, it is clear from this analysis that near-future commercial HTL plants must account for and prioritize the extra economic burden from high uncertainties associated with pioneer technologies.

LCA scenario trends do not match TEA scenarios due to different focuses and methodologies. Parameters that affect capital equipment, such as the heat exchanger U, do not play a high-impact role in life-cycle accounting. Higher biocrude yield paradoxically creates a detrimental effect on the well-to-wheels GWP, increasing from +23 to +41 g CO_2 eq MJ^{-1}. Decreasing the yield from 45% to 30% creates a net carbon credit due to the greater offset of captured CO_2 with the fixed end use emissions (75.7 g CO_2 eq MJ^{-1}). It must be emphasized that the end use emissions are an obstacle to achieving carbon neutrality in most transportation fuels (except hydrogen), unless a co-product is formed that does not produce end use emissions or displaces a high intensity traditional product. However, HTL does not allow for high-value co-products (*e.g.* bioplastics) and focuses on combustible fuel for its functional unit, which can explain the increase in GWP with improved biocrude yields. Hence, the GWP is actually negative in the low-yield scenario (-14 g CO_2 eq MJ^{-1}) since less end use emissions are attributed to the fuel products. NER sensitivity to yield is fairly straightforward; lower biocrude yield makes the NER less favorable, increasing by 26%. Increasing productivity improves the GWP metric, as paddlewheel energy duties in the cultivation step are independent of biomass

productivity and less emissions are associated with the feedstock. As such, the high-productivity scenario brings the GWP down by 14% and the low-productivity scenario increases GWP by 36%. Nutrient recycle and feed solids loading each have a moderate effect on GWP, while HTL temperature and heat of reaction have negligible effects. Feed solids loading is an important factor in NER, as the heater requires more natural gas duty to heat up biomass with high water content. With 15 wt% solids, the NER increases to 0.35, while 25 wt% solids decreases NER to 0.28. Mixed results from the scenario analysis show that it is overall challenging to optimize the sustainability metrics of HTL fuel because of the balancing effects of GWP, NER, and economics.

The scenarios in this work attempt to narrow down the uncertainty of key parameters through rigorous literature surveying. The asymmetry in impacts between scenarios highlights the importance of solidifying HTL data and optimizing operating parameters. Low biocrude yields and high temperatures diminish the economic benefit of HTL. Improving HTL toward the optimistic direction presents a massive technical challenge, as these parameters can likely only be improved through optimizing feed composition. As demonstrated in Leow et al. (2018), the range of compositions where HTL is economically favorable over other algae conversion technologies is highly conditional [109].

The scenario analysis in this work includes more parameters and studies than other HTL literature. Zhu et al. (2019) includes a sensitivity analysis of biocrude yield based on literature, but the range (35 – 60%) only encompassed three studies [13,21,110]. Nutrient recycle credits were also varied with a sensitivity of ±50% relative to the baseline (90%) [60], a much lower range than presented in the current work. The sensitivity analyses in both Jones et al. (2014) [21] and Zhu et al. (2019) [60] are performed on the total fuel selling price, which includes the cost of

biomass. In Jones et al., the biomass price is $474 per ash-free metric ton, whereas the biomass purchase cost in Zhu et al. is much higher at $1,342 per ash-free metric ton. The high biomass cost in Zhu et al. dilutes the effect of all other sensitivity variables. In this work, the scenario analysis focuses on the cost of HTL conversion alone; the cost of biomass is eliminated from the analysis and instead can be solved for by fixing the total fuel price to parity with conventional fuels.

Figure 14 presents the biomass cost constraints that are required for the total MFSP to meet cost targets of $3, $5, and $7 GGE^{-1}. An HTL contribution of $0.45 LGE^{-1} ($1.69 GGE^{-1}) in the baseline scenario (PSRK, 350 °C) constrains the feed biomass purchase price to a maximum of $413 dry metric ton^{-1} if the goal is to achieve a total $5 GGE^{-1} MFSP. As the reaction temperature decreases, the biomass price constraint becomes slightly more lenient. The price window increases to $432 ton^{-1} at 320 °C, $443 ton^{-1} at 290 °C, and $452 ton^{-1} at 260 °C. Biocrude yield is noted in the scenario analysis as the parameter with the greatest uncertainty and effect on HTL performance metrics. Consequently, yield plays a larger role than temperature in the maximum allowable biomass price. Only with high biocrude yield and a $5 GGE^{-1} fuel cost target can HTL start to allow a $571 dry metric ton^{-1} (2019$) biomass cost target outlined in the Davis et al. (2016) ORP assessment [62], which already makes optimistic assumptions on algae raceway pond technology. A low biocrude yield cannot justify the purchase of biomass at $571 ton^{-1} even for a lenient $7 GGE^{-1} target. In all yield and cost target scenarios, reaction temperature has a minimal effect on achieving said goals. Thus, while temperature and property estimation do have some impact on MFSP, economic analyses should focus on improving algae biomass production and HTL yields.

Microalgae biofuels must compete economically with petroleum diesel and biodiesels derived from other feedstocks (soy, vegetable oil, animal fats, and waste grease). The price of currently available biodiesel has been noted to follow the same price trends of diesel in the past two decades. Retail prices of biodiesel have varied between \$0.74 to \$1.28 LGE^{-1} (\$2.80 and \$4.85 GGE^{-1}) from 2008 to 2017 [111]. Though \$7 GGE^{-1} can be achieved at the current state of algal HTL technology, it is clear that aggressive efforts are necessary to bring algal fuels closer to economic parity with the current biodiesel market. The analysis in Figure 14 demonstrates a heavy burden on the algae feedstock for HTL-produced fuels to achieve \$3 or \$5 GGE^{-1} milestones within the range of biodiesel market prices.

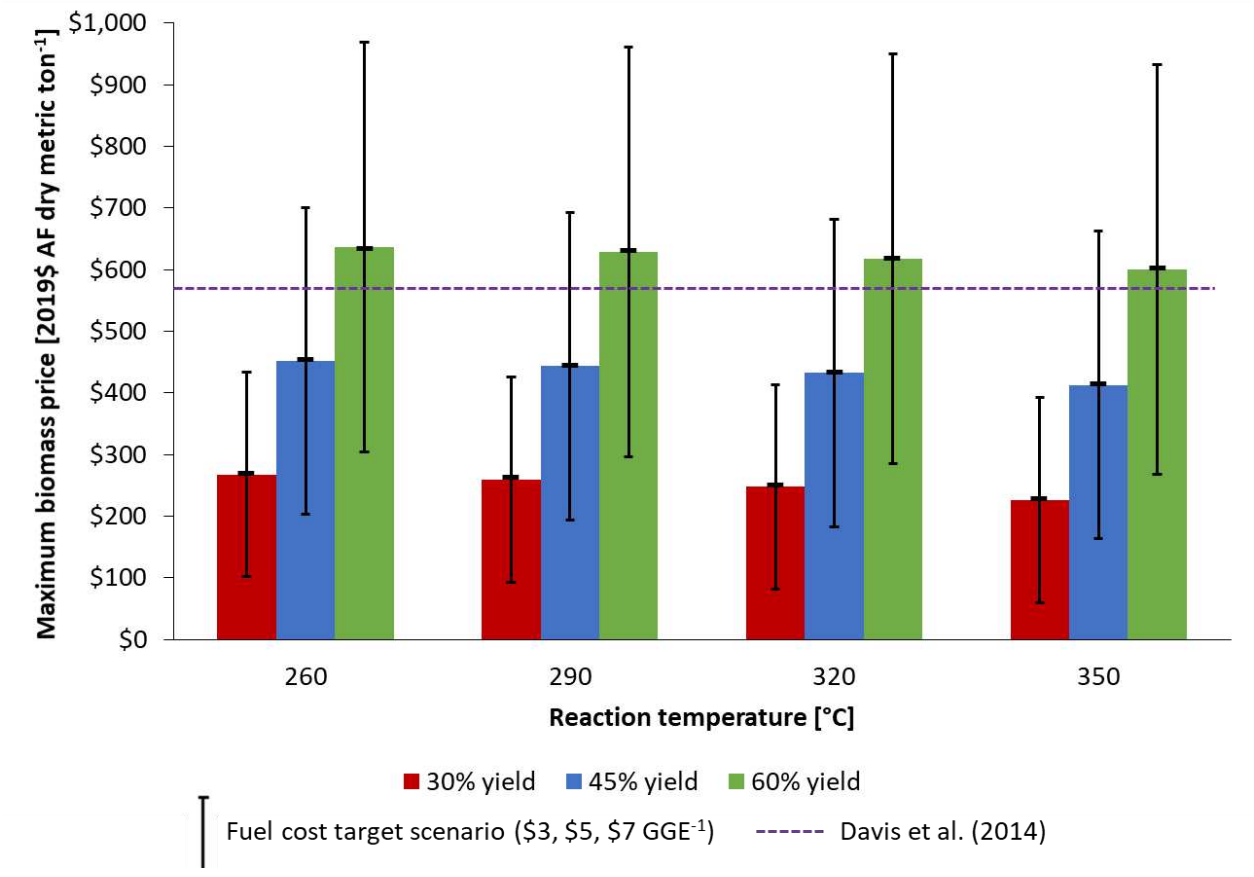

Figure 14. Maximum allowable biomass cost that can drive algal hydrothermal liquefaction to a total fuel selling price baseline milestone of \$5 per gallon gasoline equivalent (GGE) for minimum, baseline, and maximum biocrude yield bounds (30%, 45%, 60%). Error bars represent biomass price bounds to meet \$3 and \$7 GGE^{-1}. A target biomass price at \$571 metric ton^{-1} (purple line) from literature is included for comparison [62]*; scenarios above this line would meet the given fuel cost target.*

HTL is notable as a fuel-only pathway, as opposed to other processes (i.e. lipid extraction, fermentation) that produce residues with co-product potential. All scenarios in this study show that achieving even a \$5 GGE^{-1} target with realistic algae biomass costs would be exceptionally challenging for HTL conversion. Aqueous and gas products can provide recycle credits, but have little to no economic value as co-products. Char solids can contribute as a low-value co-product via carbon sequestration credits. However, these credits are projected to go up to only \$50 per ton CO_2 sequestered by 2026 [112], which would provide minimal economic returns for favoring char yields over other products. A more reasonable approach to increase the viability of HTL is to treat the process as a fuel conversion pathway for biomass residues left behind by other extraction processes. High-value products like bioplastic precursors, pigments, and nutraceuticals can be extracted first [113]. Co-HTL of other inexpensive biomass residues, like wood [114] or crude glycerol [115], can be added to extracted algae residues to increase feed solids loading, produce more energy-dense fuel, and improve the economic efficiency of HTL. More research is warranted on the integration of high-value co-product extraction processes with HTL as a residue treatment pathway and on co-conversion with other feedstocks.

The main findings of this work demonstrate a critical need for further assessment of the economic and environmental impacts of the processing of algae through HTL. The scenario analysis in this work shows that biocrude yield is the most critical parameter impacting the economic viability and environmental impact of an HTL plant. Overall improvements within the HTL system boundary, including yield, are likely limited. For HTL to be an economically viable algae fuel conversion pathway, cost improvements must come from the upstream cultivation side. Additionally, economic performance improvements from increasing yield are offset by an

increase in total greenhouse gas emissions. Co-product development alongside fuels is likely a critical path forward to generate economic credits for algal HTL and meet fuel cost targets. A transparent and readily available model, as described here, can facilitate decisions about key target areas and tradeoffs to push algal HTL toward sustainable commercialization.

3.3.5 Other considerations

The HTL system contributes \$0.45 LGE^{-1} (\$1.69 GGE^{-1}) of the fuel cost in the baseline scenario. This contribution scales by reactor length, which in turn is influenced by the reactor residence time. This is equivalent to the inverse of liquid hourly space velocity (LHSV), which is used in other assessments. Knorr et al. (2013) considered a LHSV range between 2 and 8 hr^{-1}, or a residence time range from 7.5 to 30 min. Experimental studies have used reaction times as long as 1 hour, as in Zhu et al. (2013) and Biller et al. (2011) [80,116] and as short as 3 minutes in Jazrawi et al. (2013) [117]. A generalized kinetic model can predict optimal residence times and product yields to a degree [84]. However, the complexity of the HTL reaction and inaccessibility of production-scale reactors make this model difficult to validate. Regardless of the reactor length, the current study shows that in this simple heating configuration, the significance of the reactor capital cost is roughly an order of magnitude less than the heat exchanger.

As with the heating configuration, the post-reaction separation is also greatly simplified in this analysis. In reality, gravity separation may not sufficiently separate HTL product phases due to the presence of biocrude residues lost in the aqueous phase [21]. Depending on the feed solids content, between 6.4% and 16.1% of biocrude could be present in the aqueous phase [79]. Cui et al. (2020) details the economic impact of a hexane extraction system that can recover most of the lost biocrude. Hexane contributes only 0.3% of the operational expenses, though \$440 dry ton^{-1} feed is also included in the total cost; if feedstock costs were excluded, the relative cost

contribution of hexane would increase but likely remain small. Extra capital expenses include a vacuum filter, separatory funnel, and hexane recovery distillation column, covering an additional 10% to the base HTL capital expenses [115]. More experimental results may justify the inclusion of a biocrude recovery system to the continuous HTL, which may improve biocrude yields and nutrient recovery.

This work demonstrates the importance of high nutrient recycle viability in TEA and LCA scenarios. The reference studies Jones et al. (2014) [21] and Zhu et al. (2019) [60] have assumed up to 90% nitrogen recycle from the HTL and hydrotreater aqueous streams. However, many algae species cannot tolerate certain toxic compounds from directly-recycled aqueous phase. Experimental studies have made efforts to improve the recyclability of the aqueous phase, though they also expose some limitations. *Chlorella* cultures have been reported to adapt well to the toxic effects of HTL aqueous phase, but this tolerance is very species-dependent [20]. Adsorption treatments are a novel option for dealing with toxic components of aqueous phase recycle. Chen et al. (2020) demonstrated this concept in bench-scale *Chlorella vulgaris* cultures with a 35% improvement in growth rate when fresh nitrogen was replaced with recycled nitrogen [118]. However, the removal of toxic nitrogen compounds through adsorption lost a substantial quantity of nitrogen from the recycle stream, which would place the burden back on the cultivation stage to supply more fresh nitrogen. An adsorption system would also likely require additional operating costs; Dowex 50WX8, an effective ion-exchange resin, costs a minimum of \$325 kg^{-1} without considering the cost of waste disposal [119]. The economic and environmental sustainability benefits of the recycling system would likely be offset by high regeneration costs. Sequential HTL has been proposed in Chen et al. (2017) [56], Selvaratnam et al. (2015) [57], Martinez-Fernandez et al. (2017) [58], and Gu et al. (2020) [61] as an alternative to direct HTL

to divert a greater proportion of nitrogen compounds away from the biocrude phase and into aqueous products. A low-temperature pretreatment removes a large portion of non-fuel compounds, followed by biocrude production at lower temperatures (180 – 300 °C). However, biocrude yield has been reported at the lower end, near 30%. Sequential HTL research could benefit from this analysis, but future work should further explore the balance between lower product yields and low operating temperatures.

3.4 Conclusions

This study challenges deterministic assumptions in current hydrothermal liquefaction literature by highlighting the impact of previously unaddressed uncertainties on economic and environmental performance. Modeling efforts should consider the uncertainty in high-temperature thermochemical properties. Operating temperatures below 350 °C can modestly ease energy duties and attempt to improve performance metrics; however, the economic viability of this process is ultimately limited by fuel yield and biomass cost. Global warming potential and net energy ratio are often emphasized as the key environmental impacts in biofuel literature because of their lower impacts over petroleum fuels. This work analyzed a broader spectrum of life-cycle impacts and found that biofuel derived from algal hydrothermal liquefaction performs worse than conventional fuels in some key areas, such as eutrophication potential and ecotoxicity. Results from this work show the need for continuous-scale hydrothermal liquefaction research to reinforce process models with experimental data and reduce uncertainty in critical performance areas such as product yields and nutrient recyclability. There is an open opportunity to build on modeling work by integrating hydrothermal liquefaction downstream of other conversion technologies to better demonstrate the viability of algae fuels. The open source

model supplemented with this work is meant to introduce more transparency into modeling assumptions and help pinpoint potential areas of improvement in future large-scale performance.

CH. 4: SUSTAINABILITY OF ALGAL BIOFUEL PRODUCTION PATHWAYS AS A CASE STUDY OF COMBINED FUZZY SET SCORING METHODOLOGY [f]

4.1 Introduction

Microalgae have been long investigated as a potential biofuel feedstock [120,121]. The high photosynthetic efficiency of maicroalgae allows up to one or two orders of magnitude of greater potential biofuel productivity over land crops [10,122]. However, conversion processes into biofuels are limited by the inherently high water content (approx. 80 wt% moisture) of harvested microalgae [12]. Multiple pathways have been identified for the conversion of high-moisture biomass into biofuels, bypassing the high energy duties of drying.

One major challenge of the algal biofuel production chain is simultaneously maintaining high productivity and generating biomass with optimal composition for improved fuel yields. Hydrolyzed carbohydrates readily convert to ethanol through fermentation and triacylglycerides (TAG) can be transformed into biodiesel through transesterification or similar upgrading processes. Fermentation and lipid extraction can be combined in sequence to maximize algal biofuel yield, which results in a fractionation train called Combined Algal Processing (CAP) [11]. A major downside to CAP is the difficulty of converting proteins and other cell components to fuels through biochemical pathways. One possible use for the residue biomass is to implement an anaerobic digester (AD) that can generate biogas for use as heat or power, albeit with low economic value compared to fuels or co-products. The current state of technology estimates that fractionated algal fuels with AD can be sold at a minimum fuel selling price (MFSP) of $1.15 per liter gasoline equivalent (LGE) ($4.35 per gallon gasoline equivalent (GGE)). However,

---

[f] This chapter was submitted for publication as a peer-reviewed journal article: Chen, P.H., Quinn, J.C. (Manuscript in review). Application of fuzzy set theory for the holistic sustainability assessment of algal biofuel pathways.

assumptions for these results in literature are optimistic and fixed to a particular set of input assumptions. Algal biomass is assumed to be generated with an annual productivity of 30 g m^{-2} d^{-1} and sells for $474 per dry metric ton. Moreover, the majority of the biomass composition is fuel-ready carbohydrates and lipids, with only about 15% of remaining biomass as residue [11]. The viability of fractionation pathways like CAP depends entirely on the biomass feed composition, and there is a need to compare and assess different conversion pathways on equal ground with respect to the feedstock composition and productivity.

Hydrothermal liquefaction (HTL) is a wet thermochemical reaction that serves as an alternative to CAP and only requires a single pass to convert biomass to a biocrude fuel precursor. HTL requires high temperatures and pressures (250 – 375 °C, up to 22 Mpa) to maintain subcritical conditions and avoid vaporization. A major advantage of HTL is its ability to convert proteins – along with lipids and carbohydrates – into fuel [23,84,85,116,123], but extra post-processing required for nitrogen removal must be considered. Aqueous phase byproducts have potential to be recycled back into the algae cultivation system [57,58,118] and produced gases can be used for combined heat and power (CHP) to reduce external energy demand [21,70]. Carbon sequestration credits can be claimed for char solid byproducts [59], but the monetary value and amount of char produced typically do not contribute much to reductions in production costs. Techno-economic assessments (TEA) place the minimum cost of algal HTL fuels in the range of $1.19 to $3.65 LGE^{-1}, or $4.49 to $13.80 GGE^{-1} [21,60], which is not cost-competitive with their fossil fuel counterparts. The cost of these conversion technologies is most sensitive to the cost of biomass.

Though distinct advantages and disadvantages exist between different conversion pathways, there is little work in literature that weighs the multitude of factors which characterize

the concept of sustainability. One optimization study of CAP and HTL [109] has demonstrated the ranges of biomass compositions where fuel yields or fuel prices are favored between the two conversion technologies. HTL is more economically favorable for a wider range of compositions than CAP, but has difficulty converting carbohydrates to fuel [84,85,116,123]. There are plausible situations where CAP would be the preferable conversion technology, *i.e.,* early harvest feedstocks when carbohydrate content is relatively high. Furthermore, LCA was excluded as an optimization parameter. Potential exists for CAP and HTL to be integrated in sequence to increase fuel yield, but no studies in literature have yet demonstrated the fuel production potential of CAP and HTL combined or the sustainability of this concept.

Key performance indicators for sustainable algal biofuels include (but are not limited to) minimum fuel selling price (MFSP), global warming potential (GWP), and net energy ratio (NER). Many technical assessments on algal biofuel production focus on economic targets, with little focus on robust life-cycle assessments (LCA). There is often a trade-off between economic and environmental impacts [63,124], and it is important for assessments in this field to verify that biorefinery process still meet well-defined emissions targets like the Renewable Fuel Standard [5].

Holistic scoring methodologies have been proposed in literature to assess the performance and sustainability of novel technologies. The U.S. Environmental Protection Agency (EPA) has developed the GREENSCOPE methodology, which considers the relative sustainability of a process in up to 140 indicators in the “four Es:” economics, energy, environment, and efficiency [125]. One limitation to GREENSCOPE is that scoring limits are bounded by the expected best- and worst-case performance scenarios in the state of technology and do not account for future targets. Another group [126–130] developed a similar methodology

for algal fuel systems based on the concept of fuzzy set theory. Ubando et al. (2016a) describes methodology for a "stochastic analytic hierarchy process" (SAHP) to determine the effects of five criteria (environmental impact, energy consumption, economics, social acceptability, and robustness) on an algal biorefinery. In Ubando et al. (2016b), a fuzzy mixed-integer optimization approach was used to propagate uncertainties in three objectives: product (fuel) output, environmental footprint, and profit. Although these holistic assessments are highly applicable to algal biorefinery systems, there is a lack of connection in current literature between results and realizable, concrete benchmarks. Moreover, the aforementioned studies do not highlight necessary areas of improvement for the field. The current work seeks to expand on the methodology in previous literature by establishing a sustainability scoring system for algal conversion processes based on reasonable, modern, and relevant engineering targets. Uncertainties in algal biofuel process assumptions are captured through Monte Carlo analysis (MCA) to establish probability distributions of sustainability scores. Results will highlight process improvements that commercial algal production facilities must aim for to maintain a competitive advantage over fossil fuels.

An opportunity space exists for holistic assessments of algal biofuel economics and LCA metrics, as many algal biofuel assessments focus heavily on one objective. Current assessments also generally lack a consistent methodology to evaluate sustainability metrics across different conversion pathways. In this work, engineering process models are coupled with TEA and LCA to establish comparable baseline metrics for HTL, CAP, and the integrated CAP-HTL train. Fuzzy set theory is then applied to the results to assess the degree to which algal biofuel pathways satisfy multiple sustainability metrics. Composition and biomass productivity are emphasized as key variables that influence the performance of CAP and HTL. An MCA is

included to account for uncertainty in other key parameters, such as product yields and life cycle inventory data. The goal of the work is to establish an equitable sustainability scoring system to help inform decisions for selecting HTL, CAP, or the CAP-HTL combination as a holistically sustainable algae-to-fuel pathway, instead of focusing only on a single sustainability metric. Recommendations for future directions of algal biorefineries will be discussed based on the conclusions drawn here.

4.2 Methodology

Baseline process simulation models for each of the conversion pathways were developed in the software Aspen Plus V11 (Aspentech, Inc.). To account for the potential variability in algal feedstock composition and productivity, a composition-based biomass growth model was constructed in MATLAB (MathWorks, Inc.). Aspen Simulation Workbook (Aspentech, Inc.), an Excel (Microsoft Corporation) plug-in, was used to perform the large numbers of simulations for the baseline and Monte Carlo analyses. Uncertainty distributions of process modeling parameters were developed with @RISK (Palisade) and were incorporated into overall MCAs of each algal fuel pathway. For every simulation case, TEA and LCA metrics were calculated from process model material and energy balances and translated into holistic scores based on fuzzy membership functions for each performance metric.

4.2.1 Process modeling

A process flow diagram of the algae-to-fuel pathway options is shown in Figure 15. Process modeling work was divided into two parts. Cultivation modeling included a composition-based algal growth model that was leveraged for feedstock TEA and LCA metrics. These feedstocks were then used as inputs into each of the conversion models for HTL, CAP-AD, and CAP-HTL.

4.2.1.1 Cultivation

Open raceway pond model

Commercial-scale production of algal biomass in open raceway ponds (ORP) was modeled in Excel. A reference ORP model and economic assessment [62] served as the basis for material and energy balance calculations with assumptions outlined in Table 9. Some key differences in baseline assumptions from literature included a lower average productivity of 17.5 g m^{-2} d^{-1} based on a compositional growth model [109,131], higher ash content based on literature [62,132], and higher nitrogen requirements based on a protein conversion factor of 4.78 g protein to 1 g cellular nitrogen [133].

Table 9. Key baseline inputs to cultivation, HTL, and CAP process models.

Parameter	Value	References
Cultivation		
Baseline productivity [g m^{-2} d^{-1}]	17.5	[109,131]
Facility footprint [acres]	5,000	[11]
Pond depth [m]	0.25	[11]
Protein % of protein-rich biomass [wt%]	46%	[131]
Protein to nitrogen conversion factor	4.78	[109,133]
Biomass ash content [dry wt%]	5.8% (*C. vulgaris*) 6.8% (*N. granulata*)	[62,132]
Nutrient recycle [% N or P demand]	60%	[124]
HTL		
Biocrude yield from proteins [% yield]	45%	[109]
Biocrude yield from carbohydrates [% yield]	20%	[109]
Biocrude yield from lipids [% yield]	85%	[109]
Aqueous phase yield from proteins [% yield]	48%	[109]
Aqueous phase from lipids [% yield]	15%	[109]
Solids yield from carbohydrates [% yield]	42%	[109]
Gas yield from proteins [% yield]	7%	[109]
Gas yield from carbohydrates [% yield]	38%	[109]
CAP		
Pretreatment release of fermentable carbohydrates [% yield]	90%	[62]
Ethanol yield from fermentable carbohydrates [% theoretical yield]	92%	[134]
Extracted TAG yield [% yield]	95%	[134]
Anaerobic digester hydraulic retention time [d]	20	[62]

Composition-based algae growth model

The performance of each algal biofuel production pathway is highly dependent on the composition of the feedstock. A composition-based growth model [131] was implemented to dynamically define the composition and biomass productivity of two commonly cultivated microalgae strains, *Chlorella vulgaris* and *Nannochloropsis granulata*, over time. The growth model transforms ten lumped metabolic reaction pathways into a system of kinetic equations that can be expressed and solved through state variables. It should be noted that the original model did not account for the dependent relationship between temperature and growth rate. In this work, the growth model was modified with a thermal efficiency factor, θ_T [135,136], to

incorporate temperature and light data from the third Typical Meteorological Year (TMY3) weather dataset at many potential locations across the United States [137]. In all growth simulations in this work, TMY3 data from June 1 – June 20 in Hilo, Hawaii, was used as a prime candidate dataset based on season and location to achieve high productivity values in the summer. The chosen location was assumed to be one of few regions that can support year-round algae production; however, average annual productivity was expected to fall slightly below the summer productivity values used in this work. The list of state variables with baseline initial conditions is outlined in Table C - 1.

The full system of variables and equations in the growth model is described in detail in Tables C – 2 through C – 5. Initial conditions for all state variables were assumed fixed. Protein-rich biomass is defined here as the sum of cellular proteins and other cell material, such as cell walls. As reported in Table 9, protein content is assumed to compose a fixed 46% of remaining biomass [131]. In figures, the terms "proteins" and "protein-rich biomass" are used interchangeably. Soluble nitrogen and phosphorus (S_{NO} and S_P, respectively) were based on the medium recipe of Bold's basal medium [138]. The system of linear equations was numerically solved in MATLAB using the native *ode23s* solver for stiff systems. The time step was 1 hr to match the resolution of TMY3 weather data. Total biomass density and areal productivity were calculated from the sum of volatile suspended solids (VSS) in Eq. 5 and 6.

$$X_{VSS} = X_{CPO} + X_{CH} + X_{LI} \tag{5}$$

$$Productivity = \frac{(X_{VSS,harvest} - X_{VSS,initial}) \times b_{reactor}}{(t_{harvest} - t_{initial})} \tag{6}$$

The growth model was applied to *Chlorella vulgaris* and *Nannochloropsis granulata* using parameters from modeling literature [109,131]. The key differences between the two species are the maximum growth rate parameter, $\hat{\mu}$ [109,139,140], and the accumulation rates of

stored carbohydrates and lipids. Here, the literature value of $\hat{\mu}$ for *Nannochloropsis gaditana* is substituted for *Nannochloropsis granulata*. The list of growth model parameters and their definitions can be found in Table C - 1.

4.2.1.2 Biofuel conversion

Hydrothermal liquefaction

The HTL model was previously developed for previous work by the current authors [124]. The open-source model is flexible to HTL feed compositions, product yields, and other process operating conditions that affect material or energy balances. All HTL simulations were conducted at 350 °C with a reactor residence time of 30 min. The predictive Soave-Redlich-Kwong (PSRK) equation of state was established as the most suitable model to estimate thermodynamic properties of stream components at HTL operating conditions. Product yields (Table 9) were determined by an additive yield model [109]. Aqueous phase streams were assumed to contain dissolved nitrogen and phosphorus, 60% of which was assumed to be recyclable for algal cultivation in the baseline scenarios. A CHP system was implemented to use biogas generated from HTL and upgrading processes for process heating, reducing the demand for purchased natural gas. External heat duties of HTL were minimized by maximizing the HTL heat exchanger surface area, albeit at the expense of greater capital costs.

Combined Algal Processing

An Aspen Plus model was developed for CAP with consultation from partners at the National Renewable Laboratory (NREL) [11]. In CAP, the feed stream first enters a mild hydrolysis pretreatment reactor at 150 °C with 1 wt% sulfuric acid to release fermentable carbohydrates. Hydrolyzed biomass then enters a fermentation train composed of a primary fermentation vessel (909 m^3 capacity), seed fermenters, and ethanol distillation equipment. The

remaining biomass is sent to a wet extraction column that uses agitators to separate lipids from the biomass slurry. Finally, the purified lipids are passed through a hydrodeoxygenation (HDO) unit for upgrading TAGs to fatty acid methyl esters (FAME). The final biofuel products, ethanol and FAMEs (as biodiesel and naphtha) are considered the functional product for CAP. Experimental results from the Rewiring Algal Carbon Energetics for Renewables (RACER) consortium were implemented for the baseline analysis and used as the basis for MCA distributions [134]. An anaerobic digester (AD) process was attached downstream of the main CAP model to process the protein-rich residue stream for the CAP-only pathway and is referred to as "CAP-AD" from this point forward. AD sizing information was also derived from the same reference [11].

For the integrated CAP-HTL pathway, the CAP and HTL simulations were combined as a single Aspen Plus file. The post-CAP residual stream was diverted to the HTL process model instead of AD. Heat integration was implemented with CHP to reduce energy demand for CAP-HTL using the same principle of heat duty minimization as the standalone HTL process.

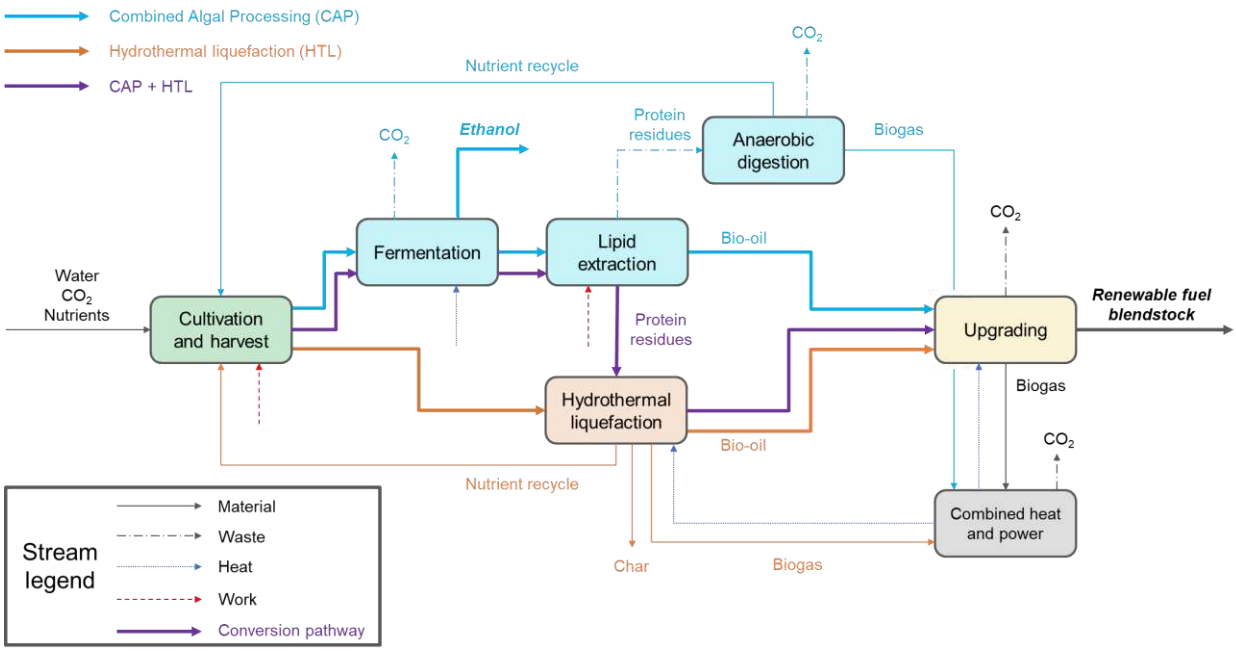

Figure 15. Process flow of downstream conversion pathways. The blue pathway represents CAP, where protein residues are sent to AD; the orange pathway represents whole-algae HTL; the purple pathway integrates CAP and HTL by diverting protein-heavy CAP residues to HTL.

4.2.2 Techno-economic analysis (TEA)

The MFSP was determined from "Nth-of-a-kind" (NOAK) economic plant assumptions, as outlined by Bioenergy Technologies Office (BETO) economic assessment standards [88], listed in Table C - 7. These parameters reflect a theoretical commercial-scale plant that has reached technological maturity and can be compared with other NOAK plant literature. The MFSP was solved one of two ways: the first method used an Excel iterative solver to calculate the product revenue required to achieve a net present value (NPV) of $0 for the plant's full 30-year lifetime. A faster solution [141] was used for bulk calculations with a large number of iterations. The second method holds true for all economic models with the same NOAK plant assumptions and follows the simple linear equation in Eq. 7. MFSPs solved with the shortcut method were validated within 6% error of MFSPs solved with the iterative method for all process models in the current work. All liquid fuel products were lumped into a single cost on an

energy equivalent (LGE or GGE) basis based on the higher heating value (HHV). The cost year of analysis was 2019, the most recent year available in the Chemical Engineering Plant Index [89].

$$Annual\ breakeven\ revenue\ [\$\ yr^{-1}] = 0.140 \times CAPEX\ [\$] + 1.0144 \times OPEX\ [\$\ yr^{-1}] \quad (7)$$

Capital cost estimates of CAP and HTL equipment were scaled from literature process models [11,124]. The capital costs of HTL upgrading equipment were scaled as a lumped system; details about hydrotreating and hydrocracking fractions were assumed unchanged from Chen and Quinn (2021). An on-site hydrogen generation plant for HTL was excluded; hydrogen was purchased instead [124]. Costs of electricity were obtained from U.S. Energy Information Administration data [92], natural gas from [93], and purchased hydrogen from [94]. Variable operating costs of other miscellaneous materials in the CAP model were taken from [11]. Fixed operating costs were derived from respective ORP and conversion modeling assessments [62,93]. Employee salaries were scaled by the cost year index for labor according to the U.S. Bureau of Labor Statistics [91]. Unit costs and cost indices were based on typical values for the United States. Detailed capital estimation parameters and operating costs are listed in Tables C – 8 through C – 12.

Capital and operating costs for cultivation were derived from a commercial-scale open raceway pond (ORP) model [62]. Key cultivation assumptions like productivity, composition, and nitrogen consumption were derived from the compositional growth model reference [131] and integrated into the ORP economic model. Although the algal growth model used nitrate as its assumed nitrogen source, the nutrient basis was kept as ammonia and diammonium phosphate for the purpose of operating costs in the uncertainty analysis.

4.2.3 Life-cycle assessment (LCA)

In all scenarios, the primary function was energy production as liquid fuel. The LCA functional unit was thus chosen as 1 MJ of biofuel. Cultivation and harvesting facilities were assumed to be co-located with conversion, so feedstock transportation impacts were negligible. Environmental impacts were evaluated with an attributional LCA approach. Consequential LCA factors, such as indirect land use change and market effects, were not considered.

Life-cycle inventory data was collected from the ecoinvent Version 3.4 database [95], with some exceptions described in the following paragraph. The "cutoff" model was applied to applicable inventory. The Tool for Reduction and Assessment of Chemicals and Other Environmental Impacts (TRACI) version 2.1 assessment method [142] was used to calculate GWP. NER was calculated as the ratio of total energy input to total fuel energy output as the HHV. An NER less than 1 is desirable given this definition.

Life-cycle impacts and energy duties of algae biomass feedstock production were derived from the algae ORP model [62]. Hydrogen life-cycle data were collected from [96]. The baseline technology was assumed to be steam-methane reforming; however, other hydrogen production technologies were considered in the uncertainty analysis. The life-cycle impacts of hydrogen were converted from the ReCiPe method to TRACI. The HHV of hydrogen was included as an energy input for the NER, as it was considered necessary in the upgrading stage to increase the energy value of the fuel product [124]. Energy required for fuel transportation and distribution was included in the LCA system boundary [67]. A standard +0.075 kg CO_2 eq MJ^{-1} from gasoline or diesel end use and +0.064 kg CO_2 eq MJ^{-1} for ethanol end use were included in the final GWP results such that the system boundary is well-to-wheel [97]. Similar to the TEA, the

nitrogen life cycle inventory data for ammonia and diammonium phosphate were used instead of sodium nitrate in the scope of cultivation and nutrient recycle.

4.2.4 Fuzzy set scoring

A holistic scoring system based on fuzzy set theory was developed to bring TEA and LCA metrics together in a single sustainability metric. Fuzzy membership functions were developed for three objectives: MFSP, GWP, and NER. Each objective parameter was assigned a satisfaction factor, λ, as a degree of satisfaction (referred to as "satisfaction score" in this work) within set thresholds. The MFSP, GWP, and NER membership functions followed a minimization shape (Figure 16) where a maximum MFSP or LCA limit was set for a "desirable" threshold ($\lambda = 1$) and another maximum limit for an "acceptable" threshold ($0 < \lambda < 1$). The desirable threshold for MFSP was set at \$0.79 LGE^{-1} (\$3 GGE^{-1}) based on average global gasoline costs, which hit a minimum in 2016 at \$0.78 L^{-1} (\$2.95 gal^{-1}). [143]. An acceptable threshold of \$1.85 LGE^{-1} (\$7 GGE^{-1}) for MFSP was chosen based on high average gasoline costs in Europe in 2020 [144]. Thresholds for GWP were based on the life-cycle GWP of petroleum diesel. The desirable threshold was based on the RFS target for advanced fuels, which mandates a 50% reduction in emissions from diesel [5]; the acceptable threshold is the diesel baseline of 0.092 kg CO_2eq MJ^{-1} [103]. The NER of conventional diesel has been established to be 0.19 [64]. The desirable target NER was rounded to 0.20 and defined as the desirable threshold in the present work, but no explicit NER goals has been specified by any literature. Hence, the acceptable limit of NER was assumed to be 1, representing an equal balance of energy input to output.

An overall satisfaction factor, λ_o, can be defined such that $\lambda_o \leq \lambda_i$ for all i objective satisfaction factors. Here, λ_o has been defined in Eq. 8 as:

$$\lambda_o = \lambda_{i,avg} \times \lambda_{i,min} \quad (8)$$

A comparison was made between CAP-AD, HTL, and the integrated CAP-HTL train across the entire compositional domain to determine λ_o as a function of feed composition. The data are presented with respect to a baseline set of membership functions defined in Figure 16.

The multitude of compositional scenarios required the Aspen Simulation Workbook (Aspentech, Inc.) extension in Excel (Microsoft Corporation). Inputs could be varied in the Excel interface to generate and store arrays of results without requiring direct changes to the original Aspen Plus model. Results stored in Excel were then exported to MATLAB (Mathworks, Inc.) to generate the key performance indicators (MFSP, GWP, and NER) for each simulation. In the baseline analysis, compositional sets were varied in the compositional space (consisting of proteins, carbohydrates, and lipids) by 5 wt% on an ash-free basis. Thus, 231 compositional sets were generated. A ternary plot diagram of compositions was generated for each pathway in Figure 15: CAP-AD, HTL, and CAP-HTL. Ternary plot and spider web plot scripts were developed in MATLAB by third parties [145,146].

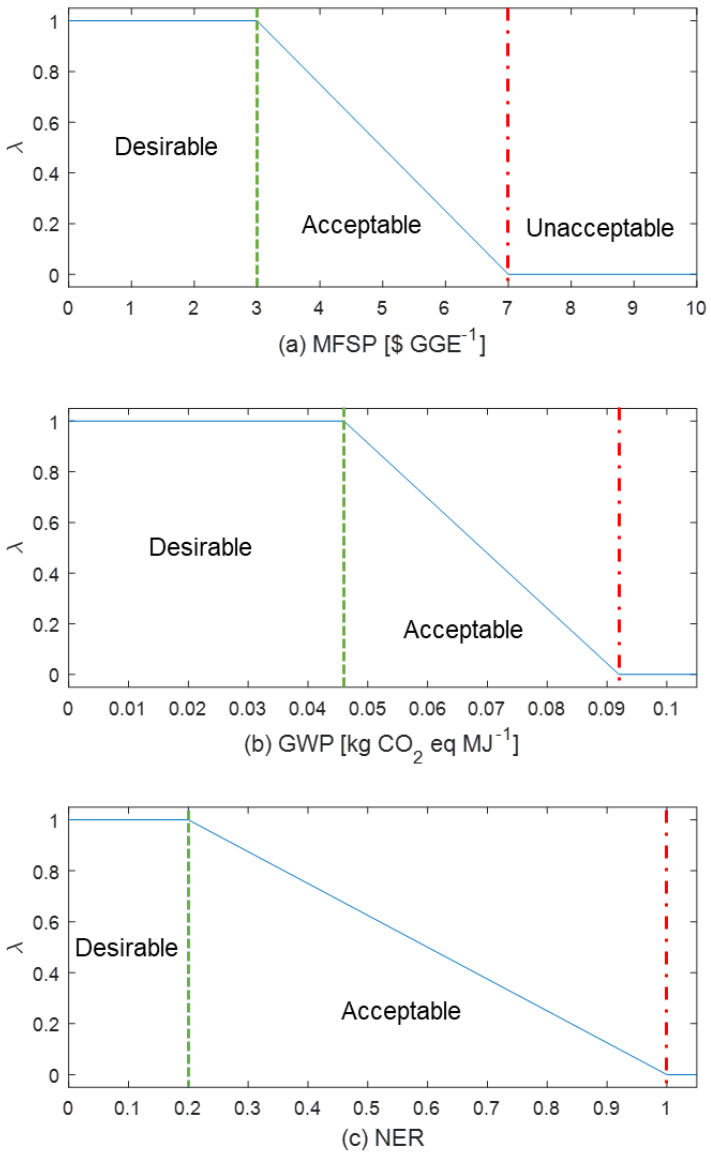

Figure 16. Linear fuzzy membership functions for objective minimization for a) MFSP, b) GWP, c) NER. Thresholds define a "desirable" region and an "acceptable" region based on the satisfaction factor, λ. The most acceptable threshold (dashed green line) corresponds to a λ of 1 and a λ of 0 is unacceptable (dot-dashed red line). The membership functions map relevant metrics to a corresponding λ value with all metrics combined into an overall satisfaction score, λ_o.

4.2.5 Uncertainty analysis

A Monte Carlo analysis (MCA) was first performed on select cultivation scenarios and the resulting feedstock metrics (biomass cost, GWP, and NER) were propagated through the given biofuel pathways (Figure 15). Probability distributions were formed for important and

uncertain parameters using the @RISK (Palisade) plug-in for Excel; distributions are listed in Table C - 5 and Table C - 6. Compositional growth model parameters were varied by ±20% to create triangular distributions. CAP yield distributions were determined by benchmarks that were established in RACER [134]. HTL yield distributions were taken from [109]. Operating cost and life cycle inventory distributions were derived from relevant studies cited in Table C - 6. Triangular distributions were selected for most parameters except for the initial value of R (chlorophyll-to-carbon ratio), which was assumed to be a normal distribution [147,148]. All scenarios were simulated for $n = 1000$ iterations. An MCA of HTL with $n = 2500$ iterations was used to determine if $n = 1000$ was adequate for convergence. The difference in mean and standard deviation between $n = 1000$ and $n = 2500$ simulations was negligible.

4.3 Results and discussion

Assumptions for the process modeling and subsequent TEA and LCA were developed from current algal biofuel literature. Fuzzy membership functions based on literature benchmarks were developed for TEA and LCA metrics and applied to all subsequent process modeling scenarios. Baseline scenarios were developed based on the current state of cultivation and fuel conversion technology. A Monte Carlo analysis (MCA) was subsequently conducted to understand the propagation of uncertainties by varying assumptions within the entire fuel production system boundary, from cultivation through end use.

4.3.1 Baseline analysis

The growth model yields a baseline *Chlorella vulgaris* summer productivity of 17.5 g m^{-2} d^{-1} using the baseline assumptions outlined in Table 9. The composition on an ash-free basis is 54% protein-rich biomass, 27% carbohydrates, and 19% lipids. This feedstock establishes the

following baseline analysis of TEA and LCA metrics of the HTL, CAP-AD, and CAP-HTL conversion pathways.

4.3.1.1 Minimum fuel selling price (MFSP)

The biomass cost for the baseline scenarios was fixed at \$0.85 (dry kg algae)$^{-1}$ based on results from the baseline cultivation process model. Combining the feedstock cost with the different conversion models results in baseline MFSPs of \$2.02, \$4.36, and \$2.24 LGE^{-1} (\$7.64, \$17.65, and \$8.98 GGE^{-1}) for HTL, CAP-AD, and CAP-HTL, respectively (Figure 17a). None of the baseline biofuel pathways achieve economic parity with their fossil fuel equivalents. In all pathways, the cost of biomass dominates the MFSP, making up 85% of the MFSP of HTL, 80% of CAP-AD, and 70% of CAP-HTL. The majority of remaining costs is attributed to the capital investment in conversion. The capital costs of HTL, CAP-AD, and CAP-HTL comprise 12%, 11%, and 18% of final costs, respectively. Operational energy costs are negligible in HTL alone, as gas generated in the HTL reaction can supply enough heating duties for CHP. However, this gas is not used for hydrogen generation as described in other HTL literature [21] and therefore energy costs in the present work are captured in cost of purchased hydrogen. Nutrient recycling can generate 4 – 5% of cost savings across all pathways assuming that the recyclability of nutrients is fixed at a baseline of 60%. As demonstrated in a previous HTL scenario analysis [124], deviating from the baseline nutrient recyclability assumption by ±30% results in modest changes in cost to the HTL system itself. However, when the high contribution of biomass cost is considered, the impact of the nutrient recycle sensitivity is greatly diluted.

4.3.1.2 Global warming potential (GWP)

Baseline GWPs are 0.031, 0.044, and 0.062 kg CO_2 eq MJ^{-1} for HTL, CAP-AD, and CAP-HTL, respectively, and presented in Figure 17b. CAP-AD yields the lowest amount of

biofuel because of the high protein content of the feed. However, the process generates large quantities of CO_2 from the residual biomass because of the AD system. In HTL and CAP-HTL, where fuel yields are much higher than in CAP-AD, fuel end use emissions create large contributions to GWP impacts when normalized to 1 MJ of produced biofuel, as more captured carbon is released back into the atmosphere as CO_2. Thus, per unit of fuel produced, CAP-AD can claim the most carbon capture credits, but the lack of a sequestered carbon product (present as biochar solids in HTL) means that more CO_2 is released back into the atmosphere. The CAP-AD and CAP-HTL systems consume more electricity and generate more associated emissions due to the power requirement in the lipid extraction phase of CAP. In summary, the baseline HTL and CAP-AD both meet the RFS target of 50% reduction in emissions compared to conventional diesel. CAP-HTL has a lower baseline GWP than conventional diesel but does not meet the 50% GWP reduction target of the RFS.

4.3.1.3 Net energy ratio (NER)

NER contributions from electricity, hydrogen, and natural gas inputs are represented in Figure 17c. The baseline NER is most favorable in HTL at 0.28 MJ input per MJ output. CAP-AD results in the worst baseline NER of 0.61, owing largely to low liquid fuel yields. CAP-HTL maintains a compromise between the two conversion processes at an NER of 0.41. CAP-HTL requires energy inputs for both HTL and CAP, but fuel yield improvements over CAP-AD make the integrated train more energetically favorable. Keeping consistent with the NER accounting methods in previous work [124], hydrogen is included as an energy input due to the inherent energetic value that hydrogen adds to the upgraded biocrude and extracted lipid products in HTL and CAP, respectively. Hydrogen is assumed to be generated from steam-methane reforming; therefore, natural gas and hydrogen are connected when considering NER in the present work.

As mentioned in Section 3.1.2, more electricity is required for CAP than for HTL. Electricity in the standalone HTL process contributes to only 36% of energy inputs due to energy recovery from biogas to electricity through CHP, while CAP-AD energy duties are divided nearly evenly between electricity (52%) and natural gas / hydrogen (32% / 16%). CAP-HTL energy duties are divided more evenly at a 42% contribution from electricity, 23% from natural gas, and 34% from hydrogen. All baseline pathways maintain a NER < 1, but none surpass the conventional diesel benchmark NER of 0.20.

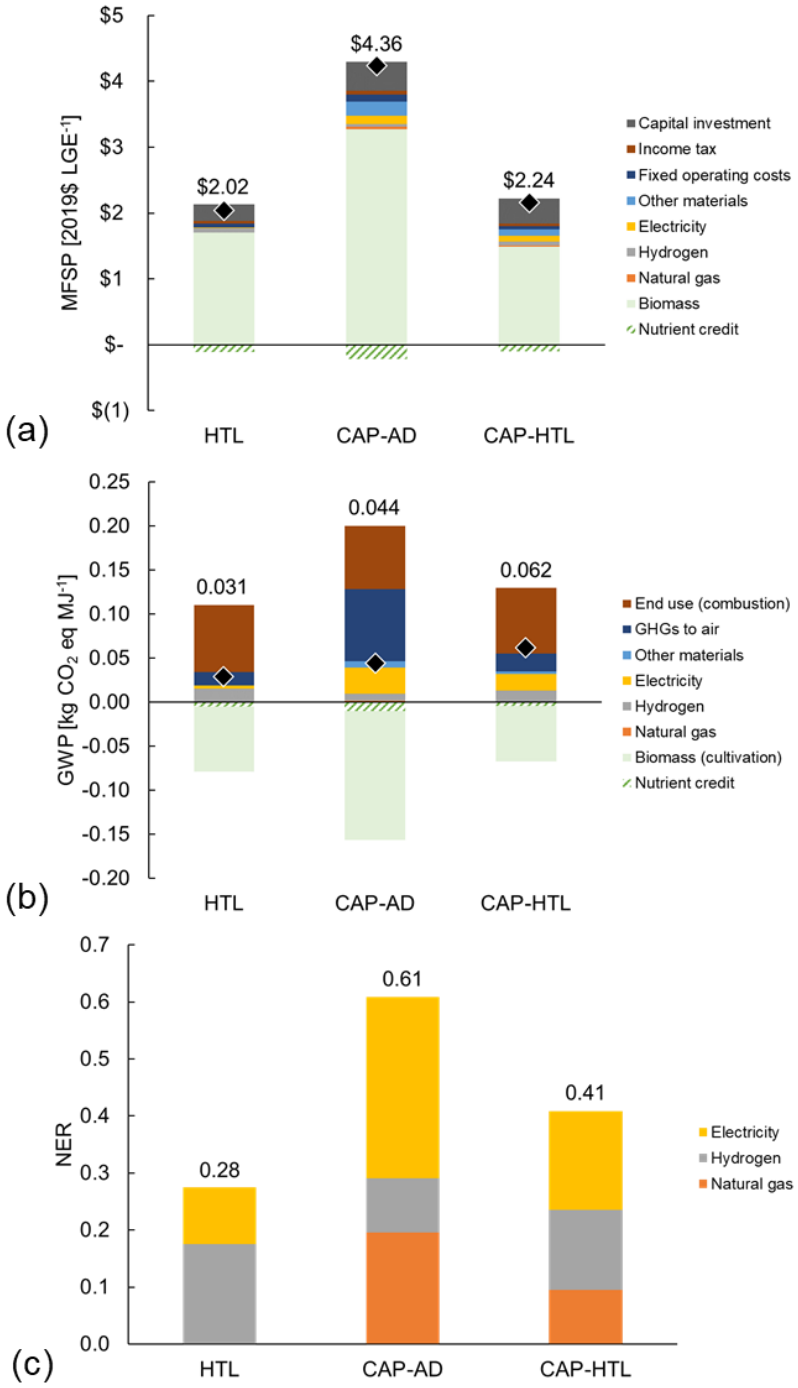

Figure 17. Breakdown plots of a) MFSP, b) GWP, c) NER of HTL, CAP-AD, and CAP-HTL by major material and energy flows. Net MFSP and GWP impacts are denoted by black diamonds.

4.3.2 Sustainability metrics as a function of biomass composition

The baseline scenarios present the performance of conversion pathways with respect to a typical feedstock given the current state of cultivation technology. However, composition is a key factor that can be manipulated in the cultivation stage to drastically change the performance of these conversion pathways. This section outlines the process modeling results that arise from varying the biomass feed composition beyond the baseline assumptions while fixing all other parameters (productivity, conversion yield, etc.) across the three conversion pathways. Results in this section are presented as ternary contour plots of λ_o over the entire domain of possible ash-free compositions. Breakdowns of λ_o by individual objectives (MFSP, GWP, NER) by composition can be found in Figures C – 2 through C – 5. Discussion focuses on optimal compositional points based on maximum λ_o values, which although infeasible to achieve, provide directions toward ideal algae compositions for different pathways.

4.3.2.1 Hydrothermal liquefaction (HTL)

A ternary contour plot of λ_o of the baseline HTL pathway as a function of composition is shown in Figure 18a. The maximum λ_o achieved is 0.46 when the feed is 100% lipids, which is impossible to achieve in phototrophic cultivation. In the additive HTL yield model, carbohydrates contribute the least to biocrude formation, proteins contribute modestly, and lipids convert readily to biocrude. Therefore, it is a prerequisite for HTL to use microalgae feedstocks with low carbohydrate content to achieve as high of fuel yield, and therefore λ_o, as possible.

In favorable compositional scenarios (high lipids and proteins), the GWP impact increases with fuel yield because of end-use emissions accounting; the more fuel that is produced, the more captured CO_2 is released back into the atmosphere. Captured carbon is considered sequestered if its end fate is biochar, which provides an opportunity for algal biofuels

to approach carbon neutrality. However, the trade-off between lower product revenue and environmental benefits is already unfavorable toward biochar production. NER is slightly favored toward low carbohydrate content, providing a minor benefit to λ_o in these scenarios. In no scenario does the NER of HTL cross the acceptable threshold of satisfaction.

MFSP is the dominant influence on λ_o between the three objectives. According to the ternary plot of MFSP λ (Figure C - 3), a line can be drawn between two compositional points (50% lipids + 50% carbohydrates to 15% lipids + 85% proteins) denoting the frontier where the MFSP objective is completely unsatisfied ($\lambda = 0$). More than half of the possible combinations of feed compositions are therefore completely unviable for the baseline HTL process. Even with high lipid content, the baseline HTL scenario indicates that current feedstock costs are too high for HTL fuels to meet economic targets.

As suggested in a harmonization study of algal biofuels [55], increasing productivity helps algal growth systems to approach sustainability targets but diminishing returns on TEA and LCA performance begin around a productivity benchmark of 35 g m^{-2} d^{-1}. In the following scenario, the baseline algae productivity was doubled to 35 g m^{-2} d^{-1}, reflecting a very optimistic, but likely necessary, cultivation target. The ternary plot of the improved productivity scenario is shown as Figure 18b. Trends in λ_o with respect to composition appear the same as the baseline scenario, but the magnitudes of λ_o approaches 1. The maximum λ_o is 0.89, which occurs where the feed is composed of 85% lipids, 0% carbohydrates, and 15% proteins. At this high-lipid range, all three objectives are near full satisfaction. However, as lipid composition approaches 100%, satisfaction of the GWP objective decreases because of the aforementioned trade-off between fuel yield and end-use emissions. It is also important to note that a high-lipid, zero-carbohydrate feedstock would be impossible to achieve without pre-processing. Outside the

range of maximum λ_o, improvements in overall satisfaction are driven by MFSP; GWP and NER are far less sensitive to changes in productivity. In compositional areas where realistic feedstocks can be generated, λ_o still trends well below 1.

4.3.2.2 Combined Algal Processing with anaerobic digestion (CAP-AD)

The maximum λ_o achieved for the baseline CAP-AD pathway is 0.32. As shown in Figure 18c, this maximum occurs near a composition of 95% lipids, 5% carbohydrates, and 0% proteins. The NER of the best-performing scenario is favorable at 0.24, but the MFSP is \$1.33 LGE^{-1} (\$5.03 GGE^{-1}) and the GWP is 0.068 kg CO_2 eq MJ^{-1}, which moderately satisfy their respective sustainability targets. One of the difficulties in implementing CAP is the inability to convert proteins to a fuel product. As carbohydrate and lipid content approach zero, the MFSP and NER approach infinity because no fuels are produced. CAP-AD is completely unviable if the lipid composition falls below approximately 50% due to low fuel yields.

As demonstrated in the baseline analysis, the cost of biomass comprises the majority of expenses by a large margin. With doubled productivity, the maximum λ_o value more than doubles to 0.65 at the compositional point of 70% lipids, 30% carbohydrates, and 0% proteins (Figure 18d), which is driven heavily by improved MFSP. The GWP and NER are far less sensitive to productivity improvements, as LCA metrics do not benefit from the principle of economy of scale. Similar to HTL, higher fuel yields improve the satisfaction of MFSP and NER objectives but also result in higher GWP from end-use emissions, driving λ_o down in favorable compositional regions. Despite improvements to λ_o overall with high productivity, the region of viable compositions for CAP-AD remains limited, requiring at least 30% lipids.

4.3.2.3 Combined Algal Processing with hydrothermal liquefaction (CAP-HTL)

Trends in λ_o of the CAP-HTL pathway with respect to composition (Figure 18e) are similar to those of the CAP-AD pathway. The maximum λ_o for the baseline productivity, 0.32, is the same as the maximum λ_o of CAP-AD and occurs at the compositional point. Outside of these unrealistically high lipid compositions, the addition of HTL to CAP allows for a wider range of viable compositions compared to CAP-AD due to the ability to process higher-protein feed into biofuel. It should be noted that HTL yields in CAP-HTL are static regardless of feed composition, as the CAP process removes almost all carbohydrates and lipids upstream of HTL, resulting in effectively a 100% protein HTL feed. At least 40% lipids are still required to stay outside the unsustainable range where $\lambda_o = 0$.

At doubled algal productivity (Figure 18f), the maximum λ_o nearly doubles to 0.63 and occurs at the compositional point of 70% lipids, 30% carbohydrates, and 0% proteins. Similar to the conclusions of the other pathways, there exists an optimization tradeoff between high fuel yields (resulting in higher satisfaction of MFSP and NER objectives) and high end-use emissions that decrease satisfaction of the GWP objective. The performance of CAP-HTL follows similar trends to CAP-AD, where high-lipid biomass is strictly favored. The major benefit of integrating CAP and HTL arises from higher fuel volumes that can be derived from all cell components. For a highly productive, carbohydrate-heavy feedstock, CAP-HTL would be the preferable fuel conversion pathway. Like HTL and CAP-AD, the ranges of GWP and NER of CAP-HTL change negligibly when productivity is doubled and improvements to λ_o stem from improving MFSP.

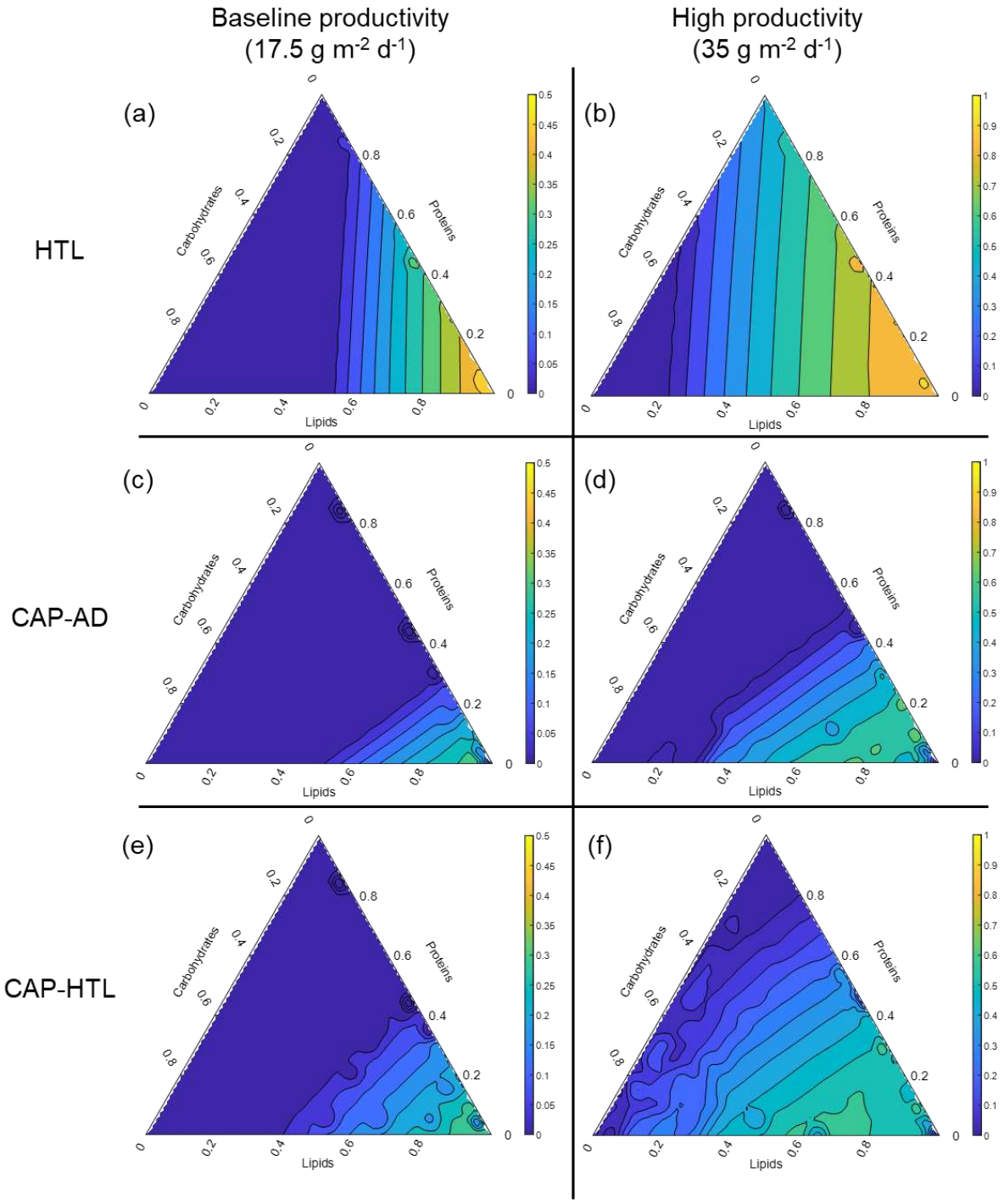

Figure 18. Ternary diagram representation of λ_o as a function of algae feed composition of each pathway. The baseline algae feedstock productivity is assumed to be 17.5 g m^{-2} d^{-1}. Scenarios presented are: a) baseline HTL, b) 2× productivity HTL, c) baseline CAP-AD, d) 2× productivity CAP-AD, e) baseline CAP-HTL, f) 2× productivity CAP-HTL. Note the different color scales for the doubled productivity scenarios (right-hand side).

4.3.3 Uncertainty analysis

In Section 3.2, key process assumptions were kept static to solely investigate the effect of composition on the viability of CAP and/or HTL as algae-to-fuel pathways considering environmental and economic considerations. In reality, many uncertainties are scattered across the entire algae-to-fuel system boundary. The following section addresses practical feedstock scenarios within the current state of cultivation technology. The fuzzy set scoring system is leveraged to highlight areas that must be improved to achieve a better probability of meeting targets in the given sustainability objectives.

4.3.3.1 Composition-based cultivation model

Composition-based growth of *Chlorella vulgaris* and *Nannochloropsis granulata* was modeled using an MCA with $n = 1000$ iterations. Two harvesting conditions were used to generate different compositions: 1) final total biomass concentration of 500 g m^{-3} and 2) 50 wt% lipids (ash-free basis). The goal of the former harvesting method is to maintain productivity in continuous operation, while the latter harvesting condition is a novel alternative to the conventional method that aims for a target biomass composition in a nutrient-starved state. With the two different harvesting methods, different compositions can be achieved with the same initial growth conditions and allow for a practical comparison of sustainability between alternative feedstocks. Compositional growth model results are compiled in Table 10 and reported in the form of mean ± standard deviation. Figure C - 1 contains growth curves of the MCA simulations for the cultivation scenarios outlined here.

Table 10. MCA ($n = 1000$) results for the compositional growth model with three hypothetical cultivation and harvesting scenarios. Results are reported as the mean ± standard deviation.

Species	Harvest condition	Areal productivity [g m^{-2} d^{-1}]	Protein-rich biomass [ash-free wt%]	Carbohydrates [ash-free wt%]	Lipids [ash-free wt%]
C. vulgaris	500 g VSS m^{-3}	18.0 ± 1.2	54 ± 0.4%	27 ± 1.2%	19 ± 1.3%
	50 wt% lipids	N/A	N/A	N/A	N/A
N. granulata	500 g VSS m^{-3}	10.1 ± 0.4	52 ± 0.4%	11 ± 0.9%	36 ± 1.0%
	50 wt% lipids	11.2 ± 0.5	36 ± 0.9%	14 ± 0.9%	50 ± 0.1%

When harvested at a total biomass density of 500 g m^{-3}, *C. vulgaris* is capable of higher productivity (18.0 ± 1.2 g m^{-2} d^{-1}) than *N. granulata* (10.1 ± 0.4 g m^{-2} d^{-1}) because of the difference in the maximum growth rate parameter, $\hat{\mu}$ [139,140]. However, there is a considerable tradeoff between productivity and favorable compositions for conversion. Baseline results from Section 3.1 demonstrated that, given the same productivity, high-lipid feedstocks achieve more favorable λ_o because of higher fuel product yields. *C. vulgaris* grown from 100 to 500 g m^{-3} in nutrient-replete conditions achieves only 19 ± 1.3 wt% lipids, which is far from the desirable high lipid content needed to meet sustainability targets. In contrast, *N. granulata* can produce 50 wt% lipids and when harvested at this condition but the productivity is limited to 11.2 ± 0.5 g m^{-2} d^{-1}. However, *N. granulata* still suffers a 38% decrease in total mean biomass productivity compared to *C. vulgaris* harvested at a fixed biomass density of 500 g m^{-3}.

Some initial conditions of the algal compositional model influence growth trajectories considerably. Changing the initial value of the state variable R (chlorophyll-to-carbon ratio) alone by ±20% causes a variability of ±10% in productivity. The initial concentration of nitrogen and phosphorus in medium causes protein-rich biomass to accumulate first and shifts biomass growth to carbohydrate and lipid accumulation when the limiting nutrient is depleted. Because of the assumptions of nitrogen content from protein (4.78 g protein to 1 g cellular nitrogen) and high protein content calculated in the growth model, nitrogen consumption is higher than

assumed in the baseline cultivation reference [62] and the cultivation system creates a GWP impact that makes meeting the RFS target difficult in all scenarios. Ash content is also species-dependent; as a marine alga, *N. granulata* is expected to accumulate more salts in the harvested biomass and therefore contains more ash than *C. vulgaris*.

4.3.3.2 Conversion Monte Carlo analysis

Typical *C. vulgaris* compositions fit better to HTL than CAP-AD or CAP-HTL. However, even with HTL, the typical *C. vulgaris* production scenario would achieve $\lambda_o > 0$ in only 15% of simulations as shown in Figure 19a. CAP-AD or CAP-HTL always fail to holistically meet sustainability objectives (Figure 19b-c). Hence, conversion MCA scenarios are presented with a hypothetically doubled *C. vulgaris* productivity in Figure 19d-f and are followed by additional scenarios where the doubled productivity is maintained with a *N. granulata* harvest of 50 wt% lipids, shown in Figure 19g-i. Additional histogram distributions of individual objectives (MFSP, GWP, and NER) can be found in Figures C – 8 through C – 10.

Fixing the *C. vulgaris* feed productivity to double the baseline (35 g m^{-2} d^{-1}) yields more favorable distributions of λ_o than the random distribution of productivity values. However, low lipid content (19 ± 1.3 wt%) still results in poor satisfaction score distributions in all three pathways. With HTL, the mean λ_o is 0.38 and varies between a minimum of 0.14 and a maximum of 0.54. CAP-AD of *C. vulgaris* performs poorly even with improved productivity. No simulations were able to achieve $\lambda_o > 0$ because of MFSP; the minimum MFSP is \$2.70 LGE^{-1} (\$10.21 GGE^{-1}), which is much greater than the target of \$0.79 LGE^{-1} (\$3 GGE^{-1}). CAP-HTL performs better than CAP-AD with a mean λ_o of 0.13 and only 0.4% of simulations resulting in $\lambda_o = 0$. Poor performance scores across all three pathways indicate that more measures beyond

pushing algal feed productivity must be implemented to improve the satisfaction scores of the sustainability objectives here.

Due to the favorability toward high lipids in all conversion pathways, algae compositions similar to *N. granulata* are desirable. If combined with high productivity, HTL of *N. granulata* achieves λ_o within a range of 0.16 to 0.78 with a mean λ_o of 0.53 as shown in Figure 19g. MFSP and GWP largely dominate the distribution of λ_o in these scenarios. Even in these favorable conditions, MFSP and NER never achieve full satisfaction of the desirable target and only 2.3% of simulations achieve the target GWP. With CAP-AD, the *N. granulata* production scenario yields $\lambda_o > 0$ in 99.8% of simulations (Figure 19h), unlike *C. vulgaris*. However, satisfaction of objectives with CAP-AD is still low; the mean λ_o is 0.10 and the maximum is 0.22. CAP-HTL falls between HTL and CAP-AD with a λ_o range between 0.16 to 0.63 and a mean λ_o of 0.48 (Figure 19i).

Given the current state of algal biofuel technology, *C. vulgaris* fed through the HTL pathway is the most realizable combination of cultivation and conversion options presented here. Although *N. granulata* can achieve more favorable compositions for fuel conversion, the higher productivity of *C. vulgaris* can compensate for its lower lipid content if HTL is used to generate higher volumes of biofuel from the protein-rich fraction. However, even the most optimal operating conditions presented here cannot satisfy the targets set in the default fuzzy membership functions given the limits of the current state of cultivation technology. MFSP remains the limiting objective in all *C. vulgaris* feedstock cases. With extremely optimistic (and likely unrealistic) compositions and productivities, CAP-AD or CAP-HTL only start to become competitive technologies with respect to sustainability metrics. Between all fuel-producing technologies with optimistic conditions, HTL can achieve the best results. The maximum λ_o in

the optimistic HTL MCA simulations is 0.78, but this indicates that all sustainability objectives cannot be fully satisfied.

To make biofuel pathways more sustainable and viable, cultivation improvements need to target highly productive strains that can also shift to rapid lipid production. This point is in contrast with a previous conclusion on HTL [23], which understates the effect of composition on HTL performance. Though high-protein biomass can still yield a moderate amount of biocrude, there is a clear gap in MFSP target satisfaction when a typical harvest composition of *C. vulgaris* is fed compared to *N. granulata*. With current algae production technology, *N. granulata*, with its natural ability to rapidly accumulate lipids, may be appropriate as a cold-season strain, as productivity would be expected to decrease compared to summer cultivation anyway.

MFSP remains the biggest driver of overall sustainability but processes that are more economically favorable tend to suffer in GWP because of the correlation between high fuel yield and higher end use emissions. There is also high uncertainty in GWP, highlighted by the optimistic *N. granulata* HTL production scenario. Life cycle inventory data of hydrogen produces a range between 2.21 and 29.5 kg CO_2eq (kg H_2)$^{-1}$ depending on production technology [96]. In the baseline GWP analysis of HTL, hydrogen contributes to 49% of the total impact. Reducing the uncertainty of conversion yields, life cycle material balances, and GWP inventory would narrow the uncertainty distribution of λ_o.

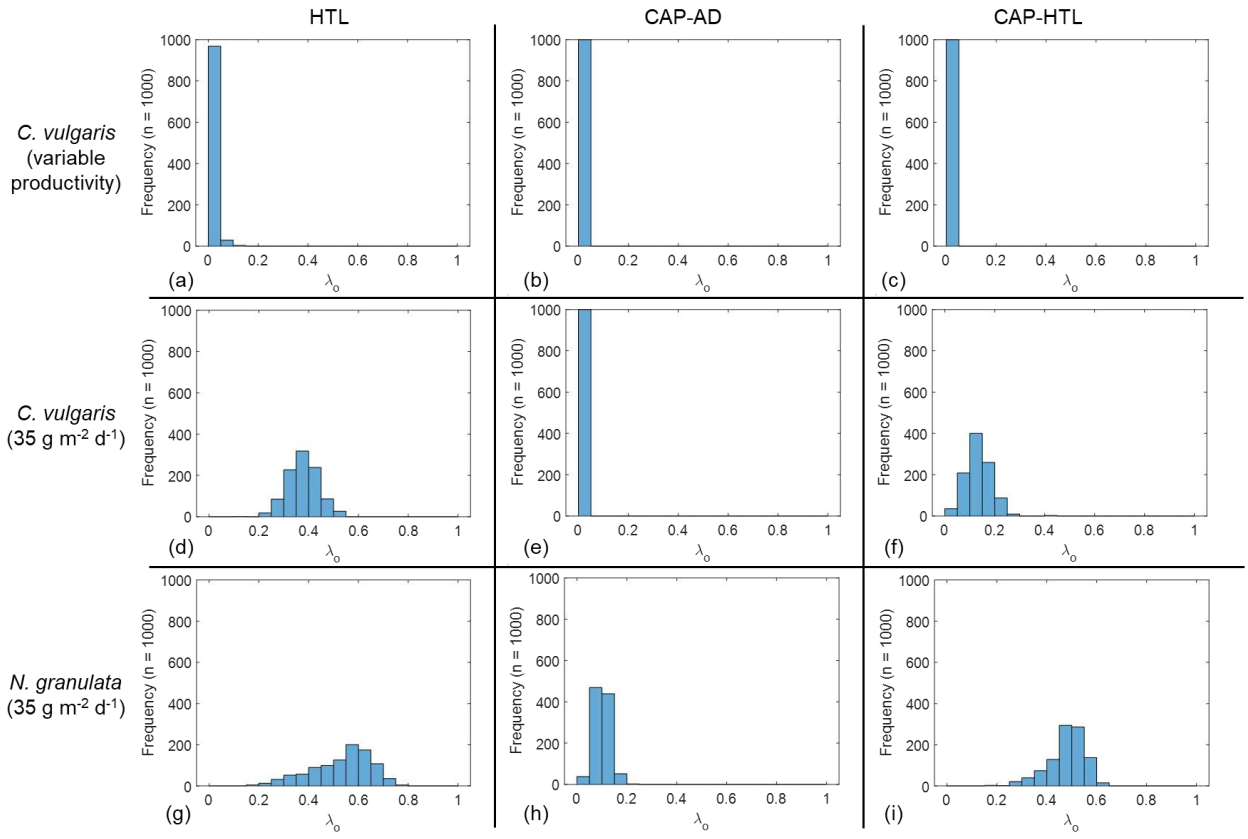

Figure 19. Monte Carlo simulation results of λ_o. Scenarios are: a) HTL, b) CAP-AD, c) CAP-HTL of the baseline C. vulgaris feedstock distributions; d) HTL, e) CAP-AD, f) CAP-HTL of C. vulgaris distributions with productivity fixed at 35 g m^{-2} d^{-1}; g) HTL, h) CAP-AD, i) CAP-HTL of N. granulata distributions with productivity fixed at 35 g m^{-2} d^{-1}.

4.4 Other considerations

Fuzzy set membership functions are not limited to the linear shapes presented in Figure 16. Satisfaction scoring criteria can follow an arbitrary nonlinear trend. For example, if GWP is even slightly above the RFS mandate, there may be a steep penalty in satisfaction past the desirable bound, resulting in a membership function that approaches a Boolean set. Alternative membership function shapes could include linear, logistic, power, exponential, and step (Boolean) functions. An example of a logistic membership function and the effect on λ_o as a function of composition can be found in Figure C - 11 and Figure C - 12. Changing the membership functions to logistic shapes results in a lower maximum λ_o of 0.32 for the baseline

HTL scenario, a 30% decrease compared to the maximum of 0.46 using linear membership functions.

Membership function bounds were based on common established targets that draw equitable comparisons to petroleum fuels. Biofuel assessments have aimed for a \$3 GGE^{-1} minimum cost target to provide renewable fuels a chance to be cost-competitive with gasoline or diesel [21,23]. RFS mandates for advanced biofuels have explicitly set a 50% life-cycle greenhouse gas reduction over their fossil fuel counterparts [5]. However, targets are subject to change by the user of the presented scoring methodology. A more ambitious cost target of \$2.50 GGE^{-1} has been cited in recent developments [149,150], which could be used to justify moving the MFSP desirable threshold. In contrast, regions outside the United States could justify more lenient fuel cost comparisons against fossil fuels. Selected gasoline prices in 2020 in East Asia ranged from \$0.85 to \$1.18 LGE^{-1} (\$3.23 to \$4.47 GGE^{-1}) and in Europe from \$0.91 to \$1.75 LGE^{-1} (\$3.43 to \$6.64 GGE^{-1}) [144].

Established biofuels like corn ethanol, sugar cane ethanol, and soy biodiesel can serve as alternative targets for comparative analysis. However, caution is advised for comparing advanced biofuels to corn ethanol, as different emissions targets exist for different renewable fuels. The RFS mandate requires only a 20% reduction in life-cycle greenhouse gas emissions from fossil fuels for corn ethanol production, as opposed to the 50% reduction mandated for advanced biofuels [5]. Additionally, corn ethanol prices can be volatile due to oversupply issues [151], which may justify the addition of another objective for product demand.

The three metrics in this work – MFSP, GWP, and NER – were chosen as major driving factors toward the adoption of new renewable fuel technologies. Sustainability objectives beyond MFSP, GWP, and NER are worth considering in future analyses of algae-to-fuel pathways. The

full set of TRACI LCA impacts were analyzed for the HTL process in previous work [124]; the impact of eutrophication from HTL, for example, was determined to be two orders of magnitude worse than equivalent fossil fuels. There is precedent in quantifying sustainability through multiple impacts in the GREENSCOPE methodology [125], which contains up to 140 impact categories across economics, energy, environment, and efficiency. However, GREENSCOPE is limited to the individual process level and is therefore, strictly speaking, not a full LCA methodology that can be applied at a system level.

The given uncertainty analysis fixes algae composition to a small range based on typical cultivation conditions. Thus, given these conditions, there may appear to be little reason to analyze the uncertainty in λ_o outside these typical compositions. However, the composition-based analysis provides results that can direct cultivation research toward necessary improvements to feed compositions. In this work, the composition-based analysis uses assumptions that are fixed across all parameters except for the composition itself. An uncertainty analysis could be combined with the composition-based analysis in this work by applying Monte Carlo analysis to each compositional point, excluding cultivation parameters. A 3-D topographical map of ternary diagrams could represent uncertainty in λ_o or individual objectives at any given compositional point.

Results from the uncertainty analysis show that the advantages of a lipid-producing strain like *N. granulata* must somehow be engineered to have improved productivity as well, which is likely a difficult task with current ORP cultivation practices. Photobioreactor (PBR) cultivation systems can generate algal biomass at higher productivities between 25 and 50 g m^{-2} d^{-1}, but the impacts of PBR production across all three sustainability objectives will likely make this tradeoff

unviable [152,153]. Future analysis on the impact of cultivation systems as additional pathway branches could be considered as an extension of the present study.

Co-products have yet to be considered in this analysis, as explorations in this field are still in the nascent stage. Single-stage HTL cannot produce high-value co-products, as algae-produced compounds are degraded in the reaction. Although λ_o values of CAP were demonstrated to be worse than HTL, CAP maintains a major advantage in its co-product flexibility to generate more economic credit and distribute the burden of life-cycle emissions. For example, the fermentation step can produce 2,3-butanediol (2,3-BDO) instead of ethanol, which can be used as a renewable chemical precursor for synthetic rubber or food additives [154]. A target co-product price of \$1 kg^{-1} [155] would value 2,3-BDO almost twice that of ethanol. The consideration of co-products alongside biofuel production would positively impact the economics and lighten the environmental impact burdens of the algal biorefining concept, thus improving the overall satisfaction score, especially for flexible biochemical processes like CAP.

Wet algae biofuel conversion processes are not limited to HTL or CAP. Sequential HTL is a multistep variant of HTL that includes a pre-processing step to remove the carbohydrate fraction from the feed before the main HTL reaction [61,150]. The carbohydrate fraction can then be converted to a lactic acid co-product to improve the products' economic value. Mild oxidative treatment (MOT) has been proposed as a less material- and energy-intensive alternative to CAP [149]. High-value carboxylic acids can be produced from oxidation of carbohydrates and proteins and treated as a co-product to extracted biofuel lipids. As these technologies continue to develop, the consideration of said alternatives would benefit greatly from holistic sustainability analyses using the scoring methodology described in this work.

4.5 Conclusions

Current conventional algal conversion pathways, HTL and CAP, struggle to achieve reasonable sustainability targets. The two processes can be combined to maximize fuel yields and improve sustainability objectives over CAP alone. Biomass productivity remains the key success factor in algae-to-fuel conversion. However, even with twice the algae productivity rates of current technology, algal biofuels are still unlikely to become holistically sustainable by current standards. A balance must be struck between productivity and favorable compositions. In all scenarios analyzed in this work, economic targets are the most difficult sustainability objective to satisfy due primarily to the high cost of biomass production. As the state of technology advances toward improving productivity, the goal of maintaining sustainable LCA metrics cannot not be ignored. Other improvements beyond productivity, such as high-value co-product pathways, must be considered to approach holistically sustainable algal biofuel production.

CH. 5: CONCLUSIONS AND RECOMMENDATIONS

5.1 Overall conclusions

When considering the viability of algal biofuels as a potential renewable energy system, every process within the system boundary must be accounted for, from nutrient recycle to fuel yield. The cost of biomass production ultimately drives the economic viability of algal fuels, which, in turn, is driven by multiple factors like nutrient recyclability and compositional targets. However, life-cycle environmental impacts of biofuels are just as important of a consideration as economic impacts. There also exists a wide range of uncertainty in the performance of algal biofuel systems due largely to data limitations at the production scale. Many literature assessments do not carry out robust uncertainty analyses of LCA despite a general inverse relationship between fuel cost and GWP.

5.2 Future directions of HTL nutrient recycle

HTL nutrient recycle can be an important assumption for the TEA and LCA of HTL systems. However, HTL-AP toxicity is an obstacle to seamless integration because it reduces productivity if added to algae cultures untreated. Experiments in this work were only performed on a particular HTL-AP stock. Other HTL-AP streams likely vary in composition. The remediation treatments explored are intended to open the field to further research in improved algal nutrient recycle. A full TEA and LCA of remediation methods (*e.g.,* adsorption columns, chromatography, waste treatment) should be conducted to see if remediation adds value to HTL as a fuel conversion system. One possible objective for future analyses is to use multiobjective optimization to search for simultaneous optima of nutrient recyclability, productivity, and TEA/LCA metrics.

5.3 Future directions of HTL modeling

Many parameters remain critically uncertain in commercial-scale HTL. Product yields influence HTL performance the most, but experimental literature does not agree on predictive yields. Different yield models tend to converge for certain biomass compositions, but deviations occur with atypical feedstocks like high-lipid algae or high-protein biomass residues. The model is flexible in calculating system flows given different yields, but improvements to component assay modeling can yield more accurate mass and energy balances.

Dynamic modeling of HTL auxiliary systems, like upgrading and gas recycle, remain underdeveloped. Commercial-scale data of HTL systems are exceptionally limited, however; at the time of this writing, only two known HTL research sites exist. HTL of a wide variety of feedstocks would vastly improve the estimation of assay compositions that are used for modeling specific compounds in Aspen Plus.

The HTL process model is publicly available, and it is encouraged that researchers take advantage of this resource and improve it. As the state of technology improves or shifts (*e.g.*, to sequential HTL), the model can be adapted to present updated results that match the improving state of technology.

5.4 Future directions of fuzzy set scoring methodology

Results from the present work show that HTL dominates over CAP as a holistically sustainable algae-to-fuels pathway. However, single-stage HTL is inflexible toward co-product credits. If co-products are introduced to improve biofuel viability, CAP has the potential to generate renewable products through all major components – carbohydrates, lipids, and residual biomass. However, high-value co-product technologies are lagging in development compared to biofuels due to their complexity and stringent production standards, and important parameters

like yields and market prices create even greater uncertainty in overall sustainability metrics. As new pathways develop, the fuzzy set scoring methodology presents a holistic and easily understandable way to analyze and interpret the concept of sustainability.

The fuzzy set scoring methodology is simple and flexible to user-defined targets. With this principle in mind, holistic sustainability analyses can easily be expanded beyond algal biofuels. Other liquid biofuels like sustainable aviation fuel can feasibly use the same objectives and membership function targets presented in this work. Membership function targets can also be based on well-established renewable fuels like corn ethanol and soy biodiesel. The importance of clearly defined sustainability objectives cannot be understated, and it is a necessary burden on the user of this methodology to be transparent about their goals and definitions.

The functional product from algal biomass does not need to be biofuel. If other renewable products can be created alongside biofuels, the displacement of non-fuel products may be an appropriate perspective to analyze the sustainability of algae production. Biofuels can be considered as a co-product in this scenario. Different metrics would serve as sustainability objectives; for example, MFSP would be irrelevant to a pathway that primarily produces bioplastics. Instead, market prices would serve as an economic objective and fuzzy membership functions would look for different targets.

REFERENCES

[1] Intergovernmental Panel on Climate Change, Assessment Report 6 Climate Change 2021: The Physical Science Basis, 2021. https://www.ipcc.ch/report/ar6/wg1/.

[2] Intergovernmental Panel on Climate Change, Climate Change 2014 Mitigation of Climate Change, 2014. doi:10.1017/cbo9781107415416.

[3] United Nations, Growing at a slower pace, world population is expected to reach 9.7 billion in 2050 and could peak at nearly 11 billion around 2100, (2019). https://www.un.org/development/desa/en/news/population/world-population-prospects-2019.html (accessed October 6, 2021).

[4] U.S. Energy Information Administration, How much ethanol is in gasoline, and how does it affect fuel economy?, (2021). https://www.eia.gov/tools/faqs/faq.php?id=27&t=10 (accessed October 6, 2021).

[5] United States Environmental Protection Agency, Overview for Renewable Fuel Standard, (2017). https://www.epa.gov/renewable-fuel-standard-program/overview-renewable-fuel-standard (accessed September 8, 2020).

[6] P.B. Thompson, The agricultural ethics of biofuels: The food vs. fuel debate, Agriculture. 2 (2012) 339–358. doi:10.3390/agriculture2040339.

[7] T. Searchinger, R. Heimlich, R.A. Houghton, F. Dong, A. Elobeid, J. Fabiosa, S. Tokgoz, D. Hayes, T.-H. Yu, Use of U.S. Croplands for Biofuels Increases Greenhouse Gases Through Emissions from Land-Use Change, Science (80-.). 319 (2008) 1238–1240. doi:10.1126/science.1151861.

[8] J. Fargione, J. Hill, D. Tilman, S. Polasky, P. Hawthorne, Land Clearing and the Biofuel

Carbon Debt, Science (80-.). 319 (2008) 1235–1238. doi:10.1126/science.1152747.

[9] R. Rapier, Cellulosic Ethanol Falling Far Short Of The Hype, Forbes. (2018). https://www.forbes.com/sites/rrapier/2018/02/11/cellulosic-ethanol-falling-far-short-of-the-hype/?sh=236767a5505f.

[10] Y. Chisti, Biodiesel from microalgae, Biotechnol. Adv. 25 (2007) 294–306. doi:10.1016/j.biotechadv.2007.02.001.

[11] R. Davis, C. Kinchin, J. Markham, E. Tan, L. Laurens, D. Sexton, D. Knorr, P. Schoen, J. Lukas, Process Design and Economics for the Conversion of Algal Biomass to Biofuels: Algal Biomass Fractionation to Lipid- and Carbohydrate-Derived Fuel Products, (2014). doi:10.2172/1159351.

[12] D.C. Elliott, P. Biller, A.B. Ross, A.J. Schmidt, S.B. Jones, Hydrothermal liquefaction of biomass: Developments from batch to continuous process, Bioresour. Technol. (2015). doi:10.1016/j.biortech.2014.09.132.

[13] D.C. Elliott, Review of recent reports on process technology for thermochemical conversion of whole algae to liquid fuels, Algal Res. 13 (2016) 255–263. doi:10.1016/j.algal.2015.12.002.

[14] D. Castello, T.H. Pedersen, L.A. Rosendahl, Continuous hydrothermal liquefaction of biomass: A critical review, Energies. 11 (2018). doi:10.3390/en11113165.

[15] P.J.L.B. Williams, L.M.L. Laurens, Microalgae as biodiesel & biomass feedstocks: Review & analysis of the biochemistry, energetics & economics, Energy Environ. Sci. 3 (2010) 554–590. doi:10.1039/b924978h.

[16] C.E. Canter, P. Blowers, R.M. Handler, D.R. Shonnard, Implications of widespread algal biofuels production on macronutrient fertilizer supplies: Nutrient demand and evaluation

of potential alternate nutrient sources, Appl. Energy. 143 (2015) 71–80. doi:10.1016/j.apenergy.2014.12.065.

[17] J.C. Quinn, T.G. Smith, C.M. Downes, C. Quinn, Microalgae to biofuels lifecycle assessment - Multiple pathway evaluation, Algal Res. 4 (2014) 116–122. doi:10.1016/j.algal.2013.11.002.

[18] A. Lee, D. Lewis, T. Kalaitzidis, P. Ashman, Technical issues in the large-scale hydrothermal liquefaction of microalgal biomass to biocrude, Curr. Opin. Biotechnol. 38 (2016) 85–89. doi:10.1016/j.copbio.2016.01.004.

[19] D.C. Elliott, T.R. Hart, A.J. Schmidt, G.G. Neuenschwander, L.J. Rotness, M. V. Olarte, A.H. Zacher, K.O. Albrecht, R.T. Hallen, J.E. Holladay, Process development for hydrothermal liquefaction of algae feedstocks in a continuous-flow reactor, Algal Res. 2 (2013) 445–454. doi:10.1016/j.algal.2013.08.005.

[20] S. Edmundson, M. Huesemann, R. Kruk, T. Lemmon, J. Billing, A. Schmidt, D. Anderson, Phosphorus and nitrogen recycle following algal bio-crude production via continuous hydrothermal liquefaction, Algal Res. 26 (2017) 415–421. doi:10.1016/j.algal.2017.07.016.

[21] S. Jones, Y. Zhu, D. Anderson, R.T. Hallen, D.C. Elliott, Process Design and Economics for the Conversion of Algal Biomass to Hydrocarbons : Whole Algae Hydrothermal Liquefaction and Upgrading, Richland, WA, 2014. doi:10.2172/1126336.

[22] B.H. Haugstad, Fuel Characterization and Process Analysis of Hydrothermal Liquefaction of Algae, University of Agder, 2017. https://pdfs.semanticscholar.org/3dde/e26ab2a8a5b86215a22f613f4191cf2ce425.pdf?_ga=2.252460169.1873111062.1566936128-1498923147.1566936128.

[23] M. Biddy, R. Davis, S. Jones, Y. Zhu, Whole Algae Hydrothermal Liquefaction Technology Pathway, U.S. Dep. Energy Tech. Rep. (2013). doi:NREL/TP-5100-58051.

[24] L. Garcia Alba, C. Torri, D. Fabbri, S.R.A. Kersten, D.W.F. Wim Brilman, Microalgae growth on the aqueous phase from Hydrothermal Liquefaction of the same microalgae, Chem. Eng. J. 228 (2013) 214–223. doi:10.1016/j.cej.2013.04.097.

[25] U. Jena, N. Vaidyanathan, S. Chinnasamy, K.C. Das, Evaluation of microalgae cultivation using recovered aqueous co-product from thermochemical liquefaction of algal biomass, Bioresour. Technol. 102 (2011) 3380–3387. doi:10.1016/j.biortech.2010.09.111.

[26] C.M. Godwin, D.C. Hietala, A.R. Lashaway, A. Narwani, P.E. Savage, B.J. Cardinale, Algal polycultures enhance coproduct recycling from hydrothermal liquefaction, Bioresour. Technol. 224 (2017) 630–638. doi:10.1016/j.biortech.2016.11.105.

[27] L. Leng, J. Li, Z. Wen, W. Zhou, Use of microalgae to recycle nutrients in aqueous phase derived from hydrothermal liquefaction process, Bioresour. Technol. 256 (2018) 529–542. doi:10.1016/j.biortech.2018.01.121.

[28] H. Chen, J. Wan, K. Chen, G. Luo, J. Fan, J. Clark, S. Zhang, Biogas production from hydrothermal liquefaction wastewater (HTLWW): Focusing on the microbial communities as revealed by high-throughput sequencing of full-length 16S rRNA genes, Water Res. 106 (2016) 98–107. doi:10.1016/j.watres.2016.09.052.

[29] L. Ruirui, R. Xia, D. Na, Y. Zhang, L. Zhidan, L. Haifeng, Application of zeolite adsorption and biological anaerobic digestion technology on hydrothermal liquefaction wastewater, Int. J. Agric. Biol. Eng. 10 (2017) 163–168. doi:10.3965/j.ijabe.20171001.2704.

[30] S.R. Shanmugam, S. Adhikari, Z. Wang, R. Shakya, Treatment of aqueous phase of bio-

oil by granular activated carbon and evaluation of biogas production, Bioresour. Technol. 223 (2017) 115–120. doi:10.1016/j.biortech.2016.10.008.

[31] M. Zheng, L.C. Schideman, G. Tommaso, W.T. Chen, Y. Zhou, K. Nair, W. Qian, Y. Zhang, K. Wang, Anaerobic digestion of wastewater generated from the hydrothermal liquefaction of Spirulina: Toxicity assessment and minimization, Energy Convers. Manag. 141 (2017) 420–428. doi:10.1016/j.enconman.2016.10.034.

[32] K. Chen, H. Lyu, S. Hao, G. Luo, S. Zhang, J. Chen, Separation of phenolic compounds with modified adsorption resin from aqueous phase products of hydrothermal liquefaction of rice straw, Bioresour. Technol. 182 (2015) 160–168. doi:10.1016/j.biortech.2015.01.124.

[33] R.S. Jackson, Postfermentation Treatments and Related Topics, Wine Sci. (2000) 355–433. doi:10.1016/b978-012379062-0/50009-3.

[34] K.A. Leiper, M. Miedl, Colloidal stability of beer, Elsevier Inc., 2009. doi:10.1016/B978-0-12-669201-3.00004-X.

[35] J.L. Faeth, P.E. Savage, J.M. Jarvis, A.M. Mckenna, P.E. Savage, Characterization of products from fast and isothermal hydrothermal liquefaction of microalgae, AIChE J. 62 (2016) 815–828. doi:10.1002/aic.15147.

[36] APHA, Standard methods for the examination of water and wastewater, 22nd ed., American Public Health Association, Washington, D.C., 2012.

[37] R.B. Madsen, P. Biller, M.M. Jensen, J. Becker, B.B. Iversen, M. Glasius, Predicting the Chemical Composition of Aqueous Phase from Hydrothermal Liquefaction of Model Compounds and Biomasses, Energy and Fuels. 30 (2016) 10470–10483. doi:10.1021/acs.energyfuels.6b02007.

[38] S. Van Wychen, L.M.L. Laurens, Determination of Total Lipids as Fatty Acid Methyl Esters (FAME) by in situ Transesterification - Laboratory Analytical Procedure (LAP) - http://www.nrel.gov/docs/fy14osti/60958.pdf, 2013.

[39] S. Van Wychen, L.M.L. Laurens, Determination of Total Solids and Ash in Algal Biomas - Laboratory Analytical Procedure (LAP) - http://www.nrel.gov/docs/fy14osti/60956.pdf, Golden, CO, 2013.

[40] S. Van Wychen, L.M.L. Laurens, Determination of Total Carbohydrates in Algal Biomass - Laboratory Analytical Procedure (LAP) - http://www.nrel.gov/docs/fy14osti/60957.pdf, Golden, CO, 2013.

[41] L. Laurens, M. Quinn, S. Van Wychen, D. Templeton, E.J. Wolfrum, Accurate and reliable quantification of total microalgal fuel potential as fatty acid methyl esters by in situ transesterification, Anal. Bioanal. Chem. 403 (2012) 167–178.

[42] R Core Team, R: A language and environment for statistical computing, (2018). https://www.r-project.org/.

[43] J. Wang, W. Zhou, H. Chen, J. Zhan, C. He, Q. Wang, Ammonium nitrogen tolerant Chlorella strain screening and its damaging effects on photosynthesis, Front. Microbiol. 10 (2019) 1–13. doi:10.3389/fmicb.2018.03250.

[44] A. Konig, H.W. Pearson, S.A. Silva, Ammonia toxicity to algal growth in waste stabilization ponds, Water Sci. Technol. 19 (1987) 115–122. doi:10.2166/wst.1987.0135.

[45] Y. Azov, J.C. Goldman, Free ammonia inhibition of algal photosynthesis in intensive cultures., Appl. Environ. Microbiol. 43 (1982) 735–9. doi:http://dx.doi.org/.

[46] Yuvraj, A.S. Vidyarthi, J. Singh, Enhancement of Chlorella vulgaris cell density: Shake flask and bench-top photobioreactor studies to identify and control limiting factors,

Korean J. Chem. Eng. 33 (2016) 2396–2405. doi:10.1007/s11814-016-0087-5.

[47] Y. Azov, Effect of pH on inorganic carbon uptake in algal cultures inorganic carbon uptake in algal cultures, Appl. Environ. Microbiol. 43 (1982) 1300–1306. http://aem.asm.org/content/43/6/1300.full.pdf+html.

[48] N.F.Y. Tam, Y.S. Wong, Effect of ammonia concentrations on growth of Chlorella vulgaris and nitrogen removal from media, Bioresour. Technol. 57 (1996) 45–50. doi:10.1016/0960-8524(96)00045-4.

[49] S. Alimoradi, H. Stohr, S. Stagg-Williams, B. Sturm, Effect of temperature on toxicity and biodegradability of dissolved organic nitrogen formed during hydrothermal liquefaction of biomass, Chemosphere. (2019) 124573. doi:10.1016/j.chemosphere.2019.124573.

[50] European Union, RES directive towards 2020, Off. J. Eur. Communities. L 269 (2015) 1–15.

[51] J. Teter, J. Tattini, A. Petropoulos, Tracking Transport 2020, Int. Energy Agency. (2020). https://www.iea.org/reports/tracking-transport-2020 (accessed January 6, 2021).

[52] J.C. Quinn, K. Catton, N. Wagner, T.H. Bradley, Current Large-Scale US Biofuel Potential from Microalgae Cultivated in Photobioreactors, Bioenergy Res. 5 (2012) 49–60. doi:10.1007/s12155-011-9165-z.

[53] J.C. Quinn, K.B. Catton, S. Johnson, T.H. Bradley, Geographical Assessment of Microalgae Biofuels Potential Incorporating Resource Availability, Bioenergy Res. 6 (2013) 591–600. doi:10.1007/s12155-012-9277-0.

[54] J.W. Moody, C.M. McGinty, J.C. Quinn, Global evaluation of biofuel potential from microalgae, Proc. Natl. Acad. Sci. U. S. A. 111 (2014) 8691–8696. doi:10.1073/pnas.1321652111.

[55] J. Cruce, A. Beattie, P. Chen, D. Quiroz, M. Somers, S. Compton, K. DeRose, B. Beckstrom, J.C. Quinn, Driving toward sustainable algal fuels: A harmonization of techno-economic and life cycle assessments, Algal Res. 54 (2021).

[56] L. Chen, T. Zhu, J.S.M. Fernandez, S. Chen, D. Li, Recycling nutrients from a sequential hydrothermal liquefaction process for microalgae culture, Algal Res. 27 (2017) 311–317. doi:10.1016/j.algal.2017.09.023.

[57] T. Selvaratnam, H. Reddy, T. Muppaneni, F.O. Holguin, N. Nirmalakhandan, P.J. Lammers, S. Deng, Optimizing energy yields from nutrient recycling using sequential hydrothermal liquefaction with Galdieria sulphuraria, Algal Res. 12 (2015) 74–79. doi:10.1016/j.algal.2015.07.007.

[58] J.S. Martinez-Fernandez, S. Chen, Sequential Hydrothermal Liquefaction characterization and nutrient recovery assessment, Algal Res. 25 (2017) 274–284. doi:10.1016/j.algal.2017.05.022.

[59] W. Kwapinski, Char production technology, Elsevier Inc., 2019. doi:10.1016/B978-0-12-814893-8.00002-X.

[60] Y. Zhu, S.B. Jones, A.J. Schmidt, K.O. Albrecht, S.J. Edmundson, D.B. Anderson, Techno-economic analysis of alternative aqueous phase treatment methods for microalgae hydrothermal liquefaction and biocrude upgrading system, Algal Res. 39 (2019) 101467. doi:10.1016/j.algal.2019.101467.

[61] X. Gu, L. Yu, N. Pang, J.S. Martinez-Fernandez, X. Fu, S. Chen, Comparative techno-economic analysis of algal biofuel production via hydrothermal liquefaction: One stage versus two stages, Appl. Energy. 259 (2020) 114115. doi:10.1016/j.apenergy.2019.114115.

[62] R. Davis, J. Markham, C. Kinchin, N. Grundl, E.C.D. Tan, D. Humbird, Process Design and Economics for the Production of Algal Biomass: Algal Biomass Production in Open Pond Systems and Processing Through Dewatering for Downstream Conversion, Natl. Renew. Energy Lab. (2016) 128. www.nrel.gov/publications.

[63] L.M.L. Laurens, J.D. McMillan, D. Baxter, A.L. Cowie, J.N. Saddler, M. Barbosa, J. Murphy, B. Drosg, D.C. Elliott, J. Sandquist, D. Chiaramonti, D. Bacovsky, State of Technology Review – Algae Bioenergy, 2017. doi:10.1017/S0959270900002288.

[64] L. Batan, J. Quinn, B. Willson, T. Bradley, Net energy and greenhouse gas emission evaluation of biodiesel derived from microalgae, Environ. Sci. Technol. 44 (2010) 7975–7980. doi:10.1021/es102052y.

[65] S. Ponnusamy, H.K. Reddy, T. Muppaneni, C.M. Downes, S. Deng, Life cycle assessment of biodiesel production from algal bio-crude oils extracted under subcritical water conditions, Bioresour. Technol. 170 (2014) 454–461. doi:10.1016/j.biortech.2014.07.072.

[66] D. Mu, R. Ruan, M. Addy, S. Mack, P. Chen, Y. Zhou, Life cycle assessment and nutrient analysis of various processing pathways in algal biofuel production, Bioresour. Technol. 230 (2017) 33–42. doi:10.1016/j.biortech.2016.12.108.

[67] E.P. Bennion, D.M. Ginosar, J. Moses, F. Agblevor, J.C. Quinn, Lifecycle assessment of microalgae to biofuel: Comparison of thermochemical processing pathways, Appl. Energy. 154 (2015) 1062–1071. doi:10.1016/j.apenergy.2014.12.009.

[68] X. Liu, B. Saydah, P. Eranki, L.M. Colosi, B. Greg Mitchell, J. Rhodes, A.F. Clarens, Pilot-scale data provide enhanced estimates of the life cycle energy and emissions profile of algae biofuels produced via hydrothermal liquefaction, Bioresour. Technol. 148 (2013) 163–171. doi:10.1016/j.biortech.2013.08.112.

[69] C.H. Sun, Q. Fu, Q. Liao, A. Xia, Y. Huang, X. Zhu, A. Reungsang, H.X. Chang, Life-cycle assessment of biofuel production from microalgae via various bioenergy conversion systems, Energy. 171 (2019) 1033–1045. doi:10.1016/j.energy.2019.01.074.

[70] D. Knorr, J. Lukas, P. Schoen, Production of advanced biofuels via liquefaction hydrothermal liquefaction reactor design, Golden, CO, 2013. doi:REPORT 30352.00/01.

[71] H. Renon, J.M. Prausnitz, Local compositions in thermodynamic excess functions for liquid mixtures, AIChE J. 14 (1968) 135–144.

[72] D.-Y. Peng, D.B. Robinson, A New Two-Constant Equation of State, Ind. Eng. Chem. Fundamen. 15 (1976) 59–64.

[73] U. Jena, K.C. Das, J.R. Kastner, Effect of operating conditions of thermochemical liquefaction on biocrude production from Spirulina platensis, Bioresour. Technol. 102 (2011) 6221–6229. doi:10.1016/j.biortech.2011.02.057.

[74] J. Yang, Q. (Sophia) He, K. Corscadden, H. Niu, J. Lin, T. Astatkie, Advanced models for the prediction of product yield in hydrothermal liquefaction via a mixture design of biomass model components coupled with process variables, Appl. Energy. 233–234 (2019) 906–915. doi:10.1016/j.apenergy.2018.10.035.

[75] P.J. Valdez, M.C. Nelson, H.Y. Wang, X.N. Lin, P.E. Savage, Hydrothermal liquefaction of Nannochloropsis sp.: Systematic study of process variables and analysis of the product fractions, Biomass and Bioenergy. 46 (2012) 317–331. doi:10.1016/j.biombioe.2012.08.009.

[76] H. Li, Z. Liu, Y. Zhang, B. Li, H. Lu, N. Duan, M. Liu, Z. Zhu, B. Si, Conversion efficiency and oil quality of low-lipid high-protein and high-lipid low-protein microalgae via hydrothermal liquefaction, Bioresour. Technol. 154 (2014) 322–329.

doi:10.1016/j.biortech.2013.12.074.

[77] D. López Barreiro, C. Zamalloa, N. Boon, W. Vyverman, F. Ronsse, W. Brilman, W. Prins, Influence of strain-specific parameters on hydrothermal liquefaction of microalgae, Bioresour. Technol. 146 (2013) 463–471. doi:10.1016/j.biortech.2013.07.123.

[78] R. Davis, D. Fishman, E.D. Frank, M.S. Wigmosta, A. Aden, A.M. Coleman, P.T. Pienkos, R.J. Skaggs, E.R. Venteris, M.Q. Wang, "Renewable Diesel from Algal Lipids: An Integrated Baseline for Cost, Emissions, and Resource Potential from a Harmonized Model. ANL/ESD/12-4; NREL/TP-5100-55431; PNNL-21437. Argonne, IL: Argonne National Laboratory; Golden, CO: National Renewable Energy, 2012.

[79] D. Xu, P.E. Savage, Effect of reaction time and algae loading on water-soluble and insoluble biocrude fractions from hydrothermal liquefaction of algae, Algal Res. 12 (2015) 60–67. doi:10.1016/j.algal.2015.08.005.

[80] Y. Zhu, K.O. Albrecht, D.C. Elliott, R.T. Hallen, S.B. Jones, Development of hydrothermal liquefaction and upgrading technologies for lipid-extracted algae conversion to liquid fuels, Algal Res. 2 (2013) 455–464. doi:10.1016/j.algal.2013.07.003.

[81] Y. Dote, S. Sawayama, S. Inoue, T. Minowa, S. ya Yokoyama, Recovery of liquid fuel from hydrocarbon-rich microalgae by thermochemical liquefaction, Fuel. 73 (1994) 1855–1857. doi:10.1016/0016-2361(94)90211-9.

[82] D. López Barreiro, B.R. Gómez, U. Hornung, A. Kruse, W. Prins, Hydrothermal Liquefaction of Microalgae in a Continuous Stirred-Tank Reactor, Energy and Fuels. 29 (2015) 6422–6432. doi:10.1021/acs.energyfuels.5b02099.

[83] E.M. Lozano, T.H. Pedersen, L.A. Rosendahl, Generic approach for the modeling of liquefied thermochemical products and biomass heat of formation. Case study: HTL

biocrude, Pyrolysis oil and assessment of energy requirements, (2019). https://arxiv.org/pdf/1908.00799.pdf.

[84] P.J. Valdez, V.J. Tocco, P.E. Savage, A general kinetic model for the hydrothermal liquefaction of microalgae, Bioresour. Technol. 163 (2014) 123–127. doi:10.1016/j.biortech.2014.04.013.

[85] S. Leow, J.R. Witter, D.R. Vardon, B.K. Sharma, J.S. Guest, T.J. Strathmann, Prediction of microalgae hydrothermal liquefaction products from feedstock biochemical composition, Green Chem. 17 (2015) 3584–3599. doi:10.1039/C5GC00574D.

[86] Pacific Northwest National Laboratory, Lower and Higher Heating Values of Fuels, Hydrog. Tools. (n.d.). https://h2tools.org/hyarc/calculator-tools/lower-and-higher-heating-values-fuels (accessed September 8, 2020).

[87] P. Rotunno, A. Lanzini, P. Leone, Energy and economic analysis of a water scrubbing based biogas upgrading process for biomethane injection into the gas grid or use as transportation fuel, Renew. Energy. 102 (2017) 417–432. doi:10.1016/j.renene.2016.10.062.

[88] W. Short, D. Packey, T. Holt, A manual for the economic evaluation of energy efficiency and renewable energy technologies, Golden, CO, 1995.

[89] S. Jenkins, 2019 Chemical Engineering Plant Cost Index Annual Average, Chem. Eng. (2019). https://www.chemengonline.com/2019-chemical-engineering-plant-cost-index-annual-average/ (accessed September 8, 2020).

[90] U.S. Bureau of Labor Statistics, Producer Price Index by Commodity: Chemicals and Allied Products: Basic Inorganic Chemicals [WPU0613], (2020). https://fred.stlouisfed.org/series/WPU0613 (accessed September 8, 2020).

[91] U.S. Bureau of Labor Statistics, Employment, Hours, and Earnings from the Current Employment Statistics survey (National), Ser. ID CEU3232500008. (2020). https://data.bls.gov/cgi-bin/srgate (accessed September 8, 2020).

[92] U.S. Energy Information Administration, Wholesale Electricity and Natural Gas Market Data, (2020). https://www.eia.gov/electricity/wholesale/ (accessed September 8, 2020).

[93] A. Dutta, M. Talmadge, J. Hensley, M. Worley, D. Dudgeon, D. Barton, P. Groenendijk, D. Ferrari, B. Stears, E.M. Searcy, C.T. Wright, J.R. Hess, Process Design and Economics for Conversion of Lignocellulosic Biomass to Ethanol, NREL Tech. Rep. NREL/TP-5100-51400. 303 (2011) 275–3000. doi:10.2172/1013269.

[94] S. Dillich, T. Ramsden, M. Melaina, Hydrogen Production Cost Using Low-Cost Natural Gas, DOE Hydrog. Fuel Cells Progr. Rec. (2012) 3–8.

[95] G. Wernet, C. Bauer, B. Steubing, J. Reinhard, E. Moreno-Ruiz, B. Weidema, ecoinvent Version 3.4, (2016). http://link.springer.com/10.1007/s11367-016-1087-8.

[96] A. Mehmeti, A. Angelis-Dimakis, G. Arampatzis, S. McPhail, S. Ulgiati, Life Cycle Assessment and Water Footprint of Hydrogen Production Methods: From Conventional to Emerging Technologies, Environments. 5 (2018) 24. doi:10.3390/environments5020024.

[97] UChicago Argonne, GREET 1, (2019). https://greet.es.anl.gov/.

[98] E.W. Merrow, K.E. Phillips, C.W. Myers, Understanding Cost Growth and Performance Shortfalls in Pioneer Process Plants, 1981.

[99] G. Shelef, A. Sukenik, M. Green, Microalgae Harvesting and Processing : A Literature Review, Haifa, Israel, 1984. doi:http://dx.doi.org/10.2172/6204677.

[100] H. Chen, Q. Fu, Q. Liao, H. Zhang, Y. Huang, A. Xia, X. Zhu, Rheological properties of microalgae slurry for application in hydrothermal pretreatment systems, Bioresour.

Technol. 249 (2018) 599–604. doi:10.1016/j.biortech.2017.10.051.

[101] N. Schneider, M. Gerber, Correlation between viscosity, temperature and total solid content of algal biomass, Bioresour. Technol. 170 (2014) 293–302. doi:10.1016/j.biortech.2014.07.107.

[102] B.H.J. Yap, G.J.O. Martin, P.J. Scales, Rheological manipulation of flocculated algal slurries to achieve high solids processing, Algal Res. 14 (2016) 1–8. doi:10.1016/j.algal.2015.12.007.

[103] United States Environmental Protection Agency, Fuels, Green Veh. Guid. (2016). https://www3.epa.gov/otaq/gvg/learn-more-fuels.htm (accessed September 29, 2020).

[104] E. Frank, A. Pegallapati, R. Davis, J. Markham, A. Coleman, S. Jones, M. Wigmosta, Y. Zhu, Life-cycle Analysis of Energy Use, Greenhouse Gas Emissions, and Water Consumption in the 2016 MYPP Algal Biofuel Scenarios, Argonne, IL, 2016. file:///C:/Users/youhe/Downloads/kdoc_o_00042_01.pdf.

[105] J. Hoffman, R.C. Pate, T. Drennen, J.C. Quinn, Techno-economic assessment of open microalgae production systems, Algal Res. 23 (2017) 51–57. doi:10.1016/j.algal.2017.01.005.

[106] National Institute of Standards and Technology, Water, NIST Chem. WebBook, SRD 69. (2018). https://webbook.nist.gov/cgi/cbook.cgi?ID=C7732185&Type=JANAFL&Table=on (accessed September 8, 2020).

[107] K.F. Tzanetis, J.A. Posada, A. Ramirez, Analysis of biomass hydrothermal liquefaction and biocrude-oil upgrading for renewable jet fuel production: The impact of reaction conditions on production costs and GHG emissions performance, Renew. Energy. 113

(2017) 1388–1398. doi:10.1016/j.renene.2017.06.104.

[108] T.H. Pedersen, N.H. Hansen, O.M. Pérez, D.E.V. Cabezas, L.A. Rosendahl, Renewable hydrocarbon fuels from hydrothermal liquefaction: A techno-economic analysis, Biofuels, Bioprod. Biorefining. 12 (2018) 213–223. doi:10.1002/bbb.1831.

[109] S. Leow, B.D. Shoener, Y. Li, J.L. Debellis, J. Markham, R. Davis, L.M.L. Laurens, P.T. Pienkos, S.M. Cook, T.J. Strathmann, J.S. Guest, A Unified Modeling Framework to Advance Biofuel Production from Microalgae, Environ. Sci. Technol. 52 (2018) 13591–13599. doi:10.1021/acs.est.8b03663.

[110] K.O. Albrecht, Y. Zhu, A.J. Schmidt, J.M. Billing, T.R. Hart, S.B. Jones, G. Maupin, R. Hallen, T. Ahrens, D. Anderson, Impact of heterotrophically stressed algae for biofuel production via hydrothermal liquefaction and catalytic hydrotreating in continuous-flow reactors, Algal Res. 14 (2016) 17–27. doi:10.1016/j.algal.2015.12.008.

[111] K. Moriarty, A. Milbrandt, E. Warner, J. Lewis, A. Schwab, 2017 Bioenergy Industry Status Report, 2016. www.nrel.gov/publications.%0Ahttps://www.nrel.gov/docs/fy18osti/70397.pdf.

[112] Office of Fossil Energy, Internal Revenue Code Tax Fact Sheet, 2019. https://www.energy.gov/sites/prod/files/2019/10/f67/Internal Revenue Code Tax Fact Sheet.pdf.

[113] B.D. Beckstrom, M.H. Wilson, M. Crocker, J.C. Quinn, Bioplastic feedstock production from microalgae with fuel co-products: A techno-economic and life cycle impact assessment, Algal Res. 46 (2020) 101769. doi:10.1016/j.algal.2019.101769.

[114] J.M. Jarvis, J.M. Billing, Y.E. Corilo, A.J. Schmidt, R.T. Hallen, T.M. Schaub, FT-ICR MS analysis of blended pine-microalgae feedstock HTL biocrudes, Fuel. 216 (2018) 341–

348. doi:10.1016/j.fuel.2017.12.016.

[115] Z. Cui, J.M. Greene, F. Cheng, J.C. Quinn, U. Jena, C.E. Brewer, Co-hydrothermal liquefaction of wastewater-grown algae and crude glycerol: A novel strategy of bio-crude oil-aqueous separation and techno-economic analysis for bio-crude oil recovery and upgrading, Algal Res. 51 (2020) 102077. doi:10.1016/j.algal.2020.102077.

[116] P. Biller, A.B. Ross, Potential yields and properties of oil from the hydrothermal liquefaction of microalgae with different biochemical content, Bioresour. Technol. 102 (2011) 215–225. doi:10.1016/j.biortech.2010.06.028.

[117] C. Jazrawi, P. Biller, A.B. Ross, A. Montoya, T. Maschmeyer, B.S. Haynes, Pilot plant testing of continuous hydrothermal liquefaction of microalgae, Algal Res. 2 (2013) 268–277. doi:10.1016/j.algal.2013.04.006.

[118] P.H. Chen, J.L. Venegas Jimenez, S.M. Rowland, J.C. Quinn, L.M.L. Laurens, Nutrient recycle from algae hydrothermal liquefaction aqueous phase through a novel selective remediation approach, Algal Res. 46 (2020). doi:10.1016/j.algal.2019.101776.

[119] Fisher Scientific, Dowex™ 50WX8-400 ion-exchange resin, ACROS Organics™, (2020). https://www.fishersci.com/shop/products/dowex-50wx8-400-ion-exchange-resin-acros-organics-3/AC335350025 (accessed September 29, 2020).

[120] J.R. Benemann, D.M. Tillett, J.C. Weissman, Microalgae biotechnology, Trends Biotechnol. 5 (1987) 47–53. doi:10.1016/0167-7799(87)90037-0.

[121] J.R. Benemann, W.J. Oswald, Systems and Economic Analysis of Microalgae Ponds for Conversion of CO2 to Biomass, Pittsburgh, PA, 1996. https://www.osti.gov/servlets/purl/493389.

[122] K.M. Weyer, D.R. Bush, A. Darzins, B.D. Willson, Theoretical maximum algal oil

production, Bioenergy Res. 3 (2010) 204–213. doi:10.1007/s12155-009-9046-x.

[123] J.D. Sheehan, P.E. Savage, Modeling the effects of microalga biochemical content on the kinetics and biocrude yields from hydrothermal liquefaction, Bioresour. Technol. 239 (2017) 144–150. doi:10.1016/j.biortech.2017.05.013.

[124] P.H. Chen, J.C. Quinn, Microalgae to biofuels through hydrothermal liquefaction: Open-source techno-economic analysis and life cycle assessment, Appl. Energy. 289 (2021). doi:10.1016/j.apenergy.2021.116613.

[125] M.A. Gonzalez, R. Smith, A Methodology to Evaluate Process Sustainability, (2003) 269–276.

[126] A.T. Ubando, A.B. Culaba, R.R. Tan, D.K.S. Ng, A Systematic Approach for Optimization of an Algal Biorefinery Using Fuzzy Linear Programming, Comput. Aided Chem. Eng. 31 (2012) 805–809. doi:10.1016/B978-0-444-59507-2.50153-0.

[127] A.T. Ubando, A.B. Culaba, K.B. Aviso, D.K.S. Ng, R.R. Tan, Fuzzy mixed-integer linear programming model for optimizing a multi-functional bioenergy system with biochar production for negative carbon emissions, Clean Technol. Environ. Policy. 16 (2014) 1537–1549. doi:10.1007/s10098-014-0721-z.

[128] A.T. Ubando, J.L. Cuello, M.M. El-Halwagi, A.B. Culaba, M.A.B. Promentilla, R.R. Tan, Application of stochastic analytic hierarchy process for evaluating algal cultivation systems for sustainable biofuel production, Clean Technol. Environ. Policy. 18 (2016) 1281–1294. doi:10.1007/s10098-015-1073-z.

[129] A.T. Ubando, A.B. Culaba, K.B. Aviso, R.R. Tan, J.L. Cuello, D.K.S. Ng, M.M. El-Halwagi, Fuzzy mixed integer non-linear programming model for the design of an algae-based eco-industrial park with prospective selection of support tenants under product price

variability, J. Clean. Prod. 136 (2016) 183–196. doi:10.1016/j.jclepro.2016.04.143.

[130] C.L. Sy, A.T. Ubando, K.B. Aviso, R.R. Tan, Multi-objective target oriented robust optimization for the design of an integrated biorefinery, J. Clean. Prod. 170 (2018) 496–509. doi:10.1016/j.jclepro.2017.09.140.

[131] J.S. Guest, M.C.M. Van Loosdrecht, S.J. Skerlos, N.G. Love, Lumped pathway metabolic model of organic carbon accumulation and mobilization by the alga Chlamydomonas reinhardtii, Environ. Sci. Technol. 47 (2013) 3258–3267. doi:10.1021/es304980y.

[132] S.M. Tibbetts, J.E. Milley, S.P. Lall, Chemical composition and nutritional properties of freshwater and marine microalgal biomass cultured in photobioreactors, J. Appl. Phycol. 27 (2015) 1109–1119. doi:10.1007/s10811-014-0428-x.

[133] S.O. Lourenço, E. Barbarino, P.L. Lavín, U.M. Lanfer Marquez, E. Aidar, Distribution of intracellular nitrogen in marine microalgae: Calculation of new nitrogen-to-protein conversion factors, Eur. J. Phycol. 39 (2004) 17–32. doi:10.1080/0967026032000157156.

[134] L.M. Laurens, Rewiring Algal Carbon Energetics for Renewables (RACER), in: BETO 2021 Peer Rev., Department of Energy Bioenergy Technologies Office, 2021.

[135] G.A. Alexandrov, Y. Yamagata, A peaked function for modeling temperature dependence of plant productivity, Ecol. Modell. 200 (2007) 189–192. doi:10.1016/j.ecolmodel.2006.07.012.

[136] J. Quinn, L. de Winter, T. Bradley, Microalgae bulk growth model with application to industrial scale systems, Bioresour. Technol. 102 (2011) 5083–5092. doi:10.1016/j.biortech.2011.01.019.

[137] S. Wilcox, W. Marion, Users Manual for TMY3 Data Sets, Golden, CO, 2008. https://www.nrel.gov/docs/fy08osti/43156.pdf.

[138] The University of Texas at Austin, Bold Basal Medium, (2019). https://utex.org/products/bold-basal-medium?variant=30991127609434 (accessed October 6, 2021).

[139] A.M. Lakaniemi, V.M. Intihar, O.H. Tuovinen, J.A. Puhakka, Growth of Chlorella vulgaris and associated bacteria in photobioreactors, Microb. Biotechnol. 5 (2012) 69–78. doi:10.1111/j.1751-7915.2011.00298.x.

[140] M. Ren, K. Ogden, B. Lian, Effect of culture conditions on the growth rate and lipid production of microalgae Nannochloropsis gaditana, J. Renew. Sustain. Energy. 5 (2013). doi:10.1063/1.4857375.

[141] J.R. Cruce, J.C. Quinn, Economic viability of multiple algal biorefining pathways and the impact of public policies, Appl. Energy. 233–234 (2019) 735–746. doi:10.1016/j.apenergy.2018.10.046.

[142] J. Bare, Tool for the Reduction and Assessment of Chemical and Other Environmental Impacts (TRACI) version 2.1, Cincinnati, OH, 2012. https://nepis.epa.gov/Adobe/PDF/P100HN53.pdf.

[143] IEA, Global fuel price changes, 2005-2019, (2020). https://www.iea.org/data-and-statistics/charts/global-fuel-price-changes-2005-2019 (accessed October 27, 2021).

[144] M. Carlier, Gasoline prices in selected countries worldwide in 2nd quarter of 2020, (2021). https://www.statista.com/statistics/221368/gas-prices-around-the-world/ (accessed October 13, 2021).

[145] C. Sandrock, S. Afshari, ternplot, (2016). doi:10.5281/zenodo.166760.

[146] J.M. Yoo, spider_plot, (2019). https://github.com/NewGuy012/spider_plot.

[147] S. Sathyendranath, V. Stuart, A. Nair, K. Oka, T. Nakane, H. Bouman, M.H. Forget, H.

Maass, T. Platt, Carbon-to-chlorophyll ratio and growth rate of phytoplankton in the sea, Mar. Ecol. Prog. Ser. 383 (2009) 73–84. doi:10.3354/meps07998.

[148] H.H. Jakobsen, S. Markager, Carbon-to-chlorophyll ratio for phytoplankton in temperate coastal waters: Seasonal patterns and relationship to nutrients, Limnol. Oceanogr. 61 (2016) 1853–1868. doi:10.1002/lno.10338.

[149] R. Davis, M. Wiatrowski, Algal Biomass Conversion to Fuels via Combined Algae Processing (CAP): 2019 State of Technology and Future Research, Golden, CO, 2020. https://www.nrel.gov/docs/fy20osti/76568.pdf.

[150] Y. Zhu, S. Jones, A. Schmidt, J. Billing, H. Job, J. Collett, S. Edmundson, K. Pomraning, S. Fox, T. Hart, A. Gutknecht, P. Meyer, M. Thorson, L. Snowden-Swan, D. Anderson, Microalgae Conversion to Biofuels and Biochemical via Sequential Hydrothermal Liquefaction (SEQHTL) and Bioprocessing : 2020 State of Technology, 2021.

[151] U.S. Energy Information Administration, Rising corn prices and oversupply push ethanol operating margins to multiyear lows, (2019). https://www.eia.gov/todayinenergy/detail.php?id=40813 (accessed December 7, 2021).

[152] J. Clippinger, R. Davis, Techno-Economic Analysis for the Production of Algal Biomass via Closed Photobioreactors : Future Cost Potential Evaluated Across a Range of Cultivation System Designs Techno-Economic Analysis for the Production of Algal Biomass via Closed Photobioreactor, Golden, CO, 2019. https://www.nrel.gov/docs/fy19osti/72716.pdf.

[153] Y. Zhu, D.B. Anderson, S.B. Jones, Algae farm cost model: Considerations for photobioreactors, Richland, WA, 2018. doi:10.2172/1485133.

[154] X.J. Ji, H. Huang, P.K. Ouyang, Microbial 2,3-butanediol production: A state-of-the-art

review, Biotechnol. Adv. 29 (2011) 351–364. doi:10.1016/j.biotechadv.2011.01.007.

[155] A.A. Koutinas, B. Yepez, N. Kopsahelis, D.M.G. Freire, A.M. de Castro, S. Papanikolaou, I.K. Kookos, Techno-economic evaluation of a complete bioprocess for 2,3-butanediol production from renewable resources, Bioresour. Technol. 204 (2016) 55–64. doi:10.1016/j.biortech.2015.12.005.

Appendix A

Table A - 1. Media recipes for modified Bold's basal medium (mBBM) and modified artificial seawater medium (MASM).

Modified Bold's basal medium (mBBM)	
Compound	**Concentration (mM)**
$NaNO_3$	10
$CaCl_2 \cdot 2H_2O$	1.70×10^{-1}
$MgSO_4 \cdot 7H_2O$	3.04×10^{-1}
K_2HPO_4	4.31×10^{-1}
KH_2PO_4	1.3
NaCl	4.28×10^{-1}
Na_2EDTA	8.92×10^{-2}
$FeCl_3 \cdot 6H_2O$	3.22×10^{-3}
$MnCl_2 \cdot 4H_2O$	7.28×10^{-3}
$ZnSO_4 \cdot 7H_2O$	3.07×10^{-2}
$CoCl_2 \cdot 6H_2O$	5.04×10^{-5}
$Na_2MoO_4 \cdot 2H_2O$	4.93×10^{-3}
$CuSO_4 \cdot 5H_2O$	6.89×10^{-3}
H_3BO_3	1.84×10^{-1}
Modified artificial seawater medium (MASM)	
Compound	**Concentration (mM)**
$NaNO_3$	10
$CaCl_2 \cdot 2H_2O$	2.0
$MgSO_4 \cdot 7H_2O$	10
KCl	8.0
KH_2PO_4	3.67×10^{-1}
NaCl	137
Tris base	8.26
Na_2EDTA	1.62×10^{-2}
$FeCl_3 \cdot 6H_2O$	4.32×10^{-3}
$MnCl_2 \cdot 4H_2O$	2.18×10^{-3}
$ZnCl_2$	8.82×10^{-4}
$CoCl_2 \cdot 6H_2O$	1.0×10^{-6}
$Na_2MoO_4 \cdot 2H_2O$	3.22×10^{-4}

Table A - 2. Iterative assignment parameters.

Assignment order	C limits	H limits	N limits	O limits	Na limits	Ion type	Error limit
1	1 - 100	4 - 200	1 - 3	1 - 6	0	Protonated	1 ppm
2	1 - 100	4 - 200	1 - 3	1 - 6	1	Adduct	1 ppm
3	1 - 100	4 - 200	4 - 6	1 - 6	0	Protonated	1 ppm
4	1 - 100	4 - 200	4 - 6	1 - 6	1	Adduct	1 ppm
5	1 - 100	4 - 200	1 - 10	1 - 10	0	Protonated	1 ppm
6	1 - 100	4 - 200	1 - 10	0	0	Protonated	1 ppm

Table A - 3. Free ammonia and ammonium concentrations (mM) derived from 10 mM NH_4Cl at pH 6.0 to 9.5.

pH	$[NH_4^+]$ (mM)	$[NH_3]$ (mM)
6.0	9.99	0.01
6.1	9.99	0.01
6.2	9.99	0.01
6.3	9.99	0.01
6.4	9.99	0.01
6.5	9.98	0.02
6.6	9.98	0.02
6.7	9.97	0.03
6.8	9.96	0.04
6.9	9.96	0.04
7.0	9.94	0.06
7.1	9.93	0.07
7.2	9.91	0.09
7.3	9.89	0.11
7.4	9.86	0.14
7.5	9.83	0.17
7.6	9.78	0.22
7.7	9.73	0.27
7.8	9.66	0.34
7.9	9.57	0.43
8.0	9.47	0.53
8.1	9.34	0.66
8.2	9.18	0.82
8.3	8.99	1.01
8.4	8.76	1.24
8.5	8.49	1.51
8.6	8.17	1.83
8.7	7.80	2.20
8.8	7.38	2.62
8.9	6.91	3.09
9.0	6.40	3.60
9.1	5.85	4.15
9.2	5.29	4.71
9.3	4.71	5.29
9.4	4.15	5.85
9.5	3.60	6.40

Table A - 4. Ash-free compositional data comparison between treatments for lipids, measured as fatty acid methyl esters (FAMEs), proteins, carbohydrates, carbon, hydrogen, and nitrogen. All data shown as the average ± standard deviation of three replicate measurements (n = 3) with exception of 200x AC and 100x DX.

	FAME	Protein	Carbohydrate	C	H	N
Control	10.74 ± 0.03	32.83 ± 0.06	23.72 ± 0.35	49.17 ± 0.14	7.39 ± 0	6.87 ± 0.02
200x untreated	11.37 ± 0.16	31.68 ± 0.96	26.23	49.68 ± 0.31	7.49 ± 0.06	6.63 ± 0.2
100x untreated	10.35 ± 0.74	35.6 ± 0.69	-	49.98 ± 0.57	7.53 ± 0.07	7.45 ± 0.14
200x AC	10.5	30.88	32.49	48.79	7.41	6.47
100x AC	10.45 ± 0.22	31.4 ± 0.13	29.09 ± 0.67	49.21 ± 0.29	7.46 ± 0.04	6.57 ± 0.03
200x DX	11.09 ± 0.2	33.82 ± 0.13	24.53 ± 1.65	50.01 ± 0.06	7.46 ± 0.03	7.08 ± 0.03
100x DX	11	33.34	25.06	49.96	7.48	6.98

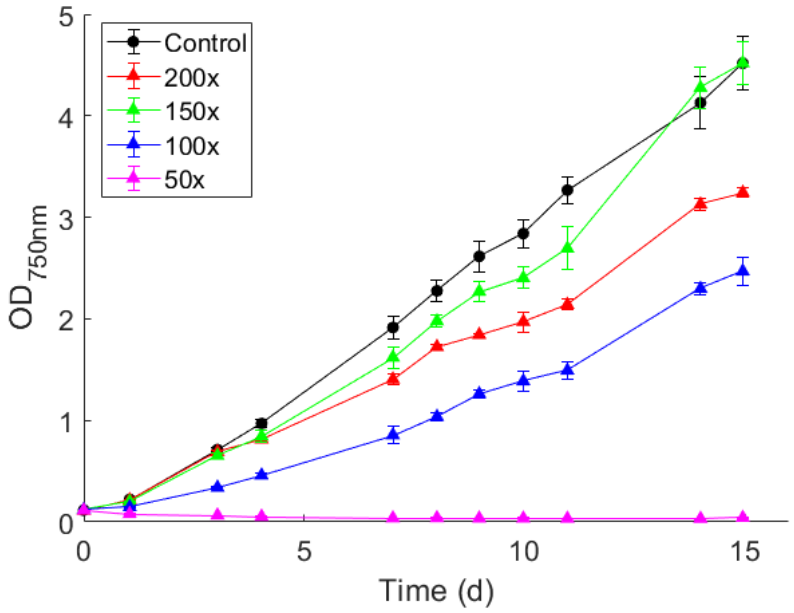

Figure A - 1. Growth of C. vulgaris *in mBBM with varying untreated HTL-AP dilutions. All treatments were grown in duplicate under constant light (50 µE) and temperature (24 °C).*

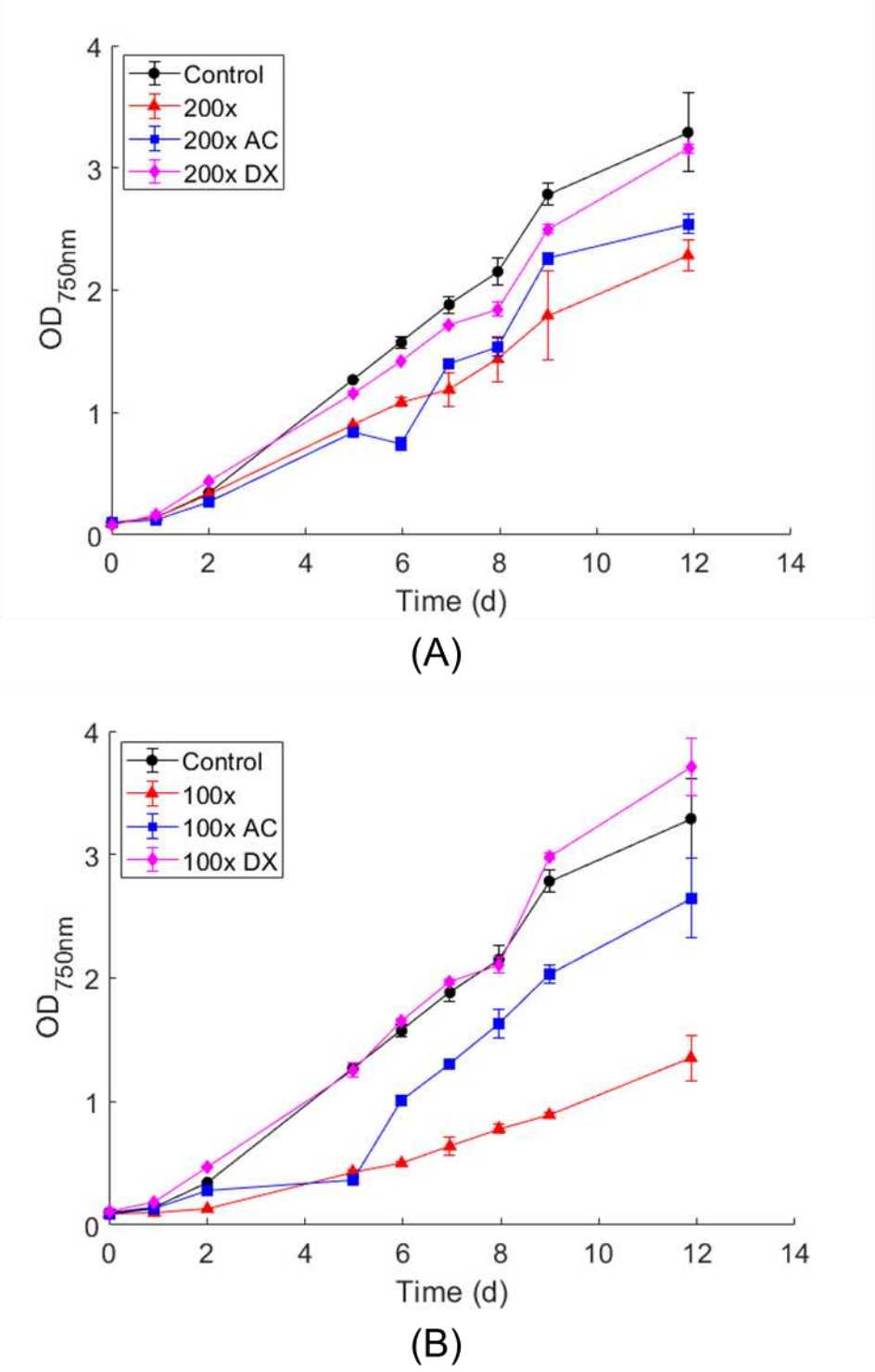

Figure A - 2. Growth of C. vulgaris *in mBBM with (A) 200x and (B) 100x dilutions of untreated, AC, and DX treated HTL-AP. Both treatments showed significant improvement in growth at 100x dilution compared to the untreated HTL-AP. DX treated HTL-AP performed especially well, performing on par with the control.*

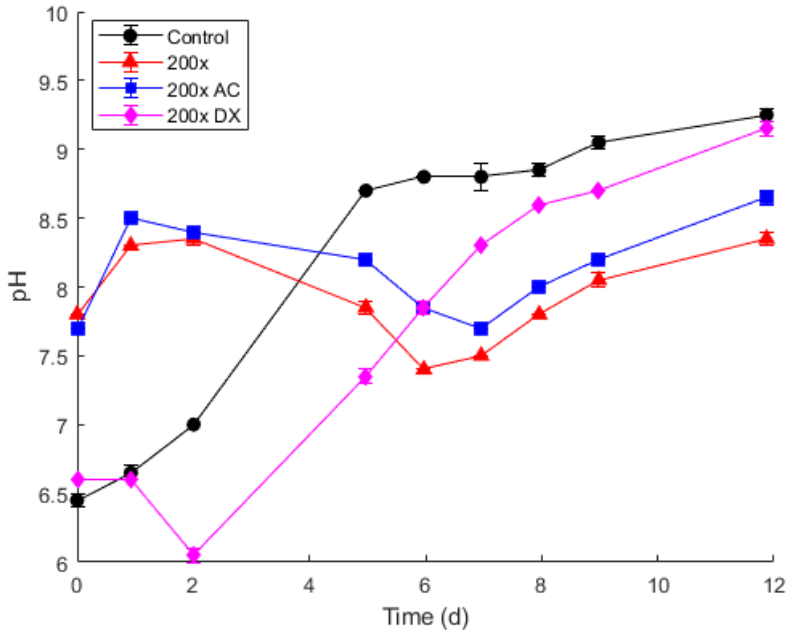

Figure A - 3. pH measurements of C. vulgaris in 200x dilutions of HTL-AP. The DX treatment was notably more buffered than the control.

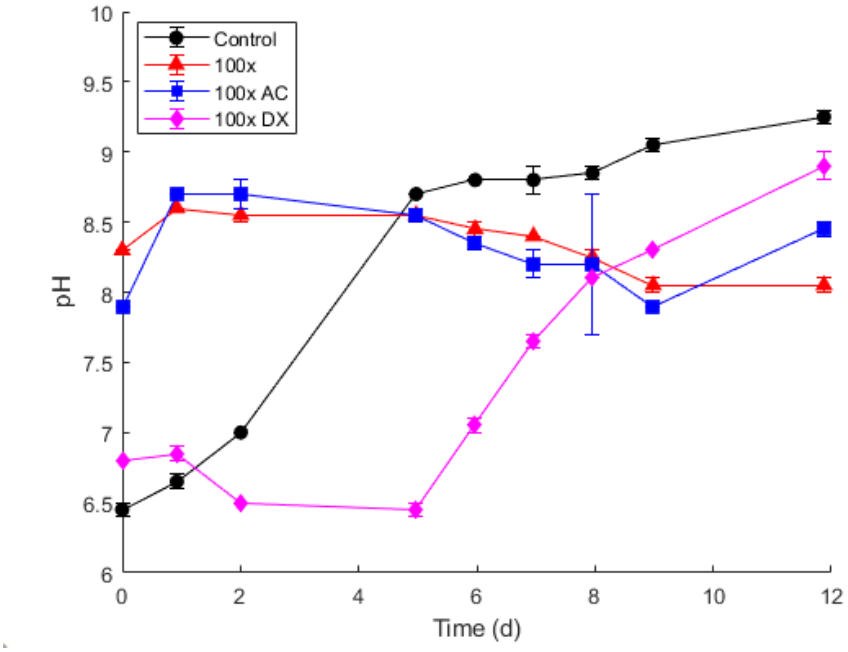

Figure A - 4. pH measurements of C. vulgaris in 100x dilutions of HTL-AP. The DX treatment was significantly buffered around the starting pH (~6.8) for much longer compared to the control and other treatments.

Appendix B

Studies with exceptionally short (< 5 min) or exceptionally long (> 60 min) residence times were not considered representative of a commercial-scale HTL system and were excluded from this work. Li et al. (2014) saw much higher biocrude yields than usual at very low temperatures (220 – 260 °C), albeit with much longer residence times, up to 90 min [76]. López Barreiro et al. (2013) reported typical yields at both low (250 °C) and high temperatures (375 °C) with a very short residence time of 5 minutes [77]. Other data were eliminated from consideration if solids loading was outside of a typical post-dewater range of 15 – 25 wt% [99]. Jena et al. (2011) pointed out that many previous HTL studies conducted experiments at 10% feed solids or lower, which is an inefficient use of capital investment [73]. López Barreiro et al. (2013) and Dote et al. (1994) only used 5 – 7 wt% solids loading, much lower than the typical harvesting range [77,81]. Knorr et al. (2013) has shown that an HTL configuration with very high biomass loading (36 wt% wood slurry) can decrease operating costs by 53% and capital costs by 85% [70]. However, this biomass loading is beyond the capability of typical algae dewatering [99] and even if that were achieved, pumping issues would likely arise.

Table B - 1. HTL feed components and mass fractions.

Component	***Aspen Plus* ID**	**Mass fraction**
Water	H2O	0.790307
Sucrose	SUCROSE	0.005119
Algae lipids	OIL	0.010237
Triacylglycerides	TAG	0.01556
Algal cell moisture	ALGH2O	0.007621
Glucan	GLUCAN	0.068552
Algae proteins	PROTEIN	0.05569
Ash	ASH	0.007166
Other cell components	ALG1CELL	0.039748

Table B - 2. HTL aqueous phase components and mass fractions based on Jones et al. (2014) [21].

Component	***Aspen Plus* ID**	**Mass fraction**
Water	H2O	0.915774
Ethanol	ETHANOL	0.003061
Acetic acid	AACID	0.009184
Glycerol	GLYCEROL	0.003061
Ammonia	NH3	0.009475
Carbon dioxide	CO2	0.002075
Formic acid	FORMIC	0.030516
Acetone	ACETONE	0.003061
Methanol	METHANOL	0.015282
1-ethyl-2-pyrrolidinone	1E2PYDIN	0.001095
N-methylthiopyrrolidone	C5H9NS	0.002823
3-hydroxypyridine	3-PYRDOL	0.004592

Table B - 3. HTL biocrude components and mass fractions based on Jones et al. (2014) [21].

Component	***Aspen Plus* ID**	**Mass fraction**
1-ethyl-2-pyrrolidinone	1E2PYDIN	0.067948
N-methylthiopyrrolidone	C5H9NS	0.010271
Ethylbenzene	ETHYLBEN	0.025546
p-cresol	4M-PHYNO	0.051093
p-ethylphenol	4EPHYNOL	0.051093
Indole	INDOLE	0.051093
7-methylindole	7MINDOLE	0.033974
Myristamide	C14AMIDE	0.033974
Hexadecanamide / Palmitic amide	C16AMIDE	0.152752
Octadecamide	C18AMIDE	0.067948
cis-9-hexadecenoic acid	C16:1FA	0.135633
N-hexadecenoic acid	C16:0FA	0.101659
Oleic acid	C18FACID	0.017119
Naphthalene	NAPHATH	0.051093
Beta-cholesterol	CHOLESOL	0.016855
Aniline	AROAMINE	0.081117
Phthalic acid	C30DICAD	0.050830

Table B - 4. Other upgraded fuel components (Jones et al., 2014) [21].

Component	***Aspen Plus* ID**
2-methylbutane	2MBUTANE
2-methylpentane	2MPENTAN
2-methylhexane	2MHEXAN
Heptane	HEPTANE
Methylcyclohexane	CC6-METH
Piperidine	PIPERDIN
Toluene	TOLUENE
3-methylheptane	3MHEPTA
Octane	OCTANE
Ethylcyclohexane	ETHCYC6
o-xylene	O-XYLENE
Nonane	C9H20
N-propylcyclohexane	PROCYC6
N-propylbenzene	C3BENZ
Decane	C10H22
N-butylbenzene	C4BENZ
Undecane	C11H24
1-butenylbenzene	C10H12
Dodecane	C12H26
1,2,3,4-tetrahydronaphthalene	1234NA
N-hexylbenzene	C6BENZ
6-methyltetralin	12346N
N-heptylbenzene	C7BENZ
N-octylbenzene	C8BENZ
1,4-dimethylcyclohexane	C10H16O4
Pentadecane	C15H32
Hexadecane	C16H34
Heptadecane	C17H36
Octadecane	C18H38
Nonadecane	C19H40
Heneicosane	C21H44
Tricosane	C23H48
Triacontane	C30H62
Phytane	PHYTANE
Diisooctylphthalate	C24H38O4
Heptyl undecyl phthalate	C26H42O4
Ammonium sulfate	N2H8SO4
Ammonium carbonate	N2H8CO3

Table B - 5. Parameters for HTL capital estimation (Knorr et al., 2013) [70].

Equipment	Unit cost	Year	Scaling variable	Base value	Scaling exponent	Installation factor
Reactor heat exchanger	$44,604,000	2012	Area	49,756 ft^2	0.7	2.2
Reactor heater	$998,850	2012	Area	6,032 ft^2	0.7	2.2
HTL reactor	$272,788	2013	Length	480 ft	1	2
Gas knockout drum	$5,600,000	2012	Volume	1 ft^3	0.7	2
Solids filter	$1,311,000	2011	Biocrude flow rate	3,689 gpm	0.6	1.7
Phase separator	$3,565,000	2011	Biocrude flow rate	3,689 gpm	0.7	2
Bio-oil heat recovery	$102,000	2012	Area	868 ft^2	0.7	2.2
Purge water cooler	$255,600	2013	Area	13,020 ft^2	0.8	2.3
Hot oil	$2,101,710	2012			1	1
Hot oil system	$1,200,500	2012	Heat duty	60 MMbtu hr^{-1}	0.6	1.8

Table B - 6. Parameters for biocrude upgrading capital estimation (Jones et al., 2014) [21].

Equipment	Unit cost	Year	Scaling variable	Base value	Scaling exponent	Installation factor
Hydrotreater and auxiliaries	$27,000,000	2007	Biocrude flow rate	6,524 bbl d^{-1}	0.75	1.51
HT hydrogen compressor	$1,385,600	2011	Hydrogen flow rate	17.1 MMscf d^{-1}	0.8	1.1
HT pressure swing absorber	$1,750,000	2004	Offgas flow rate	10 MMscf d^{-1}	0.8	2.47
Hydrocracker and auxiliaries	$25,000,000	2007	Heavy oil flow rate	2,200 bbl d^{-1}	0.75	1.51

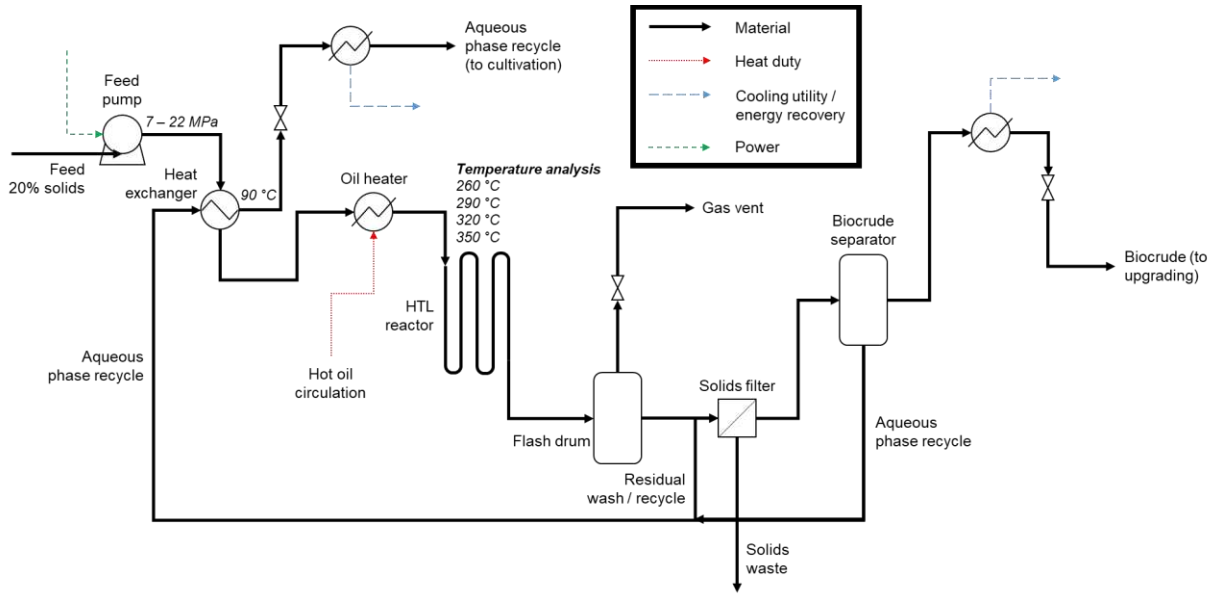

Figure B - 1. Process flow diagram of HTL reactor system. (For detailed process flow diagrams of hydrotreating and hydrocracking, refer to Jones et al. (2014) [21].*) The HTL reactor temperature varies in the temperature analysis, with a constraint on the heat exchanger to maintain 90 °C at the hot stream exit.*

Knorr et al. (2013) compared three different HTL reactor configurations based on pumping and heating considerations with a lignocellulosic feedstock. “Case A” was defined by a partial recycle of the feed stream to indirectly heat an incoming cold feed. This heating method was designed to avoid pumping issues caused by high slurry viscosity below 250 °C; however, heat integration potential was very poor due to high mass flow rates feeding into the primary heater. “Case B” was defined by simple and effective heat integration, where all of the aqueous waste was recycled as an integrated hot stream to pre-heat the reactor feed. The major downside of Case B was poor heat transfer due to high feed viscosity at colder incoming temperatures. The last scenario, “Case D,” offered a similar solution to Case A, but the incoming feed was introduced at 36.6 wt% solids and diluted before entering the reactor by mixing a portion of recycled aqueous waste [70]. It is worth noting that algae processing cannot feasibly dewater a wet biomass stream to 36.6 wt% solids without very significant energy investment. For the purposes of this work, Case A was not used due to its high energy requirements and Case D was ruled out as impractical for an algae system. Case B served as the basis for Jones et al. (2014) and was considered the best option for this study as well [21].

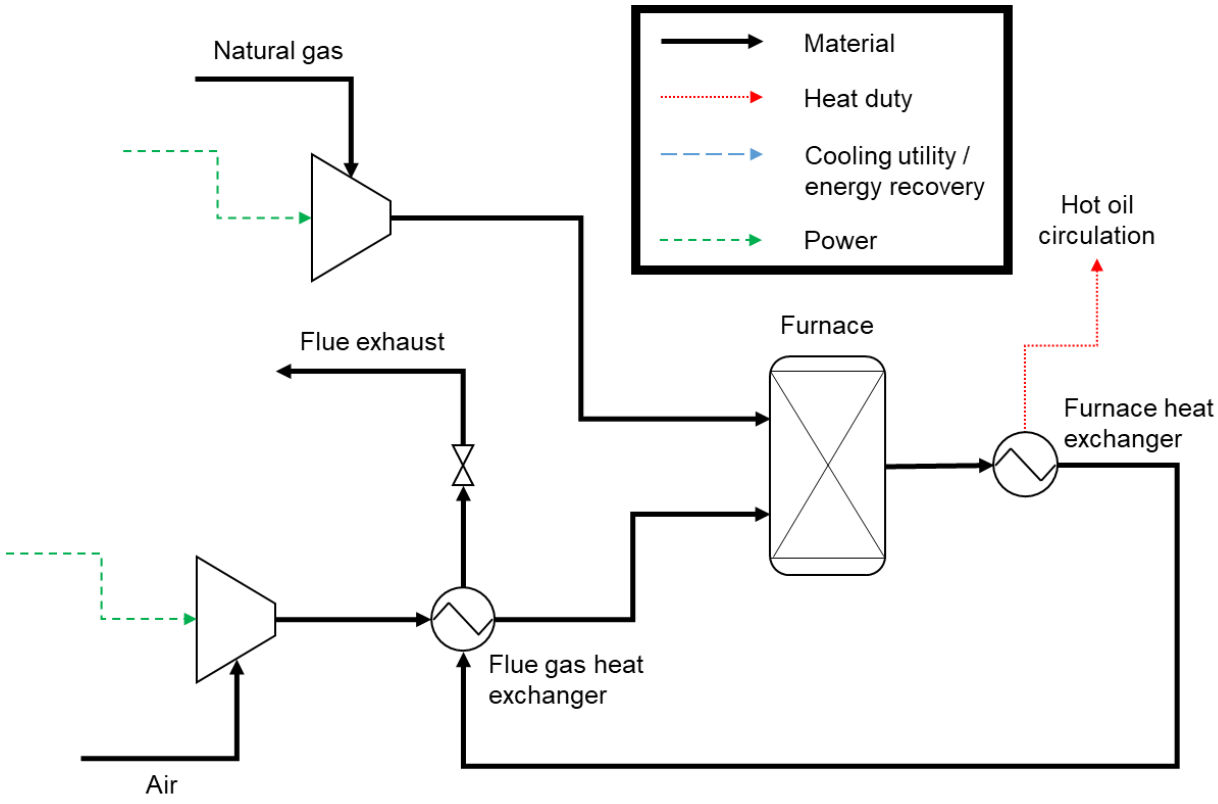

Figure B - 2. Simplified process flow diagram of natural gas heating utility for the HTL system. Heat duty for biocrude upgrading uses a very similar process, but does not require hot oil circulation.

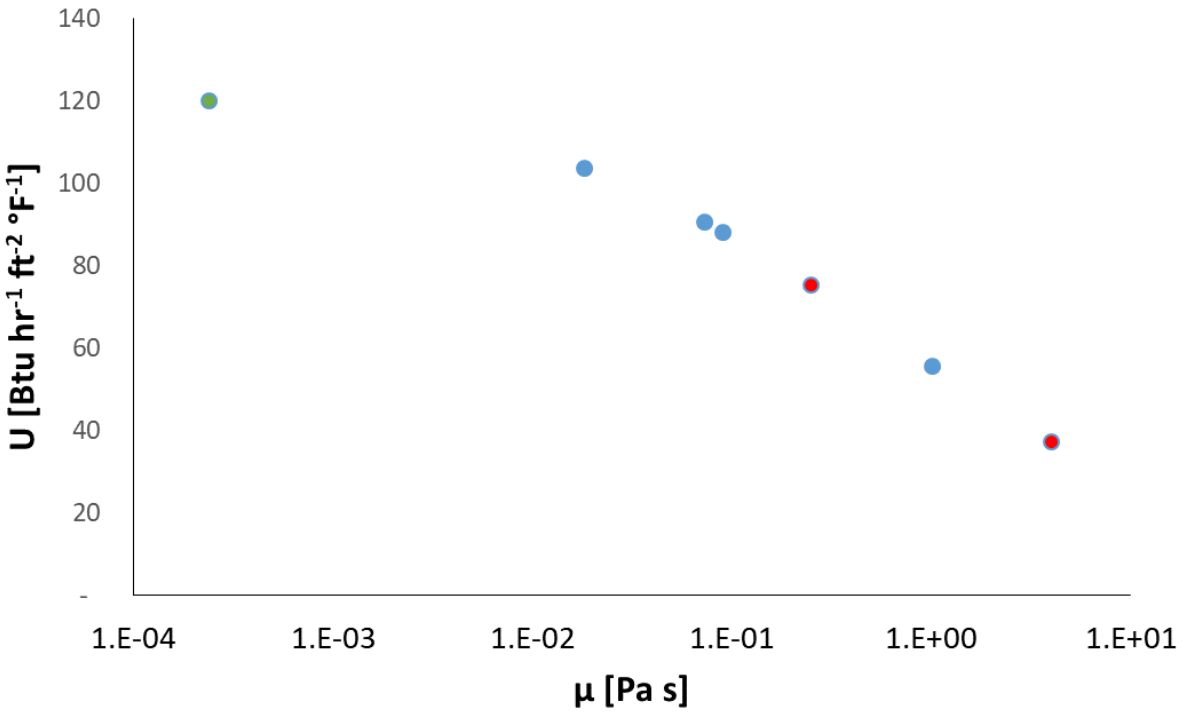

Figure B - 3. Correlation between overall heat transfer coefficient and viscosity fixed at a fouling of 150 BTU hr^{-1} ft^{-2} °F^{-1}. Viscosity values in blue were based on rheological literature on algae slurries. The green data point represents water and the red data points represent PNNL rheological studies on wood slurries (Knorr et al., 2013) [70].

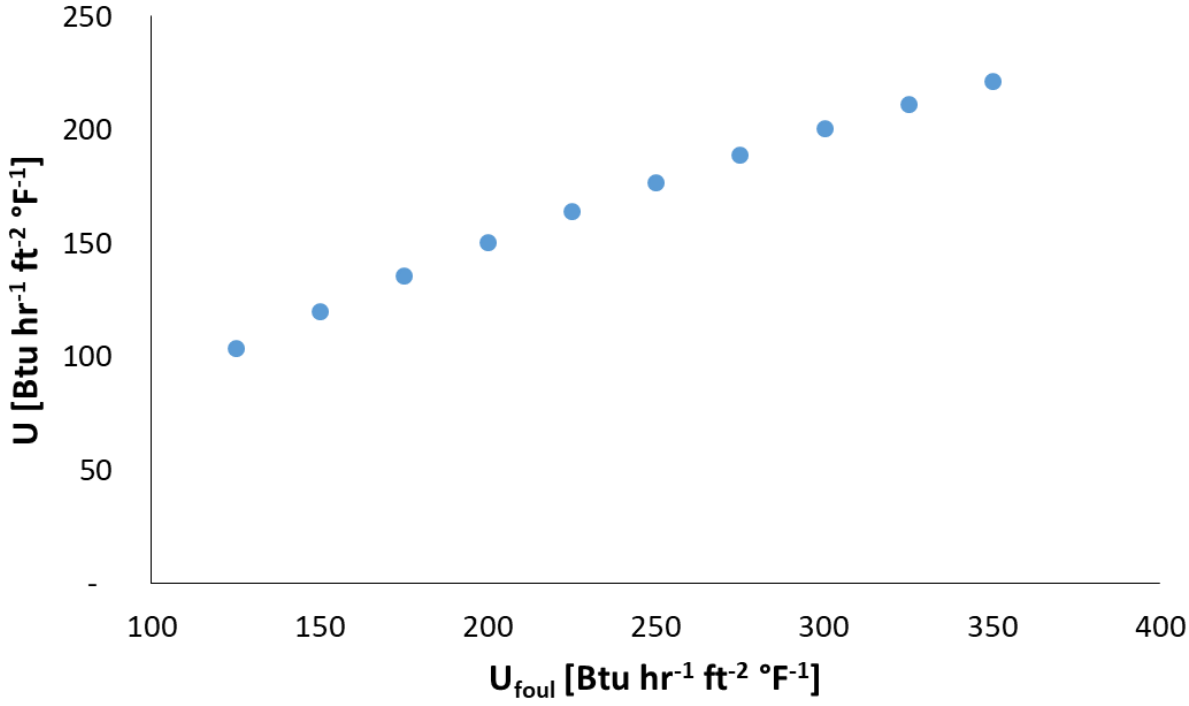

Figure B - 4. Correlation between fouling and viscosity fixed at a viscosity of 1.8×10^{-2} Pa·s (Schneider & Gerber, 2014) [101]. *Fouling values were varied from the bounds described in Knorr et al. (2013)* [70].

FOAK plant economic assumptions from Merrow et al. (1981) [98]:

$$COSTGROWTH = a + b_1(PCTNEW) + b_2(IMPURITIES) + b_3(COMPLEXITY) + b_4(INCLUSIVENESS) + b_5(PROJDEF)$$

$$PLANTPERFORM = a + b_1(NEWSTEPS) + b_2(BALEQ) + b_3(WASTE) + b_4(SOLIDS)$$

Fitting parameter	Value	Variable	Value
a	1.12196	PCTNEW	65
b_1	-0.00297	IMPURITIES	4
b_2	-0.02125	COMPLEXITY	4
b_3	-0.01137	INCLUSIVENESS	33.3
b_4	0.00111	PROJDEF	3
b_5	-0.06361	*COSTGROWTH*	*0.64*

Fitting parameter	Value	Variable	Value
a	85.77	NEWSTEPS	65
b_1	-9.69	BALEQ	4
b_2	0.33	WASTE	4
b_3	-4.12	SOLIDS	33.3
b_4	-17.19	*PLANTPERFORM*	*58.875*

$$CAPEX_{FOAK} = \frac{CAPEX_{NOAK}}{COSTGROWTH}$$

For every year i such that $PLANTPERFORM + \frac{20(i-1)}{100} < 100$,

$$OPEX_{var,FOAK,i} = \left(OPEX_{var,NOAK}\right)\left(PLANTPERFORM + \frac{20(i-1)}{100}\right)$$

Appendix C

Table C - 1. List of state variables expressed in the compositional growth model [131]*. Initial conditions listed in this table were fixed for all scenarios (except R, which was varied in the uncertainty analysis).*

State variable	Definition	Initial condition	References
R	Chlorophyll to biomass carbon ratio	0.03 g g^{-1}	[148]
X_{CPO}	Concentration of carbon-accumulating phototrophic organisms (CPO) / remaining biomass	3.9×10^{-3} C-mol L^{-1} (100 g VSS m^{-3})	[62]
X_{CH}	Molar concentration of storage carbohydrates	$0.01 \times X_{CPO}$	
X_{LI}	Molar concentration of storage lipids	$0.01 \times X_{CPO}$	
S_{CO_2}	Molar concentration of soluble carbon dioxide	3.3×10^{-2} mol L^{-1}	Saturation concentration
S_{O_2}	Molar concentration of soluble oxygen	2.4×10^{-4} mol L^{-1}	Saturation concentration
S_{NO}	Molar concentration of soluble nitrate	8.8×10^{-4} mol L^{-1}	[138]
S_P	Molar concentration of soluble phosphorus	1.2×10^{-4} mol L^{-1}	[138]
X_N	Molar concentration of cell-associated nitrogen	$0.2 \times X_{CPO}$	[109,131]
X_P	Molar concentration of cell-associated phosphorus	$0.02 \times X_{CPO}$	[109,131]

Table C - 2. List of variables and their baseline values in the compositional growth model.

Variable	Baseline value / Equation	Units	References
β_1	2.9	N/A	[109,131]
β_2	3.5	N/A	[109,131]
η_{dark}	0.70	N/A	[109,131]
θ_T	$\frac{2f(T)}{1+f^2(T)}$	N/A	[136]
$\hat{\mu}$	1.97, *C. vulgaris* 0.52, *N. granulata* [g]	d^{-1}	[109,139,140]
ρ	1.2	N/A	[109,131]
a_c	0.049	$m^2(g\ VSS)^{-1}$	[109,131]
$b_{reactor}$	0.25	m	[62]
E_a	63	$kJ\ mol^{-1}$	[136]
$f(T)$	$e^{\frac{E_a}{RT}\left(\frac{1}{T_{opt}}-\frac{1}{T}\right)}$	N/A	[136]
f_I	$\frac{I}{I+I_n(0.25-5R)\left(\frac{I^2}{I_{opt}^2}-\frac{2I}{I_{opt}}+1\right)}$	N/A	[109,131]
f_{CH}	$\frac{X_{CH}}{X_{CPO}}$	$C\ mol\ X_{CH}\ (C\ mol\ X_{CPO})^{-1}$	[109,131]
f_{CH}^{max}	1.08, *C. vulgaris* 0.41, *N. granulata*	$C\ mol\ X_{CH}\ (C\ mol\ X_{CPO})^{-1}$	[109]
f_{LI}	$\frac{X_{LI}}{X_{CPO}}$	$C\ mol\ X_{LI}\ (C\ mol\ X_{CPO})^{-1}$	[109,131]
f_{LI}^{max}	2.03, *C. vulgaris* 3.25, *N. granulata*	$C\ mol\ X_{LI}\ (C\ mol\ X_{CPO})^{-1}$	[109]
I	$\frac{I_o}{a_c b_{reactor} X_{VSS}}(1-e^{-a_c b_{reactor} X_{VSS}})$ [h]	$\mu E\ m^{-2}s^{-1}$	[131]
I_n	TMY3 data (maximum I_o)	$\mu E\ m^{-2}s^{-1}$	[137]
I_o	TMY3 data (current incident light)	$\mu E\ m^{-2}s^{-1}$	[137]
I_{opt}	300	$\mu E\ m^{-2}s^{-1}$	[109,131]
K_{STO}	1.6	$C\ mol\ X_{CH}\ (C\ mol\ X_{CPO})^{-1}$	[109,131]
m_{ATP}	0.19, *C. vulgaris* 0.20, *N. granulata*	$mol\ ATP\ (C\ mol\ X_{CPO})^{-1}d^{-1}$	[109]
$\hat{q}_{CH}$	0.51, *C. vulgaris* 0.21, *N. granulata*	$C\ mol\ X_{CH}\ (C\ mol\ CO_2)^{-1}d^{-1}$	[109]

[g] The literature value of *Nannochloropsis gaditana* was substituted for *Nannochloropsis granulata*.
[h] The original reference multiplies the equation for I by a factor of 2 for a photobioreactor illuminated on two sides.

$\hat{q}_{LI}$	0.69, *C. vulgaris* 1.21, *N. granulata*	$C\ mol\ X_{LI}\ (C\ mol\ CO_2)^{-1} d^{-1}$	[109]
Q_{limit}	$\min\left(1-\left(\frac{Q_{N,min}}{Q_N}\right)^4, 1-\left(\frac{Q_{P_{min}}}{Q_P}\right)^4\right)$	$mol\ N\ (C\ mol\ X_{CPO})^{-1}$ or $mol\ P\ (C\ mol\ X_{CPO})^{-1}$	[109,131]
Q_N	$\frac{X_N}{X_{CPO}}$	$mol\ N\ (C\ mol\ X_{CPO})^{-1}$	[109,131]
Q_P	$\frac{X_P}{X_{CPO}}$	$mol\ P\ (C\ mol\ X_{CPO})^{-1}$	[109,131]
$\bar{R}$	8.314×10^{-3}	$kJ\ mol^{-1} K^{-1}$	Ideal gas constant
T	TMY3 data (current temperature)	$°C$ or K	[137]
T_{opt}	23	$°C$	[136]
X_{VSS}	$X_{CPO} MW_{CPO} + X_{CH} MW_{CH} + X_{LI} MW_{LI}$	$g\ VSS\ m^{-3}$	[109,131]
Y_{ATP}	4.78	$mol\ ATP\ (C\ mol\ CO_2)^{-1}$	[109,131]
Y_{CH}^{NR}	1.04	$C\ mol\ X_{CH}\ (C\ mol\ CO_2)^{-1}$	[109,131]
Y_{LI}^{NR}	0.86	$C\ mol\ X_{LI}\ (C\ mol\ CO_2)^{-1}$	[109,131]
Y_{XCPO}	0.58	$C\ mol\ X_{CPO}\ (C\ mol\ CO_2)^{-1}$	[109,131]

Table C - 3. Vector of transformation processes in the compositional growth model, collectively termed $\vec{P}$ [131].

	Process	Differential rate expression
P_1	Photoadaptation	$\left(\frac{0.2\frac{I}{I_n}}{K_{gamma}+\frac{I}{I_n}}\right)\left(0.01+0.03\left(\frac{\ln\left(\frac{I}{I_n}+0.005\right)}{\ln(0.01)}\right)-R\right)$
P_2	Nitrate uptake	$\hat{V}_{NO}\left(\frac{S_{NO}}{K_{NO}+S_{NO}}\right)X_{CPO}$
P_3	Phosphorus uptake	$\hat{V}_{P}\left(\frac{S_{P}}{K_{P}+S_{P}}\right)X_{CPO}$
P_4	Photoautotrophic growth	$\hat{\mu}Q_{limit}f_I\left(1-\frac{\rho f_{CH}+f_{LI}\frac{Y_{CH}^{NR}}{Y_{LI}^{NR}}}{K_{STO}(1-f_I)+\rho f_{CH}+f_{LI}\frac{Y_{CH}^{NR}}{Y_{LI}^{NR}}}\right)X_{CPO}$
P_5	Growth on stored carbohydrates	$\hat{\mu}Q_{limit}\max(f_I,\eta_{dark})\left(\frac{\rho f_{CH}}{K_{STO}(1-f_I)+\rho f_{CH}+f_{LI}\frac{Y_{CH}^{NR}}{Y_{LI}^{NR}}}\right)X_{CPO}$
P_6	Growth on stored lipids	$\hat{\mu}Q_{limit}\max(f_I,\eta_{dark})\left(\frac{f_{LI}\frac{Y_{CH}^{NR}}{Y_{LI}^{NR}}}{K_{STO}(1-f_I)+\rho f_{CH}+f_{LI}\frac{Y_{CH}^{NR}}{Y_{LI}^{NR}}}\right)X_{CPO}$
P_7	Degradation of stored carbohydrates for cell maintenance	$m_{ATP}\left(\frac{Y_{CH}^{NR}}{Y_{ATP}}\right)\left(\frac{\rho f_{CH}}{K_{STO}+\rho f_{CH}+f_{LI}\frac{Y_{CH}^{NR}}{Y_{LI}^{NR}}}\right)X_{CPO}$
P_8	Degradation of stored lipids for cell maintenance	$m_{ATP}\left(\frac{Y_{LI}^{NR}}{Y_{ATP}}\right)\left(\frac{f_{LI}\frac{Y_{CH}^{NR}}{Y_{LI}^{NR}}}{K_{STO}+\rho f_{CH}+f_{LI}\frac{Y_{CH}^{NR}}{Y_{LI}^{NR}}}\right)X_{CPO}$
P_9	Endogenous respiration	$m_{ATP}\left(\frac{Y_{XCPO}}{Y_{ATP}}\right)\left(1-\frac{\rho f_{CH}+f_{LI}\frac{Y_{CH}^{NR}}{Y_{LI}^{NR}}}{K_{STO}+\rho f_{CH}+f_{LI}\frac{Y_{CH}^{NR}}{Y_{LI}^{NR}}}\right)X_{CPO}$
P_{10}	Carbohydrate storage	$\hat{q}_{CH}\left(1-\left(\frac{f_{CH}}{f_{CH}^{max}}\right)^{\beta_1}\right)\max\left(\left(\frac{Q_{N,min}}{Q_N}\right)^4,\left(\frac{Q_{P,min}}{Q_P}\right)^4\right)f_I X_{CPO}$
P_{11}	Lipid storage	$\hat{q}_{LI}\left(1-\left(\frac{f_{LI}}{f_{LI}^{max}}\right)^{\beta_2}\right)\left(\frac{Q_{N,min}}{Q_N}\right)^4 f_I X_{CPO}$

Table C - 4. Stoichiometric matrix of the compositional growth model, collectively termed A [131].

	R	X_{CPO}	X_{CH}	X_{LI}	S_{CO2}	S_{O2}	S_{NO}	S_P	X_N	X_P
P_1	1	0	0	0	0	0	0	0	0	0
P_2	0	0	0	0	0	0	-1	0	1	0
P_3	0	0	0	0	0	0	0	-1	0	1
P_4	0	1	0	0	-1	$\frac{1479}{1020}$	0	0	$-Q_{N,min}$	$-Q_{P,min}$
P_5	0	1	$-\frac{Y_{CH}^{NR}}{Y_{XCPO}}$	0	$\frac{Y_{CH}^{NR}}{Y_{XCPO}} - 1$	$-\frac{Y_{CH}^{NR}}{Y_{XCPO}} + \frac{1479}{1020}$	0	0	$-Q_{N,min}$	$-Q_{P,min}$
P_6	0	1	0	$-\frac{Y_{LI}^{NR}}{Y_{XCPO}}$	$\frac{Y_{LI}^{NR}}{Y_{XCPO}} - 1$	$-\frac{145}{102}\frac{Y_{CH}^{NR}}{Y_{XCPO}} + \frac{1479}{1020}$	0	0	$-Q_{N,min}$	$-Q_{P,min}$
P_7	0	0	-1	0	1	-1	0	0	0	0
P_8	0	0	0	-1	1	$-\frac{145}{102}$	0	0	0	0
P_9	0	-1	0	0	1	$-\frac{1479}{1020}$	0	0	0	0
P_{10}	0	0	1	0	-1	1	0	0	0	0
P_{11}	0	0	0	1	-1	$\frac{145}{102}$	0	0	0	0

The system of differential rate equations is represented by the following matrix equation (Eq. S1) and solved in MATLAB's ode23s function:

$$\frac{d\vec{X}_{state}}{dt} = \theta_T(t) \times A \times \vec{P}(t) \tag{S1}$$

Table C - 5. Monte Carlo distribution limits of the growth model and production-scale cultivation parameters. If two values are listed, the first value represents Chlorella vulgaris and the second represents Nannochloropsis granulata.

Parameter	Distribution shape	Minimum	Most probable	Maximum	References
$f_{CH}^{\max}$ [C-mol carb. C-mol CPO^{-1}]	Triangular	0.97 0.37	1.08 0.41	1.18 0.45	[109]
$f_{LI}^{\max}$ [C-mol lipids C-mol CPO^{-1}]	Triangular	1.83 2.92	2.03 3.25	2.23 3.57	[109]
m_{ATP} [mol ATP C-mol CPO^{-1} d^{-1}]	Triangular	0.17 0.18	0.19 0.20	0.21 0.22	[109]
$\hat{q}_{CH}$ [C-mol carb. C-mol CPO^{-1} d^{-1}]	Triangular	0.46 0.19	0.51 0.21	0.56 0.23	[109]
$\hat{q}_{LI}$ [C-mol lipids C-mol CPO^{-1} d^{-1}]	Triangular	0.62 1.09	0.69 1.21	0.76 1.33	[109]
Initial chlorophyll:carbon ratio (R) [g Chl-a (g CPO)$^{-1}$]	Normal ($P = 99.9\%$)	0.01	0.03	0.05	[148]
Dewatered solids content [total wt%]	Triangular	15%	20%	20%	[99,124]
Ash content [dry solids wt%]	Triangular	2.8% 5.1%	5.8% 6.8%	6.1% 14.2%	[62,132]

Table C - 6. Monte Carlo distribution limits of conversion pathway parameters and other economic / life cycle inventory.

Parameter	Distribution shape	Minimum	Most probable	Maximum	References
Nutrient recycle [%]	Triangular	30%	60%	90%	[124]
CAP fermentable carbohydrate conversion [%]	Triangular	80%	88%	92%	[134]
CAP lipid extraction yield [%]	Triangular	87%	92%	95%	[134]
HTL biocrude yield from lipids [%]	Triangular	69%	85%	100%	[109]
HTL biocrude yield from proteins [%]	Triangular	42%	45%	48%	[109]
HTL biocrude yield from carbohydrates [%]	Triangular	16%	21%	26%	[109]
HTL gas yield from proteins [%]	Triangular	5%	7%	9%	[109]
HTL gas yield from carbohydrates [%]	Triangular	39%	42%	45%	[109]
HTL residence time [min]	Triangular	15	30	60	[124]
Hydrogen cost [$ kg^{-1}]	Triangular	$1.10	$1.57	$2.10	[94]
Electricity GWP [kg CO_2eq kWh^{-1}]	Triangular	0.012	0.6	1	[95]
Hydrogen GWP [kg CO_2eq kg^{-1}]	Triangular	2.21	12.13	29.54	[96]

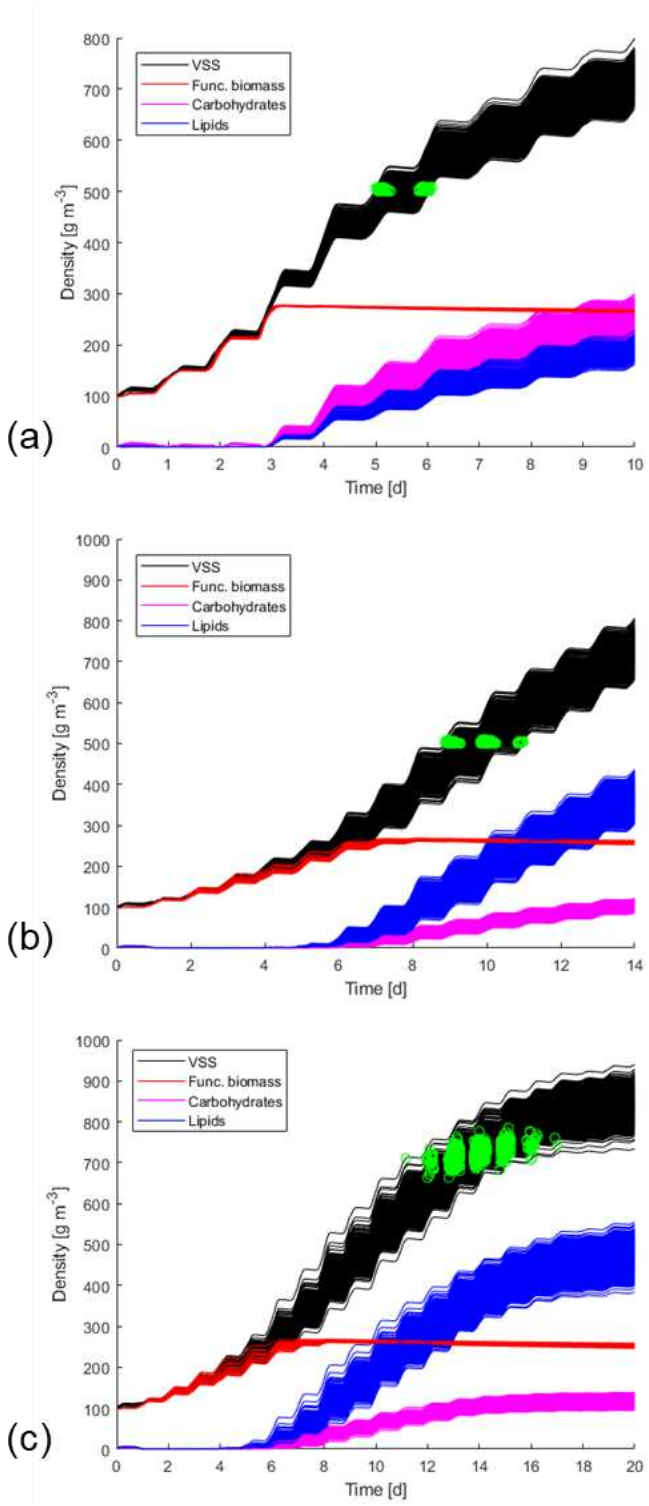

Figure C - 1. Growth curves of all Monte Carlo simulations ($n = 1000$) generated from the compositional growth model for three cultivation scenarios: a) C. vulgaris harvested at 500 g m^{-3}, b) N. granulata harvested at 500 g m^{-3}, c) N. granulata harvested at 50 wt% lipids. Green circles indicate where the harvest condition is met and where the productivity is calculated for a given simulation.

Table C - 7. Baseline "N^{th}-of-a-kind plant" economic assumptions. With these assumptions applied over the life of the plant, the objective is to find the minimum fuel selling price (MFSP) contribution such that the plant breaks even.

Parameter	**Standard value**
Internal rate of return	10%
Plant financing debt / equity	60% / 40% total capital
Plant life	30 years
Income tax rate	35%
Interest rate	8.0% annual
Debt financing term	10 years
Working capital	5% fixed capital (excl. land)
Depreciation schedule	7-year modified accelerated cost recovery system (MACRS)
Construction period	8% year 1 60% year 2 32% year 3
Plant salvage value	None
Start-up time	6 months
Start-up revenue and costs	50% revenue 75% variable costs 100% fixed costs
On-stream factor	90% (330 days per year)
Indirect capital	60% total installed capital
Base cost year	2019
On-stream factor	90% (330 days per year)
Indirect capital	60% total installed capital
Base cost year	2019

Table C - 8. Capital cost estimation of HTL equipment [21,70].

Equipment	Unit cost	Year	Scaling variable	Base value	Scaling exponent	Installation factor
Reactor heat exchanger	$44,604,000	2012	Area	49,756 ft^2	0.7	2.2
Reactor heater	$998,850	2012	Area	6,032 ft^2	0.7	2.2
HTL reactor	$272,788	2013	Length	480 ft	1	2
Gas knockout drum	$5,600,000	2012	Volume	1 ft^3	0.7	2
Solids filter	$1,311,000	2011	Biocrude flow rate	3,689 gpm	0.6	1.7
Phase separator	$3,565,000	2011	Biocrude flow rate	3,689 gpm	0.7	2
Bio-oil heat recovery	$102,000	2012	Area	868 ft^2	0.7	2.2
Purge water cooler	$255,600	2013	Area	13,020 ft^2	0.8	2.3
Hot oil	$2,101,710	2012			1	1
Hot oil system	$1,200,500	2012	Heat duty	60 MMbtu hr^{-1}	0.6	1.8
Hydrotreater and auxiliaries	$27,000,000	2007	Biocrude flow rate	6,524 bbl d^{-1}	0.75	1.51
HT hydrogen compressor	$1,385,600	2011	Hydrogen flow rate	17.1 MMscf d^{-1}	0.8	1.1
HT pressure swing absorber	$1,750,000	2004	Offgas flow rate	10 MMscf d^{-1}	0.8	2.47
Hydrocracker and auxiliaries	$25,000,000	2007	Heavy oil flow rate	2,200 bbl d^{-1}	0.75	1.51

Table C - 9. Capital cost estimation of CAP equipment [11]. *Fermentation vessel scaling variables were modified from the original reference.*

Equipment	Unit cost	Year	Scaling variable	Base value	Scaling exponent	Installation factor
A100: Pretreatment						
Flash / Solvent distillation preheater	$48,019	2007	PT heat duty	8,600 MMkcal hr^{-1}	0.6	3
Feed-effluent heat exchanger	$432,519	2007	PT heat duty	12,300 MMkcal hr^{-1}	0.6	1.6
Pretreatment reactor	$31,200,000	2013	Feed flow rate	63,166 kg hr^{-1}	0.6	1.5
PT balance of plant (BOP)	4.6% of pretreatment	2013			1	1
A200: Fermentation						
Fermentation vessel (200,000 gal)	$590,000	2009	# of vessels	1	1	2
Fermenter agitator	$21,500	2009	# of vessels	1	1	1.5
Fermenter recirculation pump	$47,200	2009	# of vessels	1	1	1.5
Seed train agitator #1	$26,000	2009	Ethanol flow rate	21,672 kg hr^{-1}	0.6	1.5
Seed train agitator #2	$43,000	2009	Ethanol flow rate	21,672 kg hr^{-1}	0.6	1.5
Seed fermenter #1	$75,400	2009	Ethanol flow rate	21,672 kg hr^{-1}	0.6	1.8
Seed fermenter #2	$116,600	2009	Ethanol flow rate	21,672 kg hr^{-1}	0.6	1.8
Seed fermenter #3	$157,600	2009	Ethanol flow rate	21,672 kg hr^{-1}	0.6	1.8
Seed fermenter #4	$352,000	2009	Ethanol flow rate	21,672 kg hr^{-1}	0.6	2
Seed fermenter #5	$1,180,000	2009	Ethanol flow rate	21,672 kg hr^{-1}	0.6	2
Fermentation BOP	8.6% of fermentation (excluding separations)	2009			1	1
Vent scrubber	$215,000	2009	Fermentation offgas flow rate	22,608 kg hr^{-1}	0.6	2.4
Ethanol distillation equipment	$3,407,000	2009	Fermentation product flow rate	30,379 kg hr^{-1}	0.6	2.4
Rectification condenser	$487,000	2010	Distillation column heat duty	23.2 MMkcal hr^{-1}	0.6	2.8
Ethanol molecular sieve	$2,601,000	2009	Ethanol flow rate	22,687 kg hr^{-1}	0.6	1.8
Solid-liquid separator (×5)	$2,152,500	2013	Residual flow rate	15,853 kg hr^{-1}	1	1.7
A300: Lipid extraction						

Lipid extraction column (×16)	$1,980,000	2013	Lipid feed flow rate	5,894 kg hr^{-1}	1	2
Solvent recovery column (×3)	$238,000	2009	Extracted product flow rate	5,599 kg hr^{-1}	0.85	2.4
Solvent recovery reboiler (×3)	$50,000	2009	Extracted product flow rate	5,599 kg hr^{-1}	0.85	3.3
A400: Lipid upgrading						
Feed pump (×2)	$129,300	2011	Lipid feed flow rate	29,274 kg hr^{-1}	0.8	1.42
Air compressor (×2)	$17,300	2011	Furnace air flow rate	3,819 kg hr^{-1}	0.6	1.82
Furnace	$241,400	2011	Furnace heat duty	2.42 MMkcal hr^{-1}	0.7	1.52
Makeup compressor (×2)	$1,621,200	2011	Hydrogen flow rate	390 kg hr^{-1}	0.6	1.09
Makeup compressor (spare)	$1,621,200	2011	Hydrogen flow rate	390 kg hr^{-1}	0.6	1.08
Recycle compressor (×2)	$1,103,700	2011	HDO offgas flow rate	14,665 kg hr^{-1}	0.6	1.13
Recycle compressor (spare)	$1,103,700	2011	HDO offgas flow rate	14,665 kg hr^{-1}	0.6	1.1
Feed effluent heat exchanger	$353,600	2011	HDO heat duty	14.3 MMkcal hr^{-1}	0.7	2.66
HDO reactor	$3,777,764	2011	Lipid product flow rate	208 bbl hr^{-1}	0.7	2
HDO effluent-water cooling heat exchanger	$321,600	2011	HDO cooling duty	4.4 MMkcal hr^{-1}	0.7	1.66
HDO CHP system	$328,500	2011	Lipid product flow rate	39,911 L hr^{-1}	0.7	2.59
Fractionation effluent heat exchanger	$92,400	2011	Frac. heat duty	1.67 MMkcal hr^{-1}	0.7	2.47
Frac. feed trim heat exchanger	$17,000	2011	Frac. heat duty	2.39 MMkcal hr^{-1}	0.7	5.03
Fractionation column	$311,600	2011	Lipid product flow rate	25,644 kg hr^{-1}	0.6	1.67
Frac. reflux pump	$5,800	2011	Lipid product flow rate	25,644 kg hr^{-1}	0.8	6.81
Frac. air cooling	$15,600	2011	Cooling duty	2.50 MMkcal hr^{-1}	0.7	4.63
Frac. 3-phase separator	$33,300	2011	Lipid product flow rate	25,644 kg hr^{-1}	0.7	5.73
Naphtha air cooler	$29,400	2011	Cooling duty	0.068 MMkcal hr^{-1}	0.7	2.32
A500: Residue processing						

Anaerobic digester	Variable size (see Davis et al., 2014) [11]	2012			0.6	1.11
A600: Combined heat and power (CHP)						
HP steam-ethanol heat exchanger	$23,900	2009	Fermentation cooling duty	5,400 MMkcal hr^{-1}	0.6	2.47
HP steam-lipids heat exchanger	$23,900	2009	Lipid extraction cooling duty	5,400 MMkcal hr^{-1}	0.6	2.47
Natural gas HP boiler	$1,279,300	2012	HP steam flow rate	1.28×10^6 kg hr^{-1}	0.6	1
Natural gas LP boiler	$1,203,500	2012	LP steam flow rate	1.28×10^6 kg hr^{-1}	0.6	1
A700: Utilities and storage						
Cooling tower system	$1,375,000	2010	Cooling water flow rate	1.00×10^7 kg hr^{-1}	0.6	1.5
Plant air compressor	$28,000	2010	Feed flow rate	83,333 kg hr^{-1}	0.6	1.6
Chilled water package	$1,275,750	2010	Cooling duty	14,200 MMkcal hr^{-1}	0.6	1.6
Clean-in-place system	$694,000	2009	Feed flow rate	83,333 kg hr^{-1}	0.6	1.8
Cooling water pump (×3)	$94,557	2010	Cooling water flow rate	1.10×10^7 kg hr^{-1}	0.8	3.1
Makeup water pump	$6,864	2010	Process water flow rate	155,564 kg hr^{-1}	0.8	3.1
Process water circulator pump	$15,292	2010	Process water flow rate	518,924 kg hr^{-1}	0.6	1.8
Instrument air dryer	$15,000	2009	Feed flow rate	83,333 kg hr^{-1}	0.6	1.8
Plant air receiver	$16,000	2009	Feed flow rate	83,333 kg hr^{-1}	0.6	3.1
Process water tank #1	$250,000	2009	Process water flow rate	451,555 kg hr^{-1}	0.7	1.7
Biodiesel storage tank	$670,000	2009	Biodiesel flow rate	11,341 kg hr^{-1}	0.7	1.7
Ethanol storage tank	$670,000	2009	Ethanol flow rate	11,341 kg hr^{-1}	0.7	1.7
Naphtha storage tank	$87,057	2009	Naphtha flow rate	378 kg hr^{-1}	0.7	1.7
Firewater storage tank	$501,000	2009	Feed flow rate	83,333 kg hr^{-1}	0.7	1.7
Tankage BOP	20% of A700	2009			1	1

Table C - 10. Variable operating costs used across the algal biofuel production system.

Material	Unit cost	Year	References
Carbon dioxide	\$0.0204 lb^{-1}	2011	[62]
Water	\$0.00022 kg^{-1}	2011	[62]
Ammonia	\$0.3862 lb^{-1}	2011	[62]
Diammonium phosphate (DAP)	\$0.315 lb^{-1}	2011	[62]
Electricity	\$0.0682 kWh^{-1}	2019	[92]
Natural gas	\$0.232 kg^{-1}	2011	[93]
Hydrogen	\$1.57 kg^{-1}	2012	[94]
Sulfuric acid	\$0.095 kg^{-1}	2016	[11]
Flocculant	\$2.205 kg^{-1}	2011	[11]
Hexane	\$1.115 kg^{-1}	2010	[11]

Table C - 11. Fixed operating costs of ORP production [62].

Position	Salary	# of employees	Year
Plant manager	\$155,400	1	2011
Plant engineer (civil)	\$81,935	2	2011
Plant engineer (environmental)	\$83,244	2	2011
Maintenance supervisor	\$60,257	1	2011
Maintenance technician	\$42,286	12	2011
Lab manager	\$59,200	1	2011
Lab technician	\$42,286	1	2011
Shift supervisor	\$50,743	4	2011
Module operator - production	\$26,872	56	
Module operator - inoculum	\$44,038	8	2011
Module operator - dewatering	\$38,536	9	2011
Clerks and secretaries	\$38,057	3	2011
Labor burden	90% total salaries		
Maintenance	0.5% ORP + 3% harvesting CAPEX		
Property insurance	0.7% fixed capital		

Table C - 12. Fixed operating costs of fuel conversion plants [93].

Position	**Salary**	**# of employees**	**Year**
Plant manager	$147,000	1	2009
Plant engineer	$70,000	2	2009
Maintenance supervisor	$57,000	1	2009
Maintenance technician	$40,000	5	2009
Lab manager	$56,000	1	2009
Lab technician	$40,000	2	2009
Shift supervisor	$48,000	2	2009
Shift operator	$40,000	9	
Yard employee	$28,000	2	2009
Clerks and secretaries	$36,000	2	2009
Labor burden	90% total salaries		
Maintenance	3% conversion CAPEX		
Property insurance	1% fixed capital		

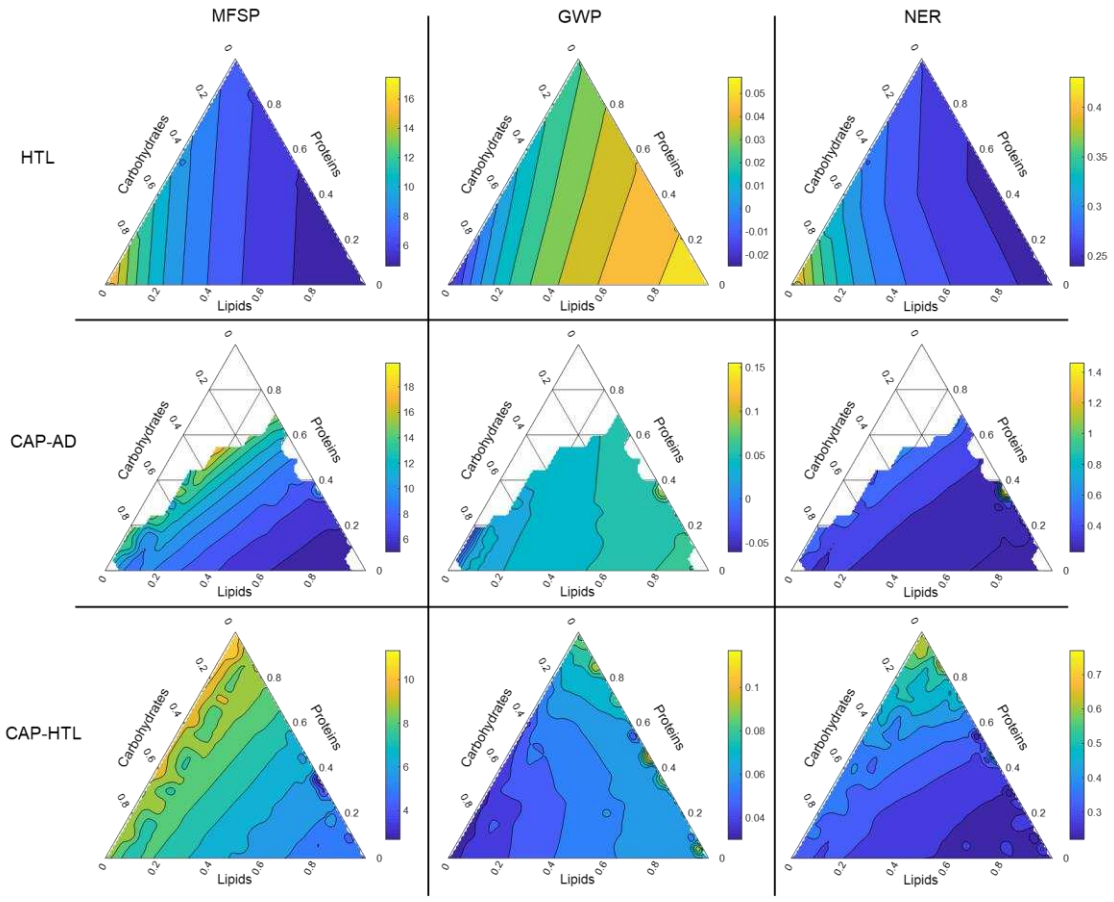

Figure C - 2. Ternary contour plots of individual objective values with respect to biomass feed composition for the baseline productivity scenario. In CAP-AD plots, compositional points were removed if the protein content was too high to yield usable fuels, with an MFSP of \$20 GGE^{-1} defined as the cap.

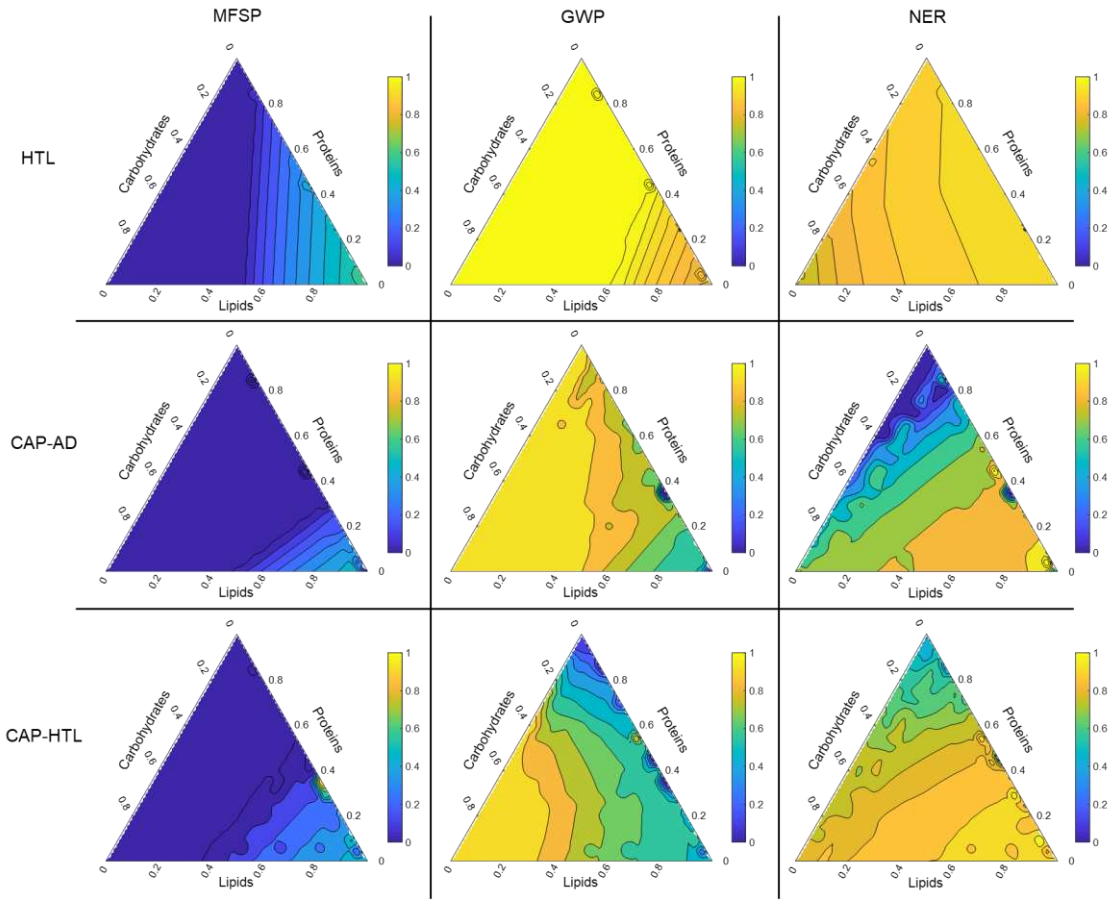

Figure C - 3. Ternary contour plots of individual λ of MFSP, GWP, and NER for the baseline productivity scenario.

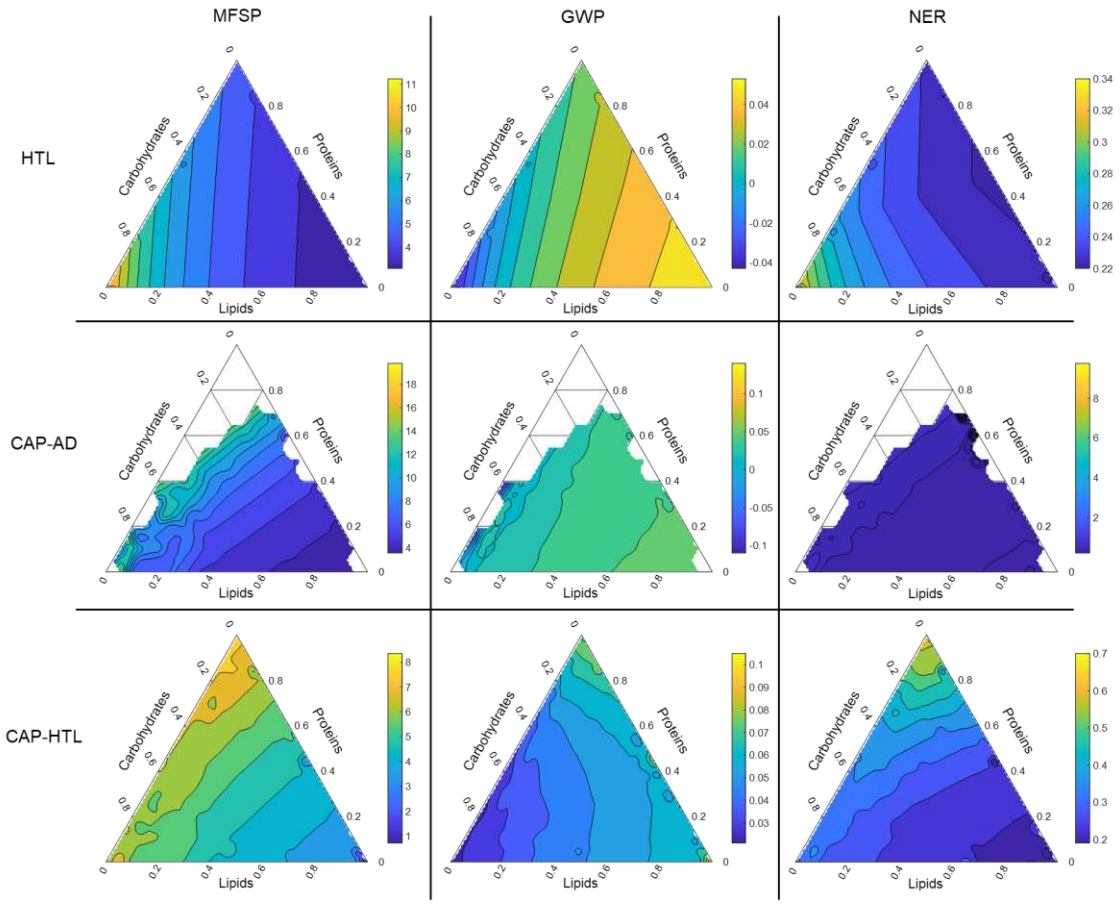

Figure C - 4. Ternary contour plots of individual objective values with respect to biomass feed composition for the doubled productivity scenario. In CAP-AD plots, compositional points were removed if the protein content was too high to yield usable fuels, with an MFSP of \$20 GGE^{-1} defined as the cap.

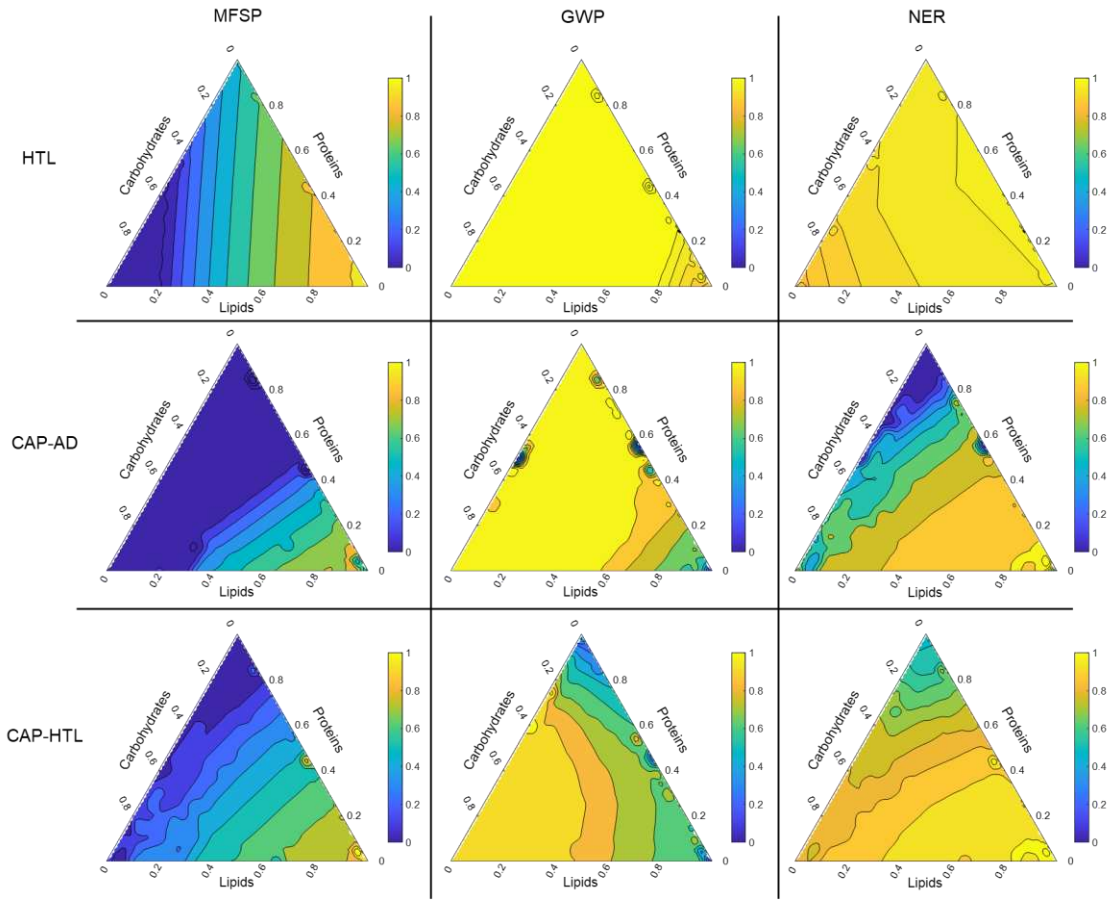

Figure C - 5. Ternary contour plots of individual λ of MFSP, GWP, and NER for the doubled productivity scenario.

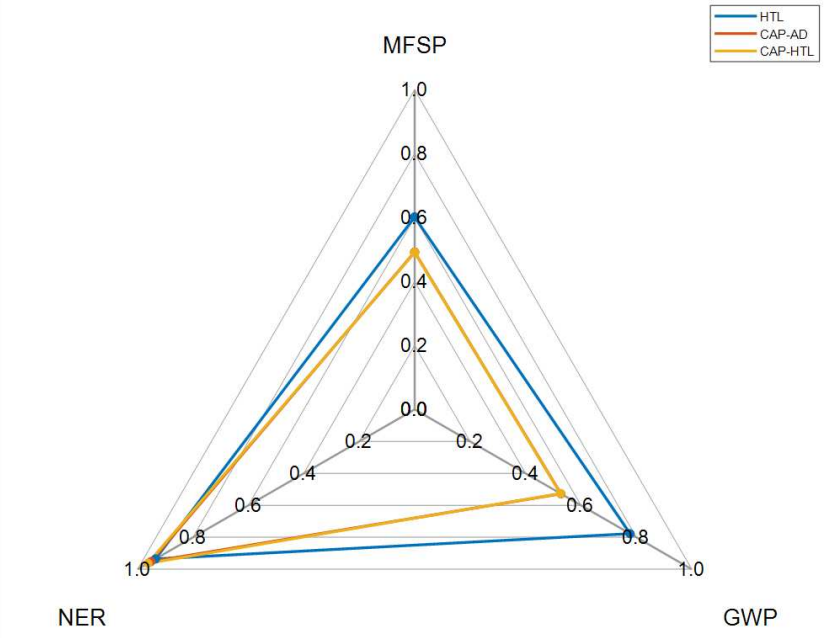

Figure C - 6. Spiderweb diagram of the best case (maximum λ_o) baseline scenarios with respect to composition of HTL, CAP-AD, and CAP-HTL. Vertices indicate the λ score of each individual objective. NER is notably the easiest objective to satisfy; MFSP is the most difficult. CAP-AD and CAP-HTL maxima are effectively identical.

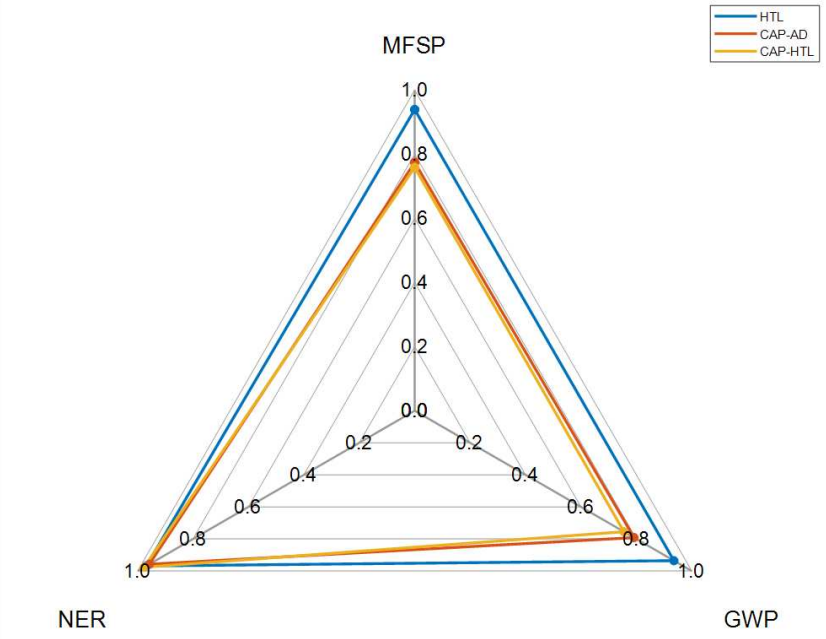

Figure C - 7. Spiderweb diagram of the best case (maximum λ_o) doubled productivity scenarios with respect to composition of HTL, CAP-AD, and CAP-HTL. Vertices indicate the λ score of each individual objective. HTL achieves near-full satisfaction in all three objectives, resulting in a favorable λ_o of 0.89. Even in the best-case scenario with doubled feed productivity, CAP-AD and CAP-HTL struggle to achieve high satisfaction scores in MFSP and GWP.

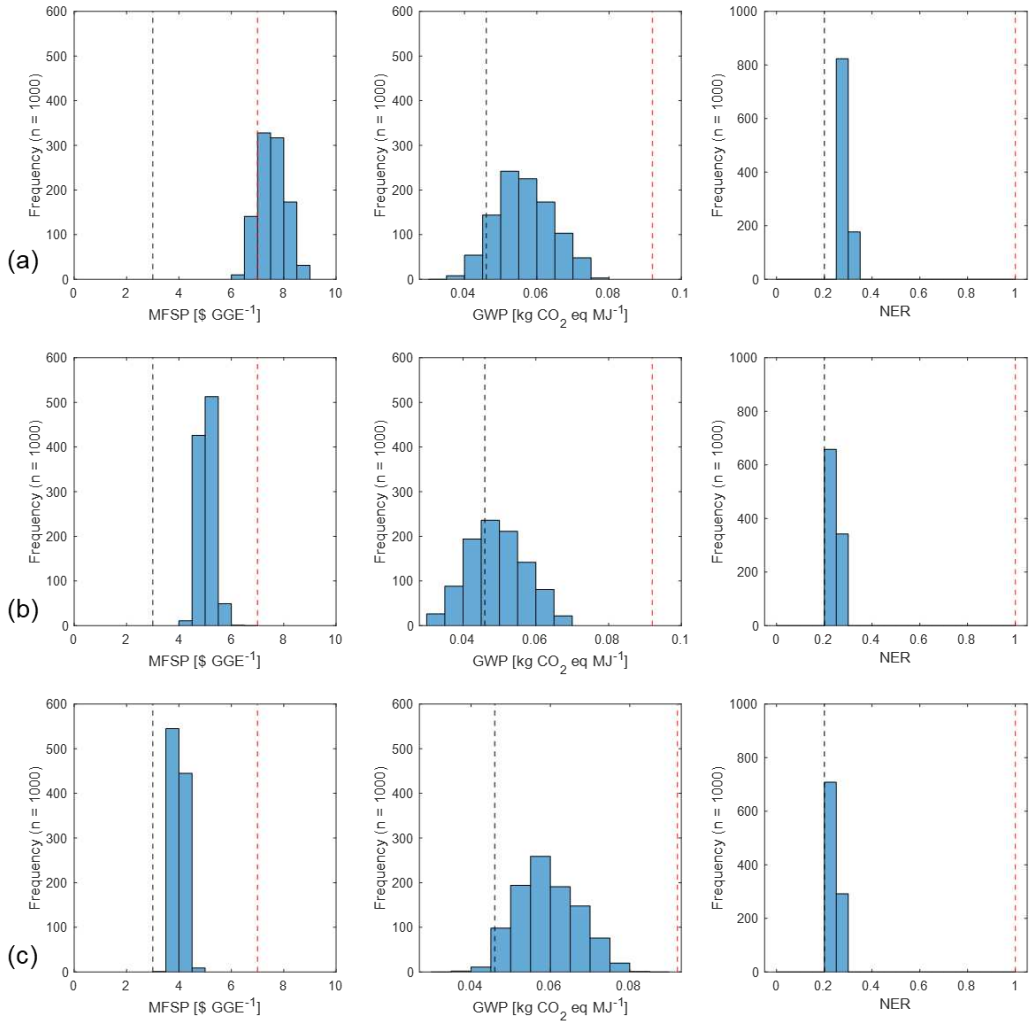

Figure C - 8. Individual breakdowns of MCA distributions of MFSP, GWP, NER, and λ_o in the normal C. vulgaris feed production scenario. a) HTL, b) CAP-AD, c) CAP-HTL.

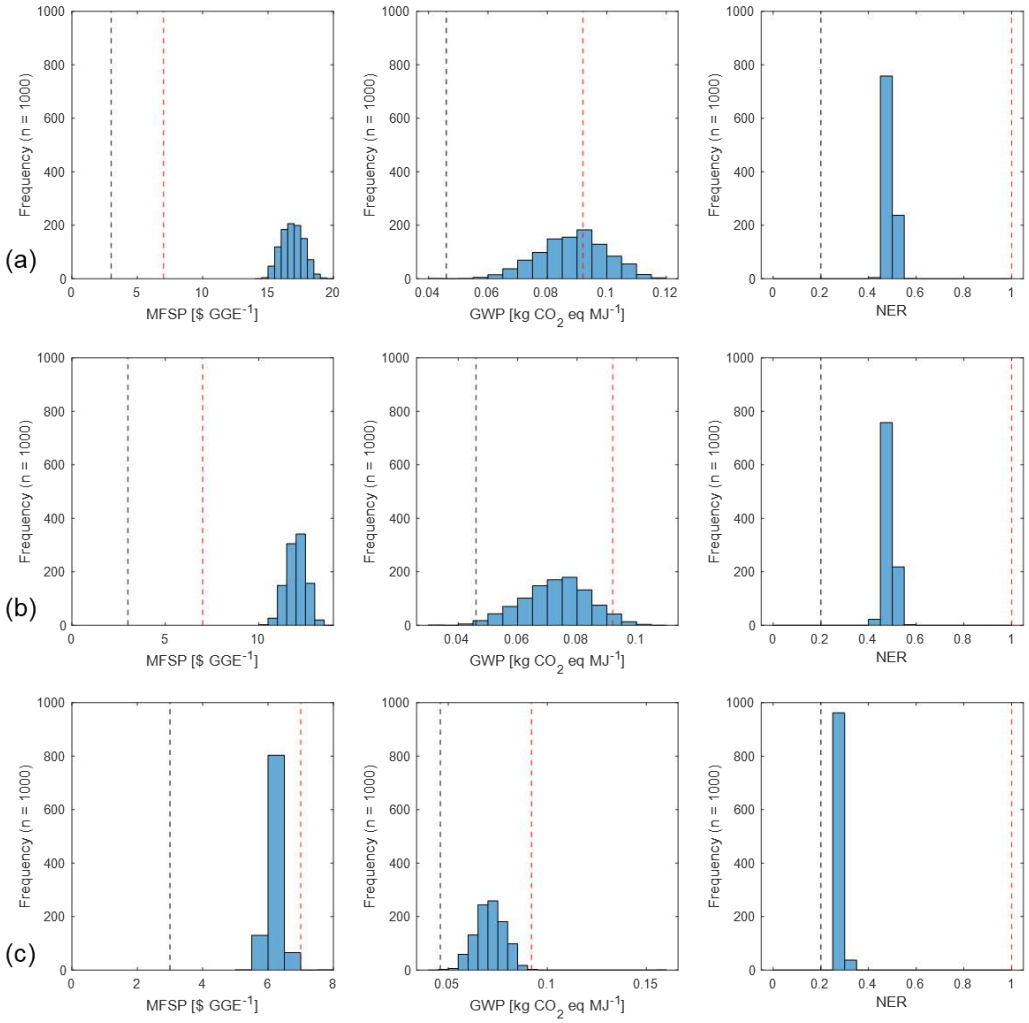

Figure C - 9. Individual breakdowns of MCA distributions of MFSP, GWP, NER, and λ_o in the doubled productivity (35 g m^{-2} d^{-1}) C. vulgaris feed production scenario. a) HTL, b) CAP-AD, c) CAP-HTL.

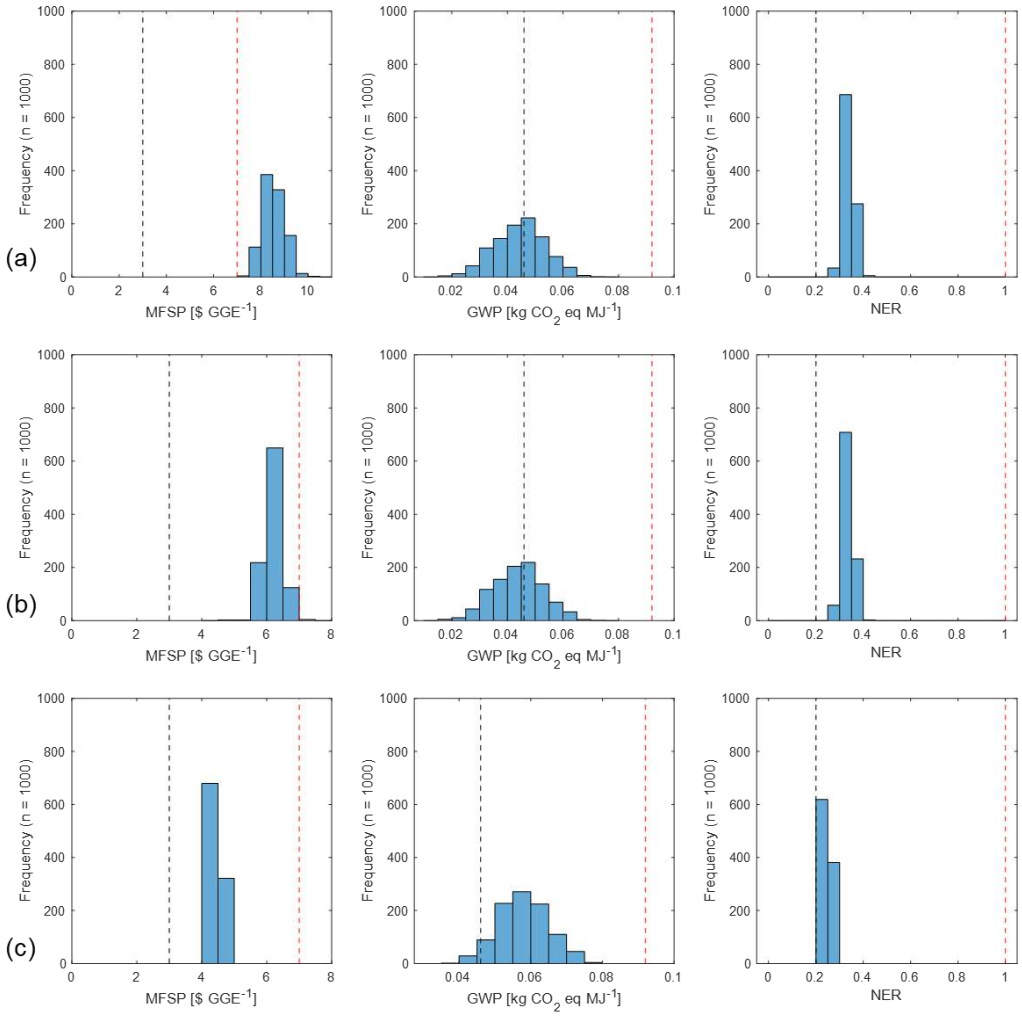

Figure C - 10. Individual breakdowns of MCA distributions of MFSP, GWP, NER, and λ_o in the doubled productivity (35 g m^{-2} d^{-1}) N. granulata feed production scenario. a) HTL, b) CAP-AD, c) CAP-HTL.

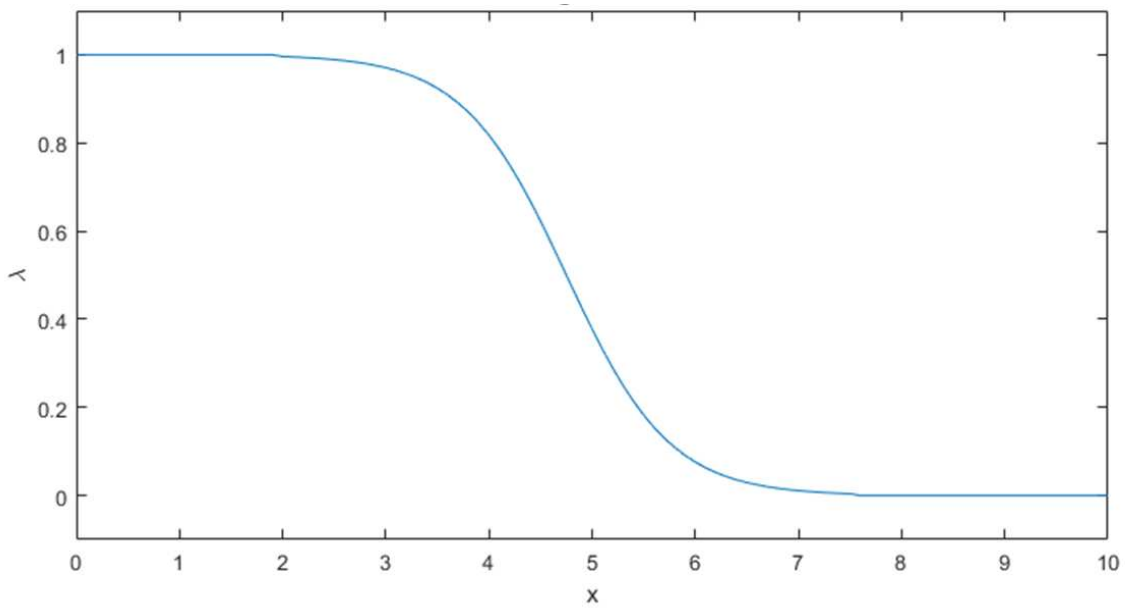

Figure C - 11. Example of a nonlinear (sigmoidal) membership function (x denotes any objective). Desirable and acceptable thresholds remain the same as linear membership functions.

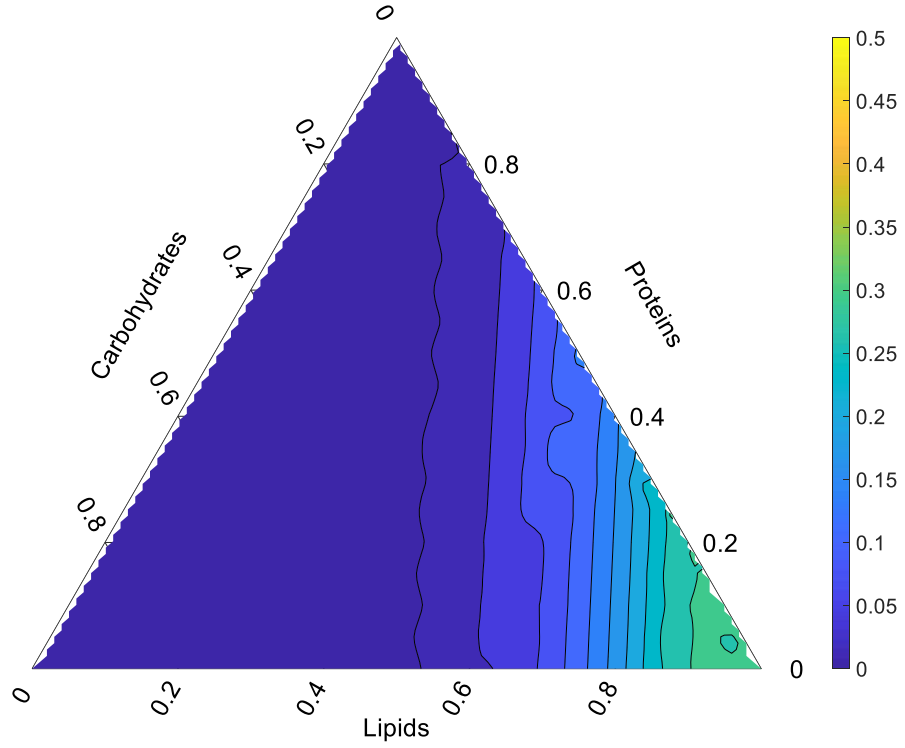

Figure C - 12. Ternary plot of λ_o of the baseline HTL pathway as a function of composition, where the membership functions have all changed from linear to smooth sigmoidal shapes. Note the difference in magnitude and contour gradients from the linear function (Figure 5a in main text). The maximum λ_o with sigmoidal membership functions is 0.32.